Report No. ACNP-62031

PATHFINDER ATOMIC POWER PLANT

REACTOR INTERNAL COMPONENTS

June 28, 1963

Submitted to

U. S. ATOMIC ENERGY COMMISSION

NORTHERN STATES POWER COMPANY

and

CENTRAL UTILITIES ATOMIC POWER ASSOCIATES

by

ALLIS-CHALMERS MANUFACTURING COMPANY
ATOMIC ENERGY DIVISION
Milwaukee 1, Wisconsin

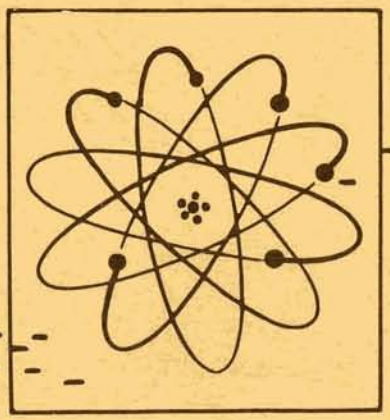

Ref: AEC Contract No. AT(11-1)-589

DISCLAIMER

LEGAL NOTICE

This report was prepared as an account of Government sponsored work. Neither the United States, nor the Commission, nor Allis-Chalmers Manufacturing Company, nor any person acting on behalf of the Commission or Allis-Chalmers Manufacturing Company:

A. Makes any warranty or representation to others, expressed or implied, with respect to the accuracy, completeness, or usefulness of the information contained in this report, or that the use of any information, apparatus, method, or process disclosed in this report may not infringe privately owned rights; or

B. Assumes any liabilities to others with respect to the use of, or for damages resulting from the use of any information, apparatus, method, or process disclosed in this report.

As used in the above, 'person acting on behalf of the Commission or Allis-Chalmers Manufacturing Company' includes any employe or contractor of the Commission, or Allis-Chalmers Manufacturing Company or employe of such contractor, to the extent that such employe or contractor of the Commission, or Allis-Chalmers Manufacturing Company or employe of such contractor prepares, disseminates, or provides access to, any information pursuant to his employment or contract with the Commission or Allis-Chalmers Manufacturing Company or his employment with such contractor.

PATHFINDER ATOMIC POWER PLANT
REACTOR INTERNAL COMPONENTS

By: D.R. Bruesewitz, J.F. Wilson,
E.C. Rothen, D.J. Nolan, J.F. Patterson, and S.P. Wnuk

Submitted to

U. S. ATOMIC ENERGY COMMISSION
NORTHERN STATES POWER COMPANY
and
CENTRAL UTILITIES ATOMIC POWER ASSOCIATES

by

ALLIS-CHALMERS MANUFACTURING COMPANY

Under
Agreement dated 2nd Day of May 1957, as Amended
between
Allis-Chalmers Mfg. Co. & Northern States Power Co.
under
AEC Contract No. AT(11-1)-589

June 28, 1963

Classification – UNCLASSIFIED

Reviewed by Lewis Klecker
Authorized Classifying Official

Approved: C. B. Graham
C. B. Graham
Manager
Nuclear Power Dept.-Greendale

ALLIS-CHALMERS MANUFACTURING COMPANY
ATOMIC ENERGY DIVISION
MILWAUKEE 1, WISCONSIN

Approved: Hibbert Hill
Hibbert Hill
Vice President-
Engineering

NORTHERN STATES POWER COMPANY
15 SOUTH FIFTH STREET
MINNEAPOLIS 2, MINNESOTA

PATHFINDER ATOMIC POWER PLANT

Reactor Internal Components

Distribution

USAEC, Chicago Operations Office-- 9800 South Cass Avenue, Argonne, Illinois	5
USAEC, Division of Reactor Development-- Washington 25, D. C.	8
USAEC, OTIE-- Oak Ridge, Tennessee ..... Offset Master plus	20
Northern States Power Company and CUAPA	26
Allis-Chalmers Manufacturing Company	39
	101

FOREWORD

This report "Reactor Internal Components" is one of a series of reports on research and development in connection with the design of the Pathfinder Atomic Power Plant.

The Pathfinder plant will be located at a site near Sioux Falls, South Dakota, and is scheduled for operation in 1963. Owners and operators of the plant will be the Northern States Power Company of Minneapolis, Minnesota. Allis-Chalmers is performing the research, development, and design as well as being responsible for plant construction.

The U. S. Atomic Energy Commission, through Contract No. AT(11-1)-589 with Northern States Power Company and Central Utilities Atomic Power Associates (CUAPA) are sponsors of the research and development program.

The plant's reactor will be of the Controlled Recirculation Boiling Reactor type with Nuclear Superheater.

TABLE OF CONTENTS

	Page
Distribution	ii
Foreword	iii
List of Illustrations	vi
1.0 Introduction	1
1A.0 Objective	1
2.0 Boiler Core Grid Plate	2
2.1 Theoretical Stress Analysis	2
2.2 Deflection Analysis	6
2.3 Experimental Stress Analysis	9
2.4 Thermal Stress Analysis	18
3.0 Boiler Core Shroud	27
3.1 Experimental Stress Analysis	27
4.0 Fuel Element Hold-Down Assembly	28
4.1 Theoretical Stress Analysis	28
4.2 Deflection Analysis of Grid Structure	48
4.3 Experimental Stress Analysis of Grid Structure	50
5.0 Steam Dryer Assembly	54
5.1 Steam Dryer Hold-Down Structure	54
5.2 Steam Dryer	58
5.3 Upper Control Rod Guide Tubes	59
6.0 Steam Separator Support Shelf	60
6.1 Theoretical Stress Analysis	60
6.2 Experimental Stress and Deflection Analysis	63
7.0 Nuclear Superheater	66
7.1 Tubes	70
7.1.1 Tube Collapsing Pressure Test	72
7.2 Superheater Lower Tube Sheet	82
7.2.1 Mechanical Stress Calculations	83
7.2.2 Thermal Gradient Calculations	88

7.3 Superheater Shrouds 95

7.3.1 Theoretical Stress Analysis 95

7.3.2 Deflection Analysis 101

7.4 Superheater Upper Shroud 103

7.4.1 Deflection Test 104

7.5 Steam Line and Superheater Support 111

7.6 Superheater Natural Frequencies 113

7.7 Superheater Tube Vibration Test 117

7.8 Superheater Orifice Flow Test 132

7.9 Superheater Water Flow 138

7.10 Superheater Seal Test 143

7.11 Superheater Tube Weld Test 147

LIST OF ILLUSTRATIONS

Fig. No.	Title	Page
1.1	Reactor Internal Assembly	3
1.2	Cutaway Model of Reactor	4
2.1	Boiler Core Grid Plate	5
2.2	Grid Plate Load Test Rig	12
2.3	Grid Plate Dial Indicator Locations	13
2.4	Strain Gage Locations on Bottom Surface of Grid Plate	16
2.5	Isometric Plot of Radial and Circumferential Stress Along Line X-X of Grid Plate	17
2.6	Plot of Temperature Distribution Through Top Plate of Grid Structure	18
2.7	Distribution of Thermal Stress Due to Gamma Heating in Top Plate of Grid Structure	24
3.1	Boiler Core Shroud Assembly	29
4.1	Fuel Element Hold-Down Assembly (4 sheets)	30
4.2	Loading on Fuel Element Hold-Down Grid Structure	36
4.3	Fuel Element Hold-Down Grid Section (two sheets)	37
5.1	Steam Dryer Final Assembly (two sheets)	55
6.1	Steam Separator Support Shelf	61
6.2	Steam Separator Support Shelf Dial Indicator Locations	62
7.1	Superheater Shell Assembly (two sheets)	67
7.2	Collapsed Unsupported Superheater Container Tube (Typical)	75
7.3	Collapsed Mock-up Superheater Assemblies	78
7.4	Collapsing Pressure of Tubes with Side and End Loading as a Function of Wall Thickness to Diameter Ratio	81
7.5	Spherical Grid Plate Free Body Diagram	84

LIST OF ILLUSTRATIONS

Fig. No.	Title	Page
7.6	Representative Section of Spherical Grid Plate	87
7.7	Temperature Gradient 3/4 in. Thick Section Plate	91
7.8	Temperature Gradient I in. Thick Section Plate	92
7.9	Stress Distribution on Inside Surface of Superheater Grid Plate	93
7.10	Stress Distribution on Outside Surface of Superheater Grid Plate	94
7.11	Superheater Baffle Energy Method Analyses	97
7.12	Stress and Deflection Loading Diagrams (3 sheets)	98
7.13	Test Setup for Baffle Pressure Test	105
7.14	Plot of Baffle Deflection Vs Internal Pressure Edges not Restrained	108
7.15	Plot of Baffle Deflection Vs Internal Pressure Edges Restrained at Sixteen Locations	109
7.16	Pathfinder Superheater Steam Line	112
7.17	Plot of Heat Flux Vs Steam Gap Thickness for Steam Line Header	115
7.18	Superheater Vibration Analysis - Wave Forms	116
7.19	Superheater Tube Vibration Test Loop	119
7.20	Superheater Vibration Test Section	120
7.21	Vibration of Tube Bundle Suspended in Air	125
7.22	Vibration of Tube Bundle in Air with Tube Sheets Guided on Three Sides	125
7.23	Vibration of Tube Bundle in Air with Tube Sheets Guided on Four Sides	125
7.24	Tube Vibration with 69 GPM and 3.15 FPS Water Flow	126

LIST OF ILLUSTRATIONS

Fig. No.	Title	Page
7.25	Tube Vibration with 190 GPM and 6.30 FPS Water Flow . . .	126
7.26	Tube Vibration with 96 GPM and 4 FPS Water Flow and 24 GPM Air Flow	126
7.27	Tube Vibration with 180 GPM and 6.75 FPS Water flow and 24 GPM Air Flow	126
7.28	Interface Frequency	126
7.29	Interface Frequency with 190 GPM Water Flow	127
7.30	Vibration of Tube (94 in. between tube sheets) Suspended in Air	127
7.31	Calibration Beam	127
7.32	Deflection with Single Phase Flow 96 GPM and 3.15 FPS . .	127
7.33	Deflection with Single Phase Flow 190 GPM and 6.30 FPS. .	127
7.34	Deflection with Two Phase Flow 190 GPM Water 24 GPM Air and 4 FPS	128
7.35	Deflection with Two Phase Flow 180 GPM Water 24 GPM Air and 6.75 FPS.	128
7.36	Calibration Beam for 94 in. Span Tube Section at Zero Flow	128
7.37	Deflection of 94 in. Span Tube with Single Phase Flow 190 GPM and 6.3 FPS	128
7.38	Deflection of 94 in. Tube with Two Phase Flow 190 GPM Water 24 GPM Air and 7.1 FPS	128
7.39	Dynamic Deflection Calibration at Zero Flow	131
7.40	Dynamic Deflection with 190 GPM and 6.3 FPS Water Flow . .	131
7.41	Superheater Orifice Flow Test Loop Schematic Diagram . .	134
7.42	Pressure Drop Across Transition Tube with Various Sized Orifice Diameters, d_o	135

LIST OF ILLUSTRATIONS

Fig. No.	Title	Page
7.43	Pressure Drop Across Intermediate Tube Sheet for Various Sized Orifice Diameters, d_o	136
7.44	Average Resistance Coefficient as a Function of B Ratio	139
7.45	Pressure Drop Across Superheater	144
7.46	Superheater Seal Test Assembly	145
7.47	Sketches of Various Tube to Tube Sheet Joint Designs	148
7.48	Surface Appearance of Joint Designs After Welding	149
7.49	Austenite Plus Ferrite Structure	151
7.50	Two Methods of Measuring Distortion of Tube Sheet	152
7.51	Method Used to Determine Strength of Weld	153
7.52	Sections Through Tube-to-Sheet Welds	154
7.53	Over-all View of Test Holder	157
7.54	View of Loose Crud Collected on Surfaces	158
7.55	View Showing Lack of Weld Penetration in Proper Area	158
7.56	View Showing Oxide at End of Weld Penetration	159
7.57	View Showing Bent Surface of 316 SS 25/32 in. Diameter Tube	159
7.58	View Showing Bent Surface of Inconel Sheet	160
7.59	View Showing Oxide at End of Weld Penetration	160
7.60	View Showing Outside Surface of 316 SS Fully Annealed	161
7.61	View Showing Bent Surface of 316 SS 11/16 in. Diameter Tube	161
7.62	View Showing Layer of Oxide Between Tube and Collar	162
7.63	View Showing Outside Surface of 316 SS Expanded Tube	162

1.0 INTRODUCTION

The Pathfinder Reactor is a 66 MWe, direct cycle boiling water reactor with an internal nuclear superheater, controlled circulation, and internal steam separation. The mechanical arrangement, water circulation and steam circulation are shown in Figure 1.1.

Feedwater enters the 11 ft I.D. reactor vessel at the feedwater distribution ring near the bottom of the downcomer region, where it mixes with recirculating water. The water is then withdrawn from the vessel and pumped back through the core region, where a portion of it is generated into steam. The steam water mixture is then forced up into the two-phase interface, where a percentage of the steam is released from the water at the interface. The remaining mixture of steam and water passes into the downcomer region, where most of the remaining steam is removed from the water by centrifugal type separators. Steam from both the separators and interface flows through a mesh-type dryer and into the centrally located superheater where its temperature is raised from 489 to 825 F. The steam leaves the superheater through the main steam line located at the bottom of the reactor vessel.

Figure 1.2 shows a scale model of the reactor internals.

1A.0 OBJECTIVE

To provide descriptive information on major reactor internal components,

to report on the test programs related to component development, and to describe methods used in component design analysis.

2.0 BOILER CORE GRID PLATE (SEE FIGURE 2.1)

The grid plate supports and locates the boiler fuel elements and the boiler core shroud. The grid plate is a rigid sandwich type structure consisting of two annular, perforated plates joined at the periphery by a cylindrical ring. Additional rigidity is gained from 96 cylindrical spacers, which serve as sleeves for boiler fuel element nozzles. The sandwich type structure supplies rigid support, and reduces thermal stresses in the plate. Further reduction of thermal stresses in the plate is accomplished by circulating coolant between the inner surfaces of the sandwich plating.

The grid plate is bolted to a skirt which is welded to the reactor vessel. A cylindrical shroud is attached to the periphery of the grid plate. The shroud supports the fuel element hold-down structure and separates the annular coolant downcomer region from the core.

2.1 Theoretical Stress Analysis*

The mechanical stresses present in the boiler core grid plate were determined as follows:

1. The maximum deflection of the annular sandwich structure was determined from analogous methods.

* Nomenclature for analysis is defined on pp. 25

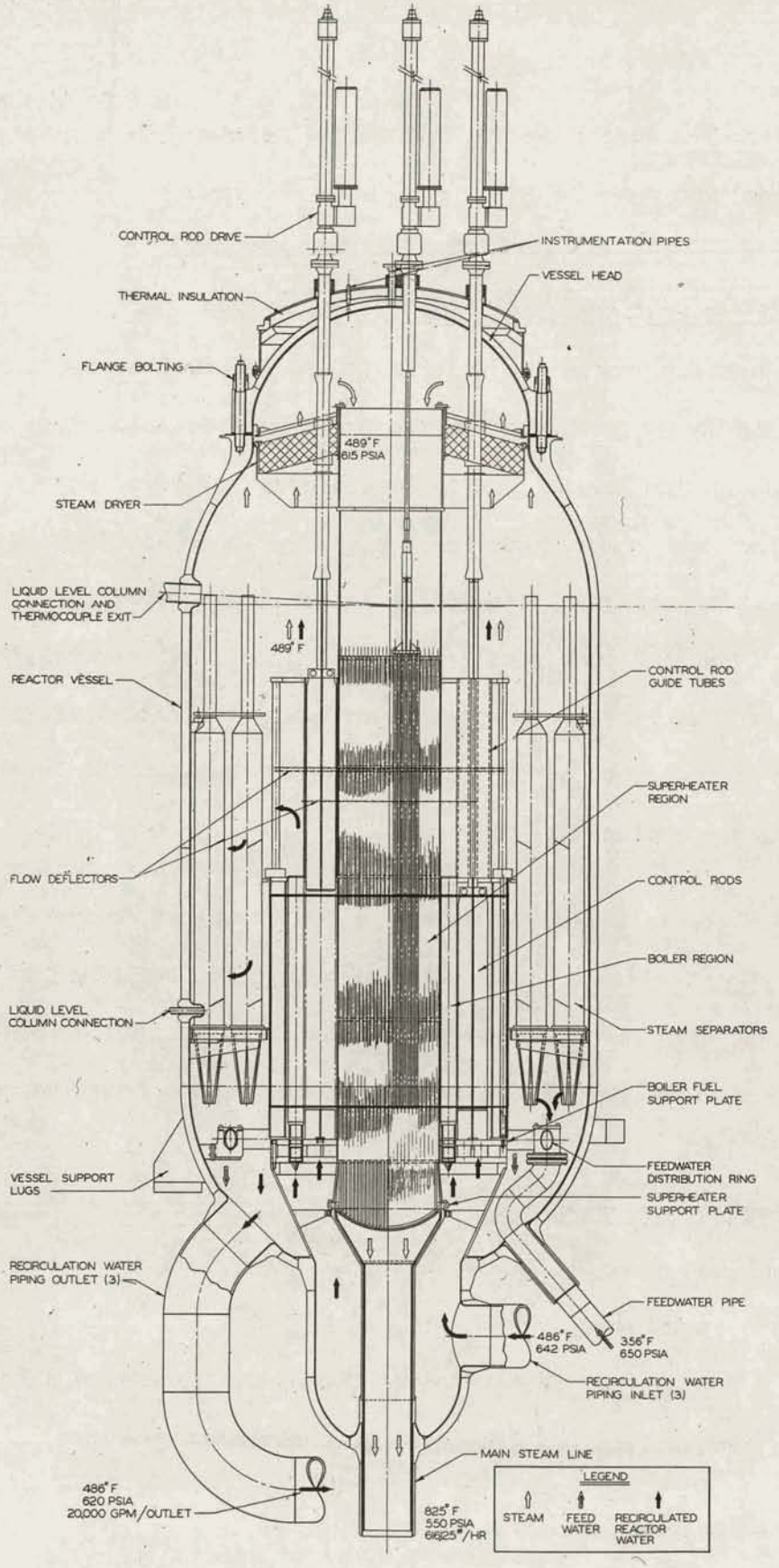

Figure 1.1 - Reactor Internal Assembly (206530)

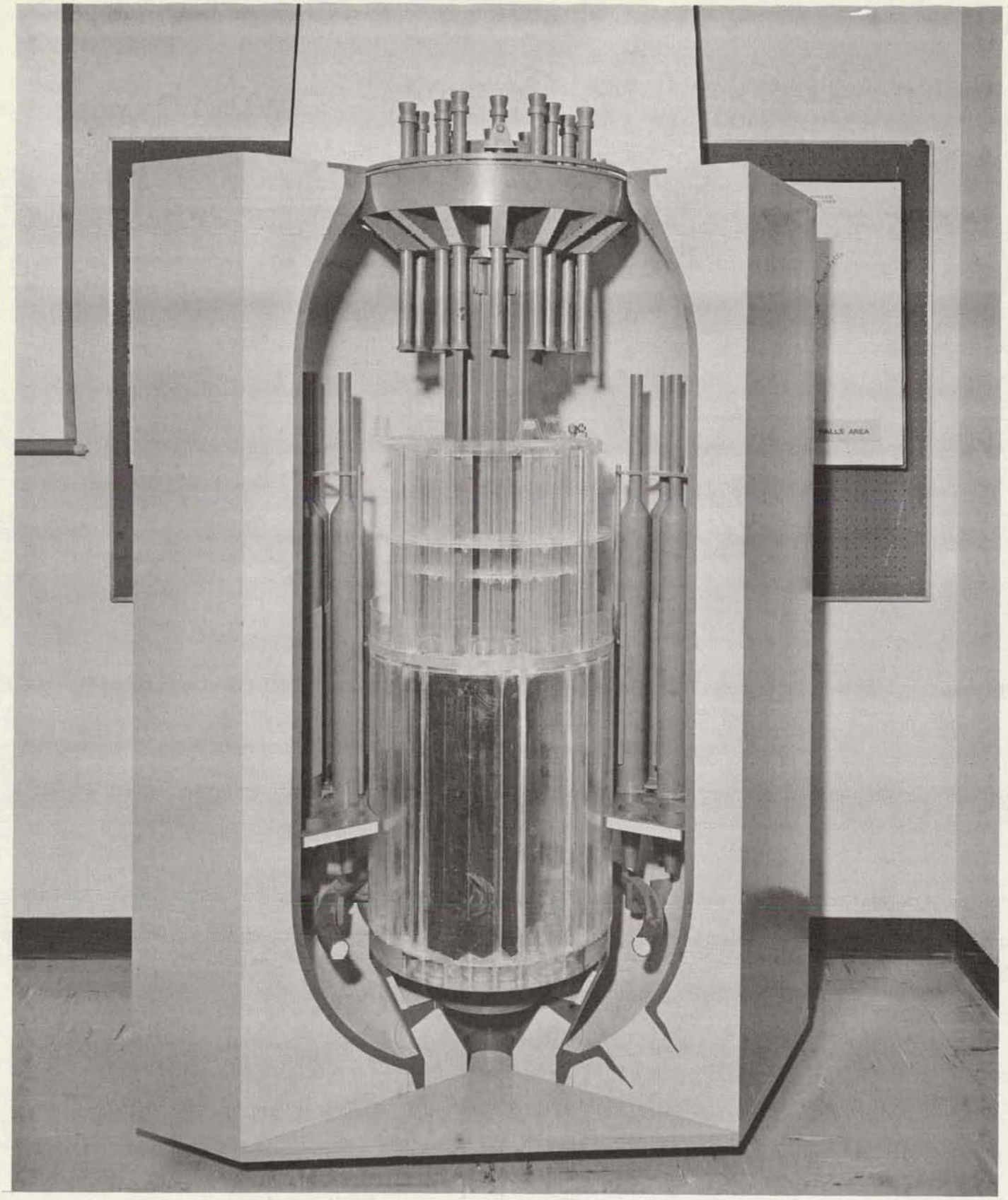

Figure 1.2 - Cutaway Model of Reactor (213994)

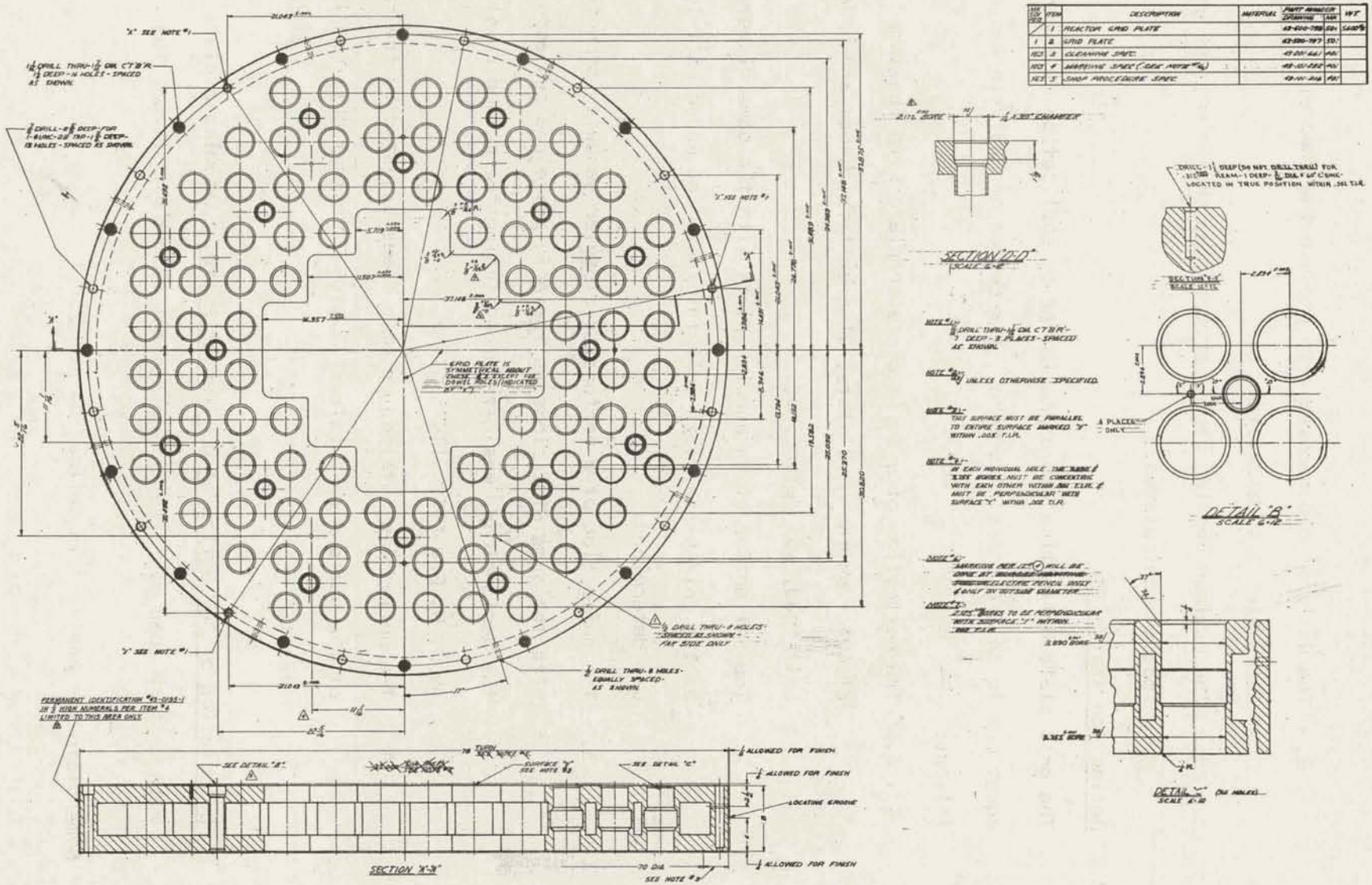

Figure 2.1 - Boiler Core Grid Plate (43-500-798)

2. The uniform load necessary to produce the theoretical maximum deflection was calculated.

3. The maximum bending stress produced by the determined uniform load was calculated.

2.2 Deflection Analysis*

The grid plate deflection was approximated by application of known equations to an analogous structure. The method of analysis was as follows:

1. The deflection of a solid circular plate with the same diameter as the grid plate, with unit thickness and under unit load, was determined.

2. The deflection of an annular plate with the same diameter as the grid plate, with unit thickness and under unit load, was determined.

3. The deflection of a perforated circular sandwich structure, with the same dimensions as the grid plate and subjected to the design load, was determined, using the method developed by G. H. Eng (Ref. 1).

4. The deflection obtained in step 3 was adjusted by the ratio of the deflection obtained in step 2 to that obtained in step 1.

Calculation of Deflection of a Circular Plate. Assuming a plate with uniform load over the entire surface with edges fixed, the

* Nomenclate for analysis is defined on pp. 25

maximum deflection was computed by the following formula, as given in Roark, (Ref. 2):

$$Y_{max} = \frac{3\,w\,(m^2 - 1)\,a^4}{16\,E\,m^2 t^3} \qquad (2.1)$$

After performing the necessary calculation:

$$Y_{max} = 0.0139 \text{ in.}$$

Calculation of Deflection of an Annular Plate. The annular plate is also assumed to be under uniform load with the outside edge fixed and supported. From Reference 2:

$$Y_{max} = \frac{3\,w\,(m^2 - 1)}{16\,m^2 E\,t^3}\left(a^4 + 5b^4 - 6a^2b^2 + 8b^4 \ln a/b - \frac{[8b^6\,(m+1) - 4a^2b^4\,(3\,m+1) - 4a^4b^2\,(m+1) \ln a/b]}{a^2\,(m-1) + b^2\,(m+1)} + \frac{[16a^2b^4\,(m+1)\,(\ln a/b)^2 - 4a^2b^4 + 2a^4b^2\,(m+1) - 2b^6\,(m-1)]}{a^2\,(m-1) + b^2\,(m+1)}\right) \qquad (2.2)$$

After computation

$$Y_{max} = 0.0080 \text{ in.}$$

The ratio of deflection of circular to annular plate is:

$$\text{Ratio} = \frac{0.0139 \text{ in.}}{0.0080 \text{ in.}} = 1.74$$

Calculation of Deflection of Circular Sandwich Structure. The calculation of the deflection of a circular perforated sandwich structure requires a knowledge of the shear and flexural rigidity of the structure. Approximate values can be obtained by modifying data reported by G. H. Eng (Ref. 1) for a similar structure.

$$Y_{max} = Y_o \left[1 + \frac{16\, D_x}{a^2 \left(C + \frac{t_1 + t_2}{2} \right) G_c} \right] \tag{2.3}$$

Where:

$$Y_o = \frac{q\, a^4}{64\, D_x} \tag{2.4}$$

$$D_x = n_w\ D \tag{2.5}$$

$$D = \frac{E_f\, t_1\, t_2 \left(C + \frac{t_1 + t_2}{2} \right)^2}{(1 - \nu^2)\ (t_1 + t_2)} \tag{2.6}$$

After performing the indicated calculations

$$Y_{max} = 0.0085 \text{ in.}$$

The conversion ratio between the circular and annular plates, determined previously, is now applied to the calculated deflection of the circular sandwich structure to predict the maximum deflection of the annular sandwich structure.

$$Y_{max} = (0.0085/1.74) = 0.0049 \text{ in.}$$

Uniform Load Producing Calculated Deflection. Using Equation (2.2), the distributed load producing the computed deflection is calculated:

$$Y_{max} = 0.0049 = \frac{3w\ (m^2 - 1)}{16\ m^2\ E\ t^3}\ (12.47 \times 10^5)$$

Thus: $w = 4.9\ lb/in^2$

Calculation of Bending Stress Produced by Uniform Load. The bending stress at the outer edge of each annular plate can be readily calculated from the formula as given in Roark (Ref. 2):

$$S_{max} = \frac{3w}{4\ t^2}\left[a^2 - 2b^2 + \frac{b^4(m-1) - 4b^4(m+1)\ \ln a/b + a^2b^2\ (m+1)}{a^2\ (m-1) + b^2\ (m+1)}\right] \quad (2.7)$$

Thus: $S_{o_{max}} = 1040$ psi

In the same manner the bending stress at the inner edge can be found. From Roark (Ref. 2)

$$S_{max} = -\frac{3w\ (m^2-1)}{4\ mt^2}\left[\frac{a^4 - b^4 - 4a^2b^2\ \ln a/b}{a^2(m-1) + b^2(m+1)}\right] \quad (2.8)$$

Thus: $S_{i_{max}} = 495$ psi

2.3 Experimental Stress Analysis*

Since the validity of the assumption used in the theoretical analysis

* Nomenclature for analysis is defined on pp. 25

could not be verified readily, a quarter scale plexiglas II model was constructed. This enabled a direct measurement of stresses and deflections in the model, and the results were converted to stresses and deflections applicable to the Pathfinder grid plate by principles of similitude.

A comparison of significant characteristics of both the model and Pathfinder grid plate are given in Table 2.1.

TABLE 2.1 COMPARISON OF MODEL AND REACTOR GRID PLATE

Parameters	Reactor	Model
Material	304L SS	Plexiglas II
Operating Temperature, ^{o}F	489	72
Relative Linear Dimension, in.	1.0	0.250
Total Load, lb	33,600	Variable
Modulus of Elasticity, psi	25.5×10^6	0.480×10^6
Poisson's Ratio	0.317	0.35

The test apparatus used is shown in Figure 2.2. To insure uniform support along the periphery of the model, the model was seated in the support stand ring with plastic steel. A uniformly distributed load of 1860 lbs was imposed on the grid plate with an inflatable diaphragm. Dial indicators were mounted beneath the model at the locations shown in Figure 2.3. Corresponding reactor grid-plate deflections were calculated by the equation:

$$Y = \frac{1}{N} \cdot \frac{P}{P_M} \cdot \frac{E_M}{E} \cdot Y_M \qquad (2.9)$$

The model deflections measured and the grid-plate deflections calculated by Equation (2.9) are given in Table 2.2. Results indicate a deflection of 0.0029 in. in the reactor, which is within design limits. Since recirculation flow tends to reduce the total load, the value is conservative.

TABLE 2.2 DEFLECTION IN MODEL AND REACTOR GRID PLATE

Location	Model Deflection (in.)	Predicted Reactor Deflection (in.)
1	0.0263	0.00223
2	0.0240	0.00204
3	0.0006	0.00005
4	0.0247	0.00209
5	0.0066	0.00056
6	0.0136	0.00115
7	0.0146	0.00124
8	0.0336	0.00287

Upon completion of the deflection test, a stress analysis program was conducted to determine the magnitude and location of the maximum circumferential and radial stresses. A stress-coat analysis was made to determine the direction of principle stresses in the model. No attempt was made to obtain quantitative results from the stress-coat, because strain gages were used to obtain this data. Stress-coat ST 1207 was applied to the model according to standard procedures.

Thin cellophane sheets were placed over a one-eighth segment of the stress-coated model, and the stress trajectories were traced with pen and ink. These cellophane sheets were used to lay out the strain-gage locations and also to check the gage orientation after placement.

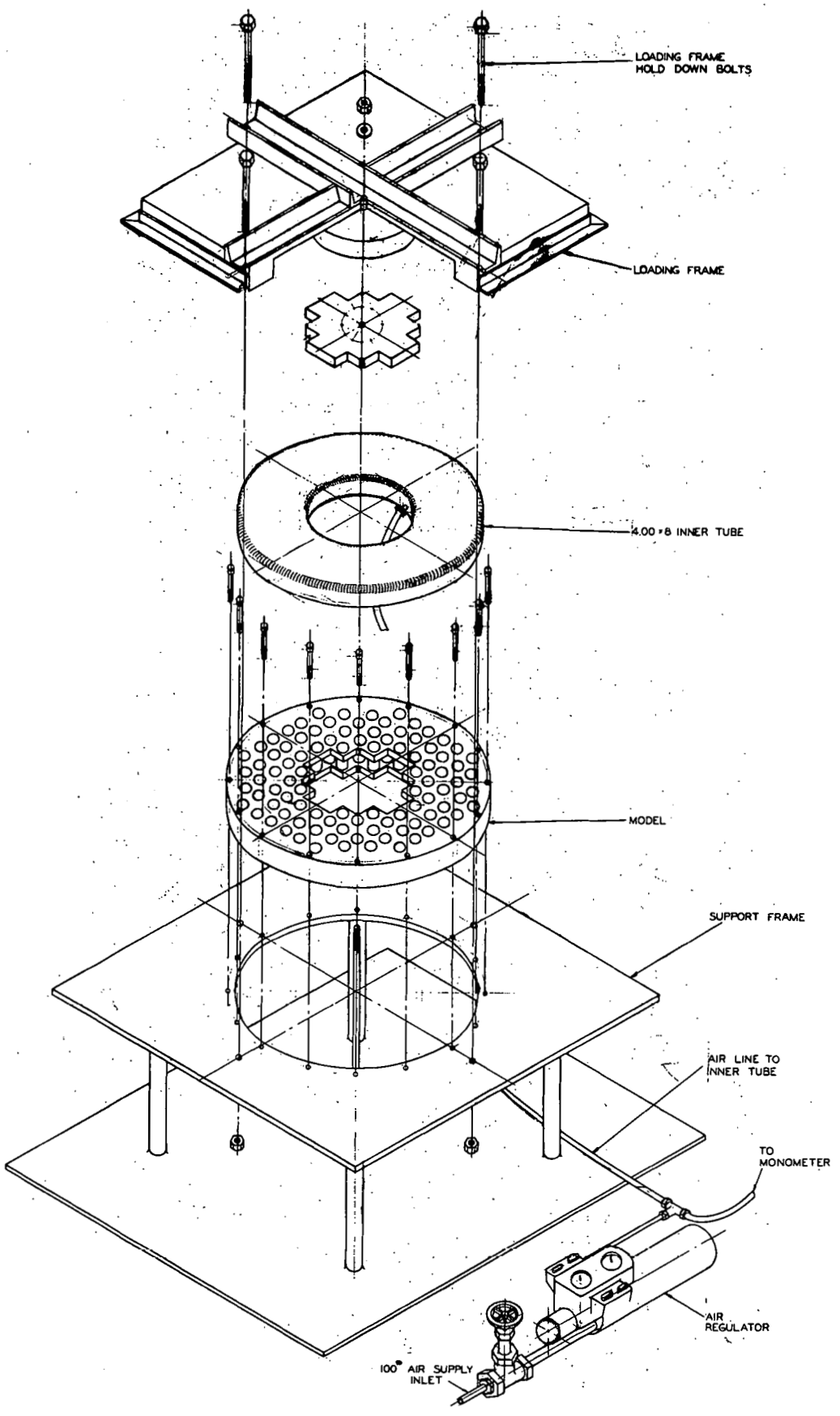

Figure 2.2 - Grid-Plate Load Test Rig (43-401-069)

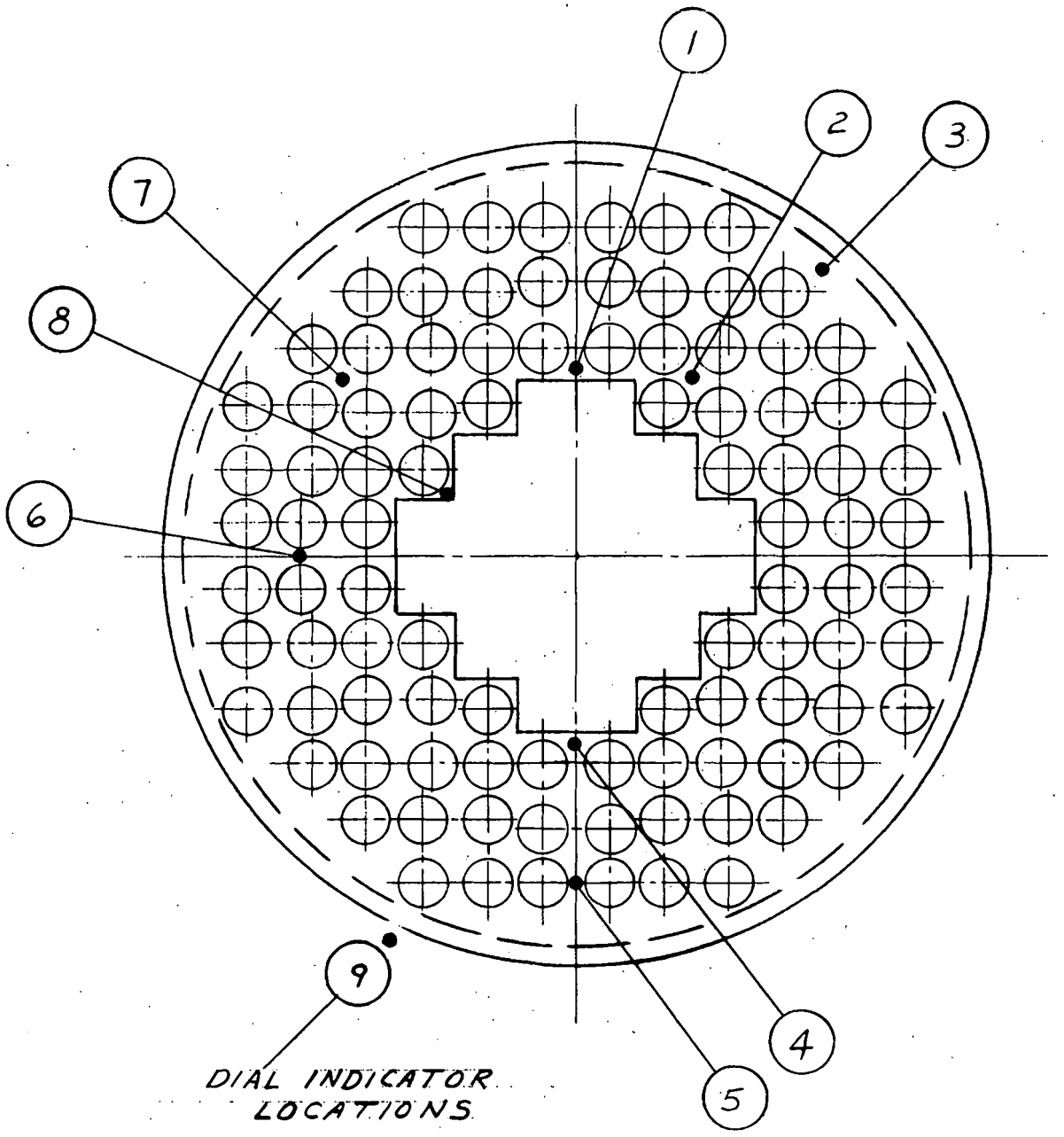

Figure 2.3 - Grid-Plate Dial Indicators Locations (43-024-174)

Because of model size, it was not practical to place two strain-gage rosettes at many of the points where stress values were desired. In narrow regions, foil gages with a 1/32 in. gage length were the largest gages that would fit. To put one gage on top of another was impossible because of interference with the soldered lead-wire connections. Since stress is a linear function of the load on the model, it was decided to place one set of single gages in one principle stress direction, load the model, and obtain all strain readings. Then remove all the gages and place the orthogonal set in the same location and load again to the same value.

The 1/32 in. foil gages were bonded to the model with Eastman 910 cement and moisture-proofed with TATNAL GW-1 moisture-proofing compound. Type A-18 wire gages were bonded with Duco cement. A thin layer of Duco smeared over the installation was used for moisture proofing.

Five foil rectangular rosettes were located on the shear tubes. These rosettes were placed on the tubes before assembly of the model. One rosette was destroyed during fabrication.

A 20-channel Ellis switch-and-balance unit and an Ellis BAM-1 strain indicator were used to make the strain measurements. Since the plastic model was sensitive to temperature changes the entire test stand was placed in a draft-free enclosure. The usual problem of gage heating due to the poor thermal conductivity of the plastic material was no

problem with the Ellis strain indicator. Since the gain control regulates the power to the bridge, it was only necessary to adjust the gain to a value low enough that no significant drift occurs. With this procedure, it was possible to use only one A-18 gage mounted on a separate piece of plastic to compensate for all A-18 gages on the model. Only one foil compensating gage was used for all the foil gages.

The model was loaded by pressurizing the inflatable diaphragm slowly until 17 in. of mercury was reached. With mercury pressure at 17 in. and a total applied load of 1570 lbs on the grid plate model, the principle stresses were computed from the measured principle strains by the equation:

$$\sigma_{12} = \frac{E}{1 - \nu^2} (\epsilon_{12} + \nu \epsilon_{21}) \qquad (2.10)$$

Table 2.3 is a summary of the stresses referring to the gage locations in Figure 2.4.

A plot of the circumferential and radial stresses along the line of symmetry $X - X^1$ is shown in the isometric sketch, Figure 2.5.

The maximum stress developed in the model (Table 2.3) is a circumferential stress of 498 psi. The corresponding reactor grid-plate stress was calculated as follows:

$$S = 1/(N)^2 \quad (P/P_M)\ S_M$$

$$S = 654 \text{ psi}$$

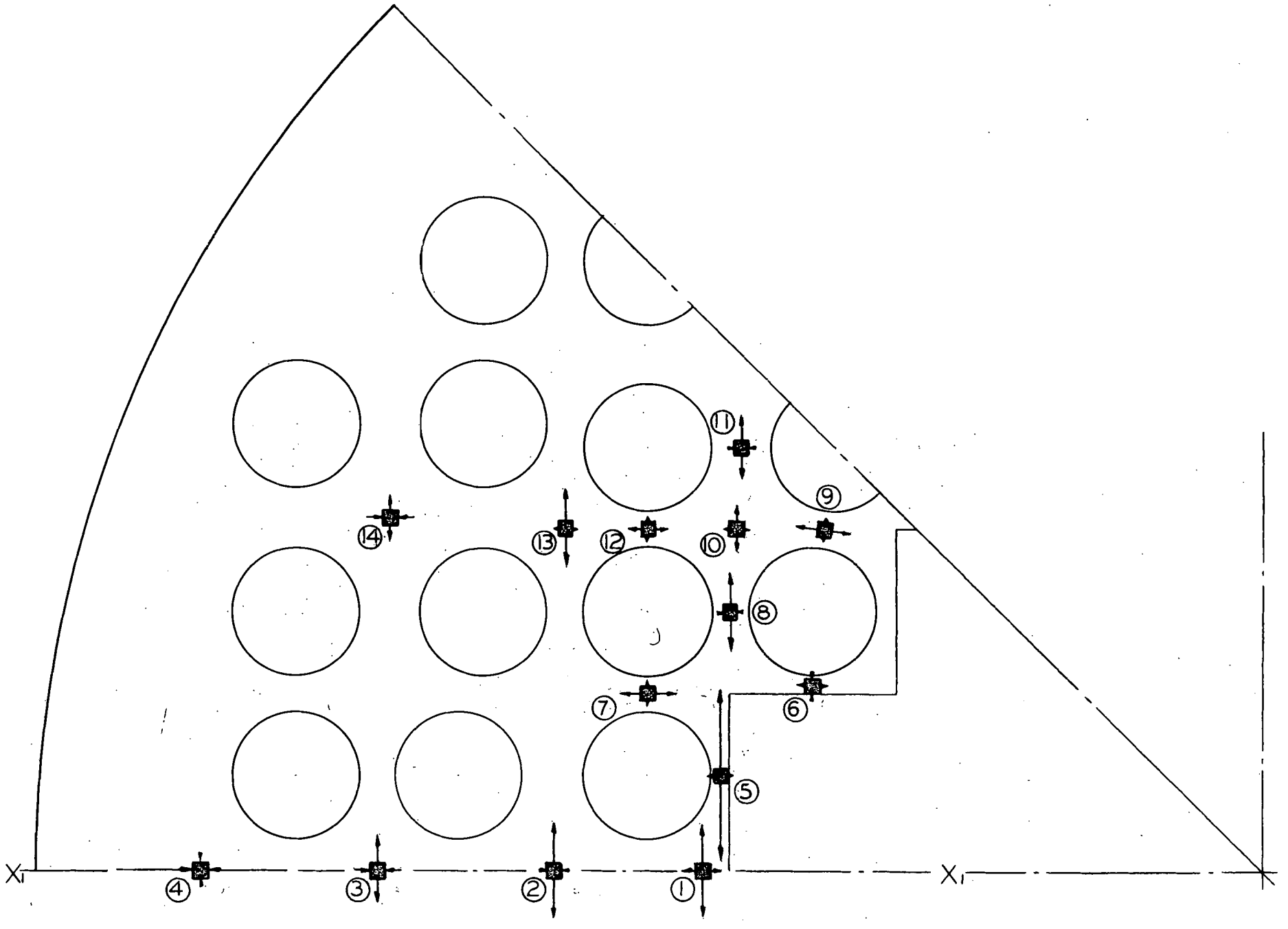

Figure 2.4 - Strain Gages Locations on Bottom Surface of Grid-Plate (43-024-126 PS)

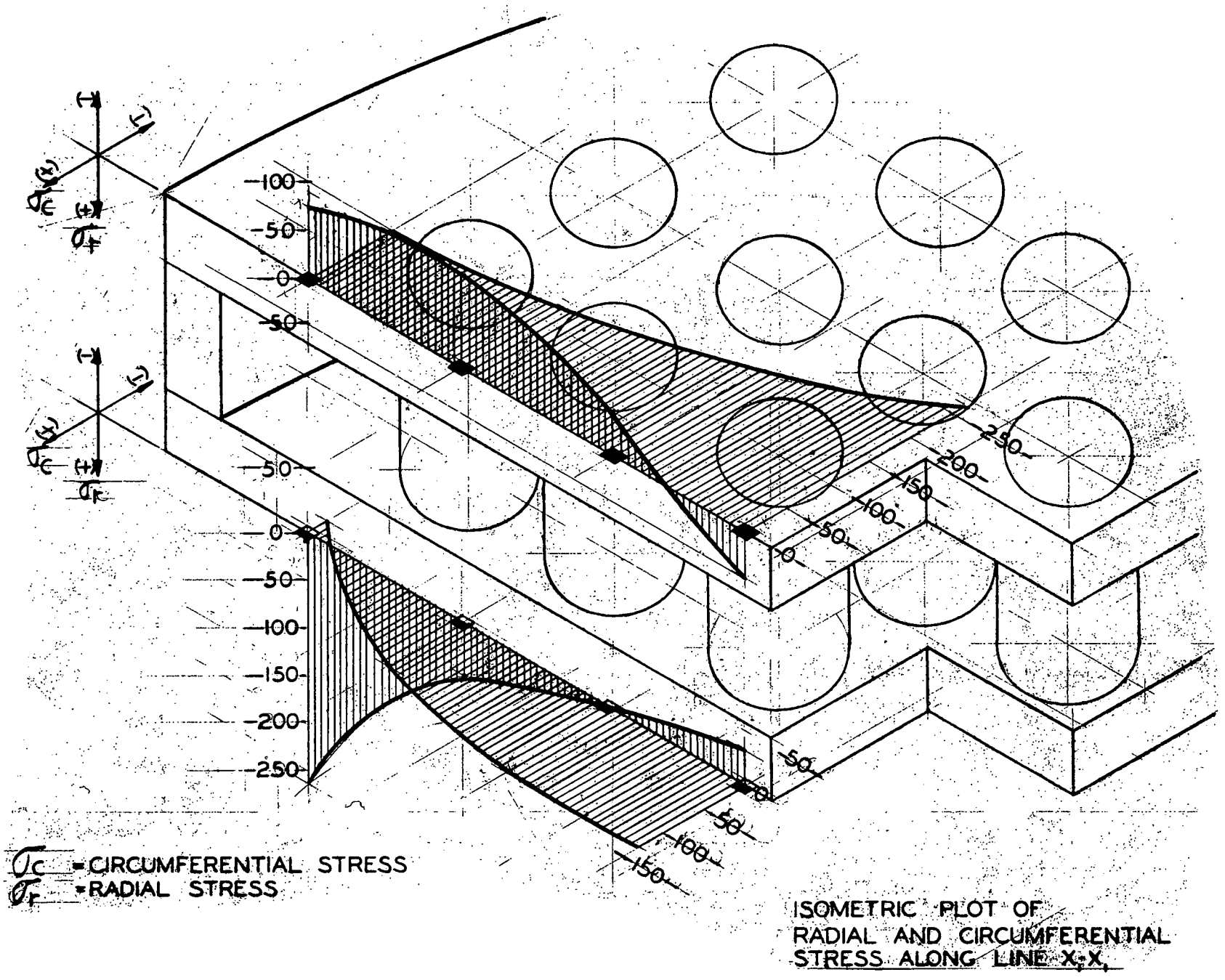

Figure 2.5 - Isometric Plot of Radial and Circumferential Stress along Line X-X of Grid-Plate (43-024-125 PS)

TABLE 2.3 PRINCIPLE STRESS IN GRID PLATE MODEL

Gage Location*	Top Surface σ_c	Top Surface σ_r	Bottom Surface σ_c	Bottom Surface σ_r
1	-268	-50	130	33
2	-186	43	131	-1
3	-123	106	92	-56
4	-104	79	-262	-24
5	-498	-15	244	12
6	-53	-16	20	-11
7	-271	-213	65	12
8	-231	-24	108	-7
9	-139	-49	69	1
10	-129	-58	54	13
11	----	----	71	-9
12	-63	32	33	12
13	-149	-28	91	6
14	-89	29	56	-50

*Strain gage location refers to positions indicated on Figure 2.4.

2.4 Thermal Stress Analysis

Thermal Stress in the Grid Plate Due to γ Heating. γ-ray absorption within the top plate of the sandwich structure produces non-uniform heating. A typical temperature plot is shown in Figure 2.6.

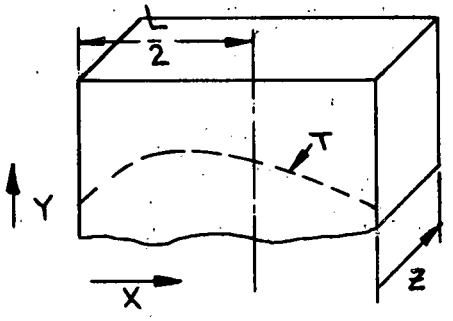

Figure 2.6 Plot of Temperature Distribution through Top Plate of Grid Structure.

The horizontal thermal expansion, αT, is suppressed by applying to each element the compressive stress:

$$\sigma_y = -\alpha T E \tag{2.12}$$

The tensile forces in the beam due to heating have the resultant:

$$\Sigma F_T = \int_o^L T E \, dx \tag{2.13}$$

For a thin slab (z is small) and at a distance (x) from the ends of the slab, the distributed tensile stress is:

$$\sigma_T = \frac{1}{L} \int_o^L \alpha T E \, dx \tag{2.14}$$

The stress in the slab can be obtained by superimposing the tensile and compressive stresses for the case where the temperature distribution is symmetrical:

$$\sigma = \frac{1}{L} \int_o^L \alpha T E \, dx - \alpha T E \tag{2.15}$$

In the case of γ heating, the temperature distribution is not symmetrical. Therefore, in addition to Equation (2.15), a couple is formed which must be resisted by forces within the slab, thus giving rise to bending stresses. The bending stresses are proportional

to the distance from the neutral plane. The moment developed by these stresses is:

$$M = \frac{I\sigma}{L/2 - X} \tag{2.16}$$

The resultant couple formed by non-symmetrical temperature distribution is given by:

$$M = \int_o^L \alpha E T (L/2 - X)\, dx \tag{2.17}$$

To satisfy equilibrium:

$$\frac{I\sigma}{L/2} - \int_o^L \alpha E T (L/2 - X)\, dx = 0$$

or:

$$\frac{\sigma}{L/2} = \frac{12}{L^3} \int_o^L \alpha E T (L/2 - X)\, dx \tag{2.18}$$

The bending stress at any point X is:

$$\sigma_y = \frac{12 (L/2 - X)}{L^3} \int_o^L \alpha E T (L/2 - X)\, dx$$

or:

$$\sigma_y = \frac{6 (L - 2X)}{L^3} \int_o^L \alpha E T \frac{(L - 2X)}{2}\, dx \tag{2.19}$$

The total stress at a point X in a thin slab is given by:

$$\sigma_T = -\alpha T E + \frac{1}{L} \int_o^L \alpha T E\, dx$$

$$+ \frac{6(L - 2X)}{L^3} \int_o^L \alpha E T \frac{(L - 2X)}{2}\, dx \tag{2.20}$$

The grid plate is not thin in the z direction, and the mean value of T is not zero, therefore, Eq. (2.20) must be modified as follows:

$$\sigma_y = \sigma_z = -\frac{\alpha T E}{1-\nu} + \frac{1}{L(1-\nu)}\int_o^L \alpha T E \, dx$$

$$+ \frac{6(L-2X)}{(1-\nu)L^3}\int_o^L \alpha E T \frac{(L-2X)}{2} dx \qquad (2.21)$$

The temperature, $T_{(X)}$, is expressed by:

$$T_{(X)} = \frac{Q_o}{K\mu^2}\left[(e^{-\mu L}-1)\frac{X}{L} - e^{-\mu X} + 1\right]$$

(See Eq. (2.27) for derivation)

Substituting in Eq. (2.21):

$$\sigma_y = \sigma_z = -\frac{\alpha E}{1-\nu}\left(\frac{Q_o}{K\mu^2}\right)\left[(e^{-\mu L}-1)\frac{X}{L} - e^{-\mu X} + 1\right]$$

$$+ \frac{\alpha E}{L(1-\mu)}\left(\frac{Q_o}{K\mu^2}\right)\int_o^L \left[(e^{-\mu L}-1)\frac{X}{L} - e^{-\mu L} + 1\right] dx$$

$$+ \frac{6(L-2X)}{(1-\nu)L^3}\left(\frac{Q_o \alpha E}{K\mu^2}\right)\int_o^L \left[(e^{-\mu L}-1)\frac{X}{L} - e^{-\mu X} + 1\right]$$

$$\left[\frac{L-2X}{2}\right] dx \qquad (2.22)$$

Performing the required integration:

$$\sigma_y = -\frac{\alpha E}{1-\nu}\left(\frac{Q_o}{K\mu^2}\right)\left[(e^{-\mu L}-1)\frac{X}{L} - e^{-\mu X} + 1\right]$$

$$+\frac{\alpha E}{L(1-\nu)}\left(\frac{Q_o}{K\mu^2}\right)\left[e^{-\mu L}\left(\frac{L}{2}+\frac{1}{\mu}\right)+\frac{L}{2}-\frac{1}{\mu}\right]$$

$$+\frac{6(L-2X)}{(1-\nu)L^3}\left(\frac{Q_o\,\alpha E}{K\mu^2}\right)\left\{\frac{L}{2}\left[e^{-\mu L}\left(\frac{L}{2}+\frac{1}{\mu}\right)+\frac{L}{2}-\frac{1}{\mu}\right]\right.$$

$$\left.-\left[(e^{-\mu L}-1)\frac{L^2}{3}+\frac{e^{-\mu L}}{\mu^2}(1+\mu L)+\frac{L^2}{2}-\frac{1}{\mu^2}\right]\right\} \qquad (2.23)$$

Thus:

$$\sigma_y = \left(\frac{\alpha E}{1-\nu}\right)\left(\frac{Q_o}{K\mu^2}\right)\left\{-\left[(e^{-\mu L}-1)\frac{X}{L} - e^{-\mu X} + 1\right]\right.$$

$$+\frac{1}{L}\left[e^{-\mu L}\left(\frac{L}{2}+\frac{1}{\mu}\right)+\frac{L}{2}-\frac{1}{\mu}\right]$$

$$+\frac{6(L-2X)}{L^3}\left(\frac{L}{2}\left[e^{-\mu L}\left(\frac{L}{2}+\frac{1}{\mu}\right)+\frac{L}{2}-\frac{1}{\mu}\right]-\left[(e^{-\mu L}-1)\frac{L^2}{3}\right.\right.$$

$$\left.\left.\left.+\frac{e^{-\mu L}}{\mu^2}(1+\mu L)+\frac{L^2}{2}-\frac{1}{\mu^2}\right]\right)\right\} \qquad (2.24)$$

Figure 2.7 illustrates the distribution of thermal stresses in the top grid plate due to γ heating.

Temperature Distribution in Grid Plate. To obtain an expression for the temperature at any point through the plates, the following derivation is made:

Volumetric Heat Source (Ref. 3)

$$Q = Q_o e^{-\mu_e X} \tag{2.25}$$

$$-K\frac{d_2T}{dx^2} = Q_o e^{-\mu_e X} \tag{2.26}$$

Thus:

$$T = -\frac{Q_o}{K\mu^2} e^{-\mu_e X} + C_1 X + C_2$$

If a case where T = 0 and X = 0 is assumed

$$C_2 = \frac{Q_o}{K\mu^2}$$

Similarly, for a case where T = 0 and X = L

$$C_1 = \frac{Q_o}{LK\mu^2} e^{-\mu L} - \frac{Q_o}{LK\mu^2}$$

Thus:

$$T = \frac{Q_o}{K\mu^2}\left[(e^{-\mu L} - 1)\frac{X}{L} - e^{-\mu_e X} + 1\right] \tag{2.27}$$

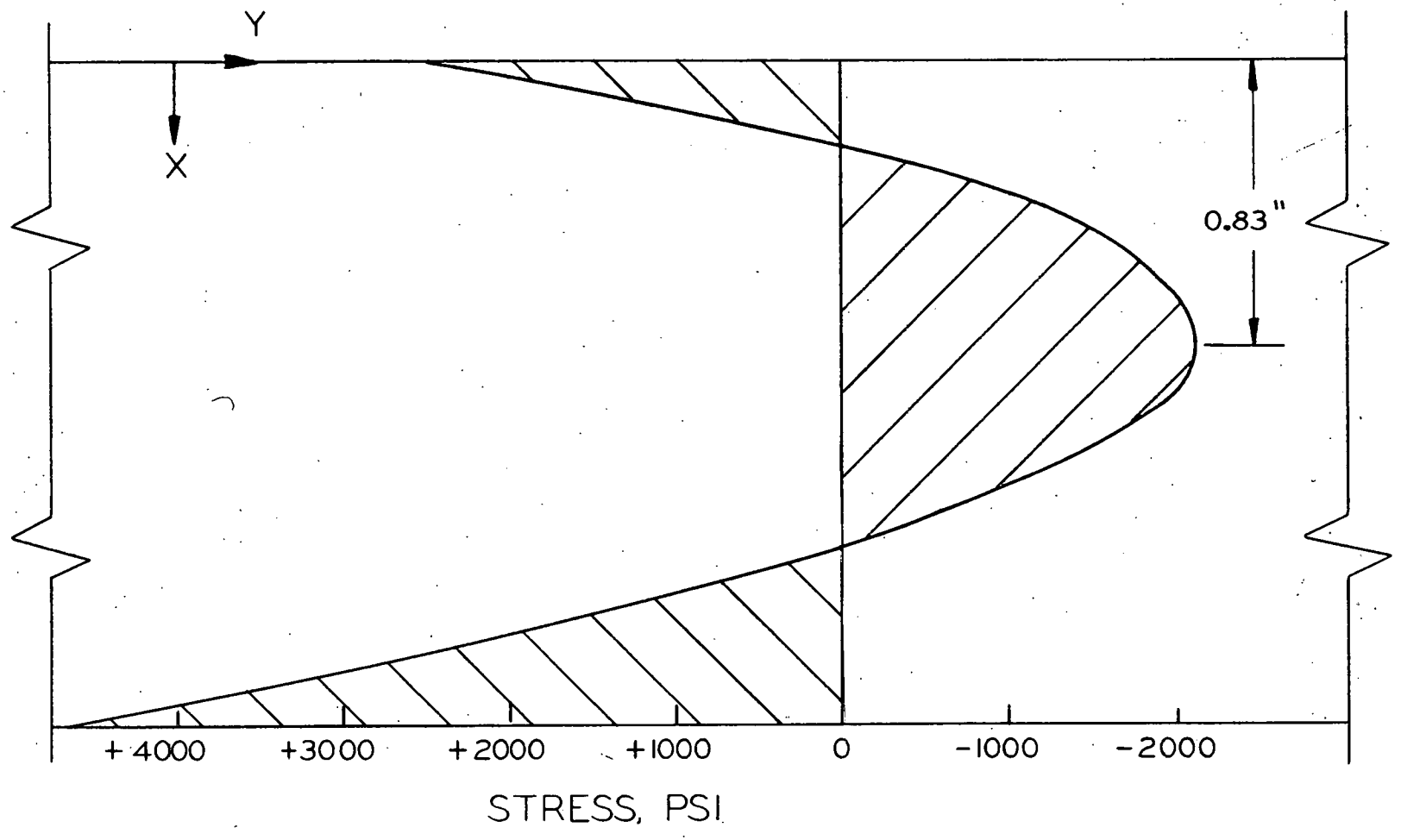

Figure 2.7 - Distribution of Thermal Stress Due to γ Heating in Top Plate of Grid Structure (43-025-156)

NOMENCLATURE - BOILER CORE GRID PLATE

a = Outside radius of circular or annular plate, in

b = Inner radius of annular plate, in

C = Core layer thickness, in

D = Flexural rigidity of sandwich structure, lb - in

D_x = Flexural rigidity of perforated sandwich structure, lb - in

E = Modulus of elasticity, psi

E_f = Modulus of elasticity, face layer, psi

G_c = Shear modulus, core layer, psi

I = Moment of inertia, in^4

K = Thermal conductivity Btu-ft/hr - ft^2

L = Length, in

M = Bending moment, lb-ft

m = Reciprocal of V, Poisson's ratio

N = Length scale

n_s = Ligament efficiency

n_w = Deflection efficiency

P = Load, lb

Q_o = Volumetric heat generation rate, Btu/ft^3 - hr

q = Normal load intensity, lb/in^2

S = Stress, psi

T = Temperature, ^oF

t = Thickness of plate

t_1 = Top plate thickness, in

t_2 = Bottom plate thickness, in

ν = Poisson's ratio

w = Unit load applied, lb/in^2

Y = Deflection, in

Y_o = Deflection neglecting shear deformation, in

α = Coefficient of thermal expansion, $in/in-^oF$

γ = Gamma ray

ϵ = Strain, in/in

μ = Absorption coefficient for gamma rays, in^{-1}

σ = Stress, psi

Subscripts

M = Model

X = x direction

Y = y direction

Z = z direction

3.0 BOILER CORE SHROUD (SEE FIGURE 3.1)

The boiler core shroud supports the fuel-element hold-down structure, and separates the annular downcomer region from the boiler core.

The Pathfinder boiler core shroud is cylindrical in shape and completely encloses the outer periphery of the core. The top and bottom plates are machined on the inside to fit the core configuration. The boiler shroud is 89 in. high and 79 in. in diam. Rigidity of the structure is maintained by suitable structural angles and gusset plates.

3.1 Experimental Stress Analysis

During reactor operation, fluid-friction forces in the core are transferred to the shroud by the fuel-element hold-down structure. To determine the effect of these forces, a quarter-scale Plexiglas model of the shroud was fabricated.

The loading on the model was supplied by a hydraulic jack and measured with a pressure gage. The stresses in the model were measured by stress coat analysis. Predicted stresses in the shroud were determined from the equation:

$$\sigma_A = \frac{\sigma_M}{N^2} \frac{(P_A)}{P_M} \qquad (3.1)$$

Where: σ_A = actual stress, psi
σ_M = model stress, psi
P_A = actual load on shroud, lbs
P_M = load on model, lbs
N = scale length factor

The maximum stress developed in the boiler core shroud was calculated to be 4400 psi, well within the limits for 304 Stainless Steel.

4.0 FUEL ELEMENT HOLD-DOWN ASSEMBLY (SEE FIGURE 4.1)

The fuel-element hold-down assembly retains the boiler fuel elements against the hydraulic forces developed by the water flowing upward through the core. Through the use of control rod guide channels, which surround each control rod in the boiler core, the hold-down assembly prevents the coolant flow from exerting lateral forces on the control rods as it flows across the core to enter the downcomer region. A flow deflector is attached to the guide tubes to break up steam channels that may be formed at the exit of the boiler fuel elements.

The grid structure of the hold-down assembly consists of a lattice of interlocking rectangular plates joined to a flange ring. The plates are slotted to form an interlocking junction with each other.

All theoretical and experimental stress analyses are based on the assumption that the vertical forces acting on the hold-down assembly are resisted only by the grid structure.

4.1 Theoretical Stress Analysis*

The investigation of the mechanical stresses present in the fuel-element hold-down assembly was accomplished in the following manner:

* Nomenclature for this section is given on pp. 53

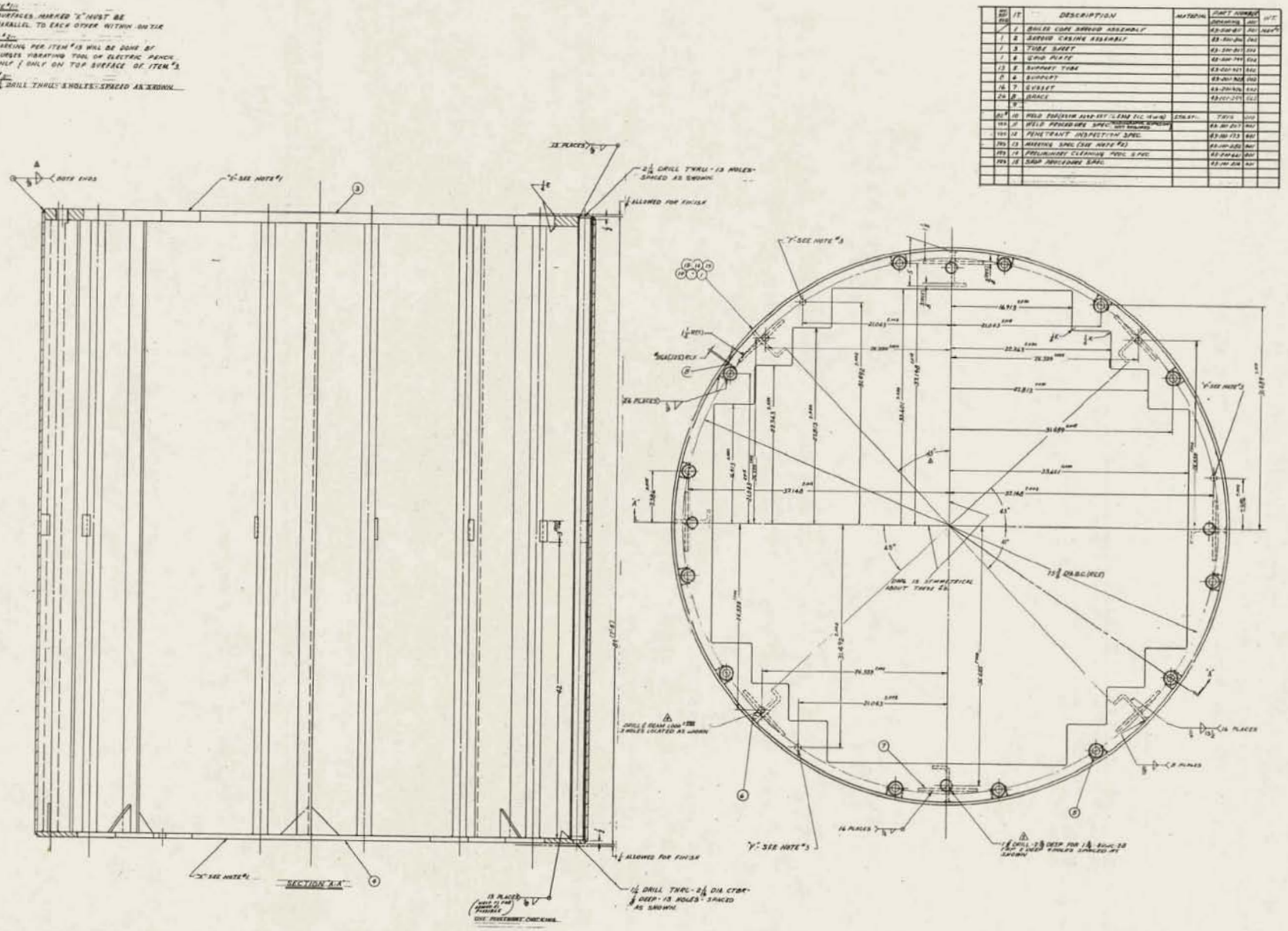

Figure 3.1 - Boiler Core Shroud Assembly (43-500-811)

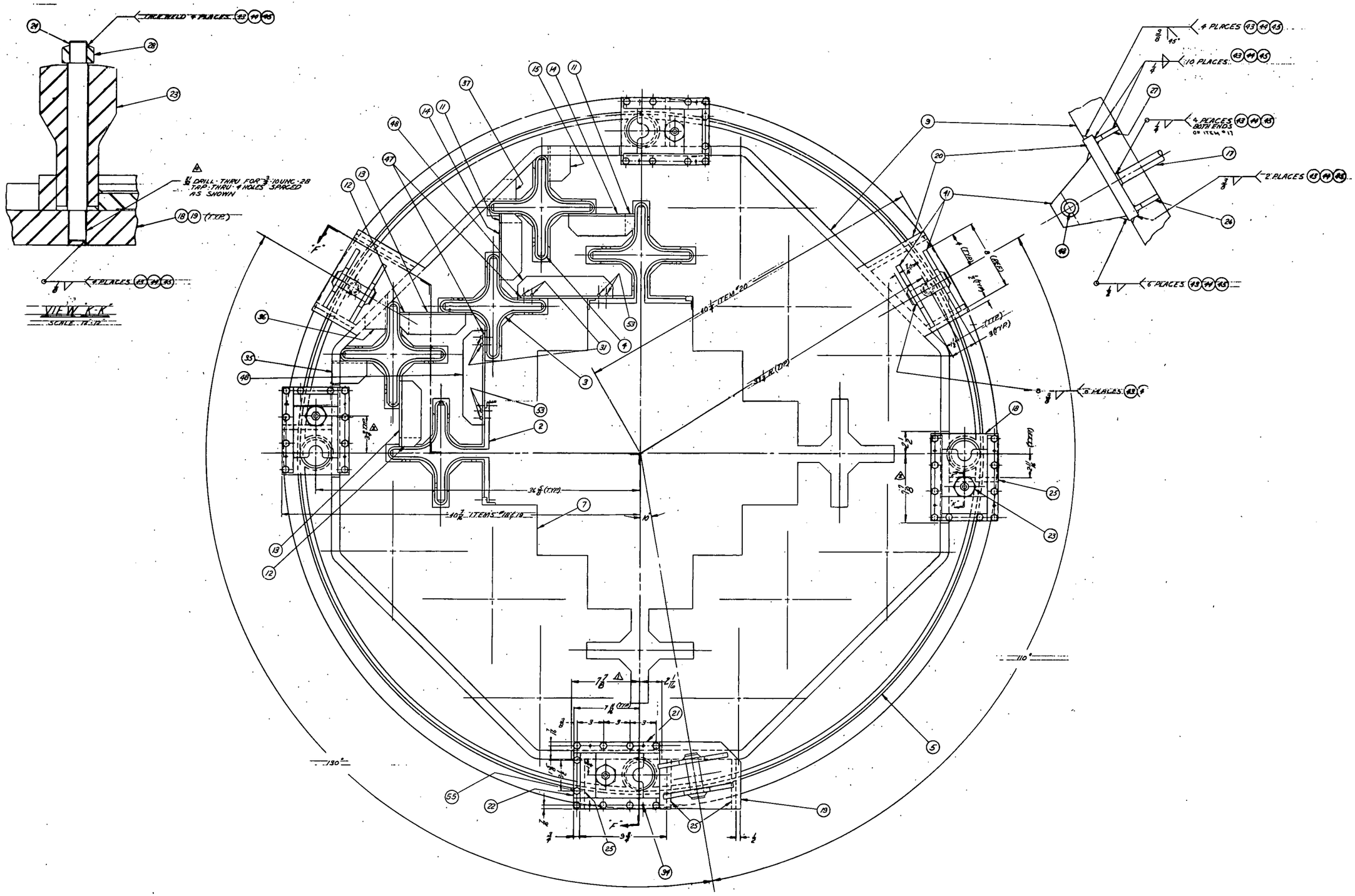

Figure 4.1 - Fuel Element Hold-Down Assembly (Sheet 1 of 4) (43-500-974)

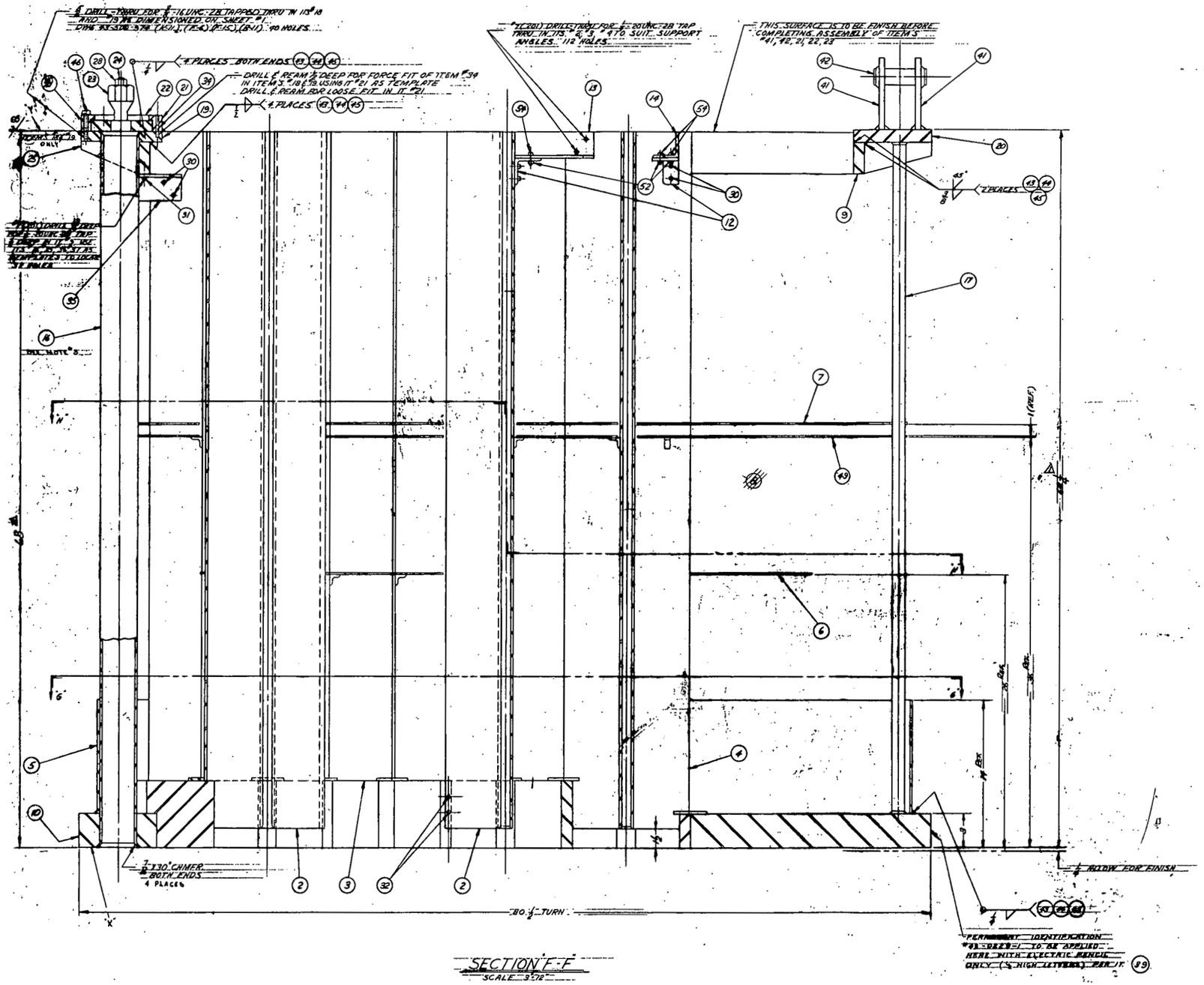

MK SOL REQ	ITEM	DESCRIPTION	MATERIAL	PART NUMBER DRAWING	MK	WT.
1	1	HOLD DOWN ASSEMBLY		43-500-974	501	1900 #
1	2	INNER GUIDE TUBE ASSEMBLY		43-401-265	501	
1	3	INTERMEDIATE GUIDE TUBE ASSEMBLY		43-401-264	501	
8	4	OUTER GUIDE TUBE ASSEMBLY		43-401-263	501	
1	5	BAFFLE		43-301-257	502	
1	6	LOWER BAFFLE		43-300-996	502	
1	7	BAFFLE PLATE (UPPER)		43-500-995	502	
~~308~~	~~8~~	~~BAFFLE SUPPORT~~		~~43-303-285~~	~~502~~	
1	9	OCTAGON SUPPORT ASSEMBLY		43-501-007	503	
1	10	BASE PLATE ASSEMBLY		43-500-973	501	
9	11	SUPPORT ANGLE (L.W.)		43-202-293	502	
8	12	SUPPORT ANGLE (L.M.)		43-202-299	502	
8	13	SUPPORT ANGLE (A.M.)		43-202-294	502	
8	14	SUPPORT ANGLE (L.R.)		43-202-300	502	
4	15	SUPPORT ANGLE (L.W.)		43-202-301	502	
4	16	SLEEVE		43-202-237	502	
2	17	SUPPORT PIPE		43-202-308	502	
3	18	PLATE		43-202-312	502	
1	19	LIFTING PLATE		43-202-310	502	
2	20	LIFTING PLATE		43-202-311	502	
8	21	GUIDE BAR		43-202-250	502	
4	22	STOP		43-202-262	502	
4	23	SLIDE ASSEMBLY		43-301-783	501	
4	24	STUD		43-202-313	502	
6	25	GUSSET		43-202-309	502	
2	26	GUSSET		43-202-305	504	
2	27	GUSSET		43-202-306	506	
4	28	3/8-16UNC-2B KKV SEMIFINISH HEX. NUT		43-101-368	112	
180	29	3/8-16UNC-3A X 1 LG. KKV SOCKET CAP SCREW		43-MA-981	963	
112	30	1/2-20UNC-3A X 1 LG. NPT SOC. HD. CAP SCREW		43-101-381	971	
48	31	5/8-18UNC-3A X 1 LG. HEX SOC. HD. CAP SCREW		43-101-381	328	
16	32	5/8-11UNC-3A X 1 LG. SLOTTED FLAT HD. CAP SCREW		42-101-496	965	
60	33	PIN		43-701-499	379	
14	34	PIN		43-701-984	321	
4	35	SUPPORT ANGLE (R.W.)		43-202-250	506	
4	36	SUPPORT ANGLE (R.M.)		43-202-291	502	
4	37	SUPPORT ANGLE (L.M.)		43-202-302	502	
VAR.	38	FINAL CLEANING SPEC.		43-201-167	901	
VAR.	39	MARKING SPEC.		43-301-282	901	
VAR.	40	FABRICATION PROCEDURE SPEC.		43-101-216	901	
6	41	LUG		43-301-816	502	
9	42	PIN		43-202-296	502	
VAR.	43	WELDING PROCEDURE SPEC.		43-101-367	901	
10	44	WELD ROD ASTM A298-SST CLE 308	MEM 119	DNAS	0999	
VAR.	45	ZYVID PENETRANT INSPEC. SPEC.		43-MA-783	901	
32	46	3/4-10UNC-2A X 1 1/2 LG. NPT STAINLESS HEX BOLT		43-101-378	965	
8	47	SHIM		43-202-298	502	
8	48	SUPPORT ANGLE		43-249-332	502	
1	49	BAFFLE PLATE (INTERMEDIATE)		43-300-995	502	
78	50	SPACER		43-202-600	502	
78	51	1/2-20UNC-3A X 1 1/2 LG. REG. SF. HEX. BOLT		43-101-378	965	
148	52	1/2-20UNC-3B NYL. S.F. HEX. NUT		43-706-376	106	
16	53	1/4-20UNC-3A X 1 1/2 LG. HEX. SOC. HD. CAP SCREW		43-101-381	973	
32	54	1/2-20UNC-3A X 1 LG. HEX. SOC. HD. CAP SCREW		43-101-381	328	
8	55	5/8-11UNC-2A X 1 3/4 LG. HEX. S.F. HEX. BOLT		43-101-378	965	

NOTE 3:
CENTERLINES OF ITEM'S 1, 3, 5, AND 10 MUST BE PERPENDICULAR TO SURFACE MARKED "A" WITHIN .02" T.I.R.

NOTE 4:
SURFACES MARKED "B" MUST BE PARALLEL WITHIN .015 T.I.R.

Figure 4.1 - Fuel Element Hold-Down Assembly (Sheet 2 of 4) (43-500-974)

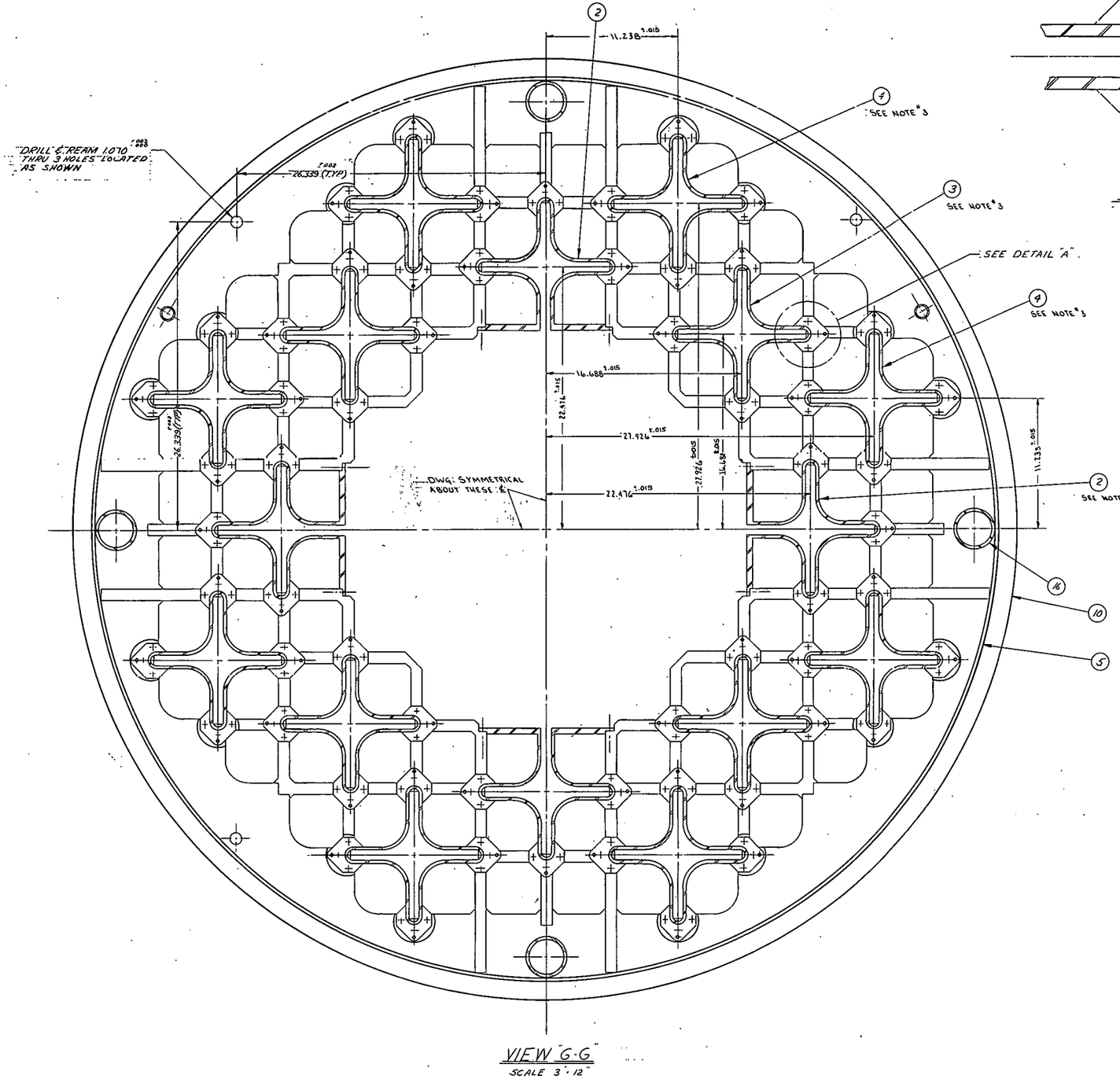

VIEW "G-G"
SCALE 3 : 12

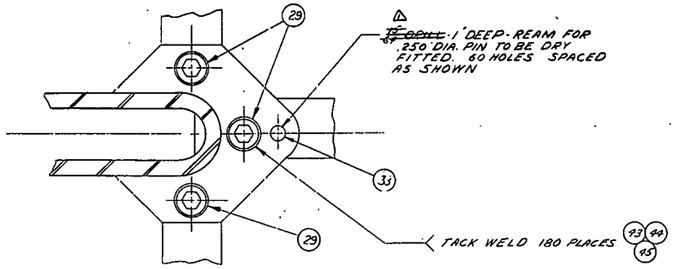

DETAIL "A"
SCALE 12 : 12

Figure 4.1 - Fuel Element Hold-Down Assembly (Sheet 3 of 4) (43-500-974)

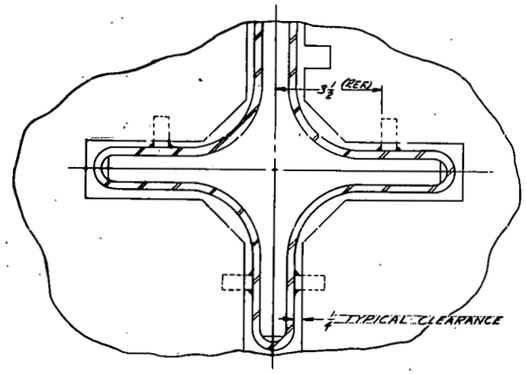

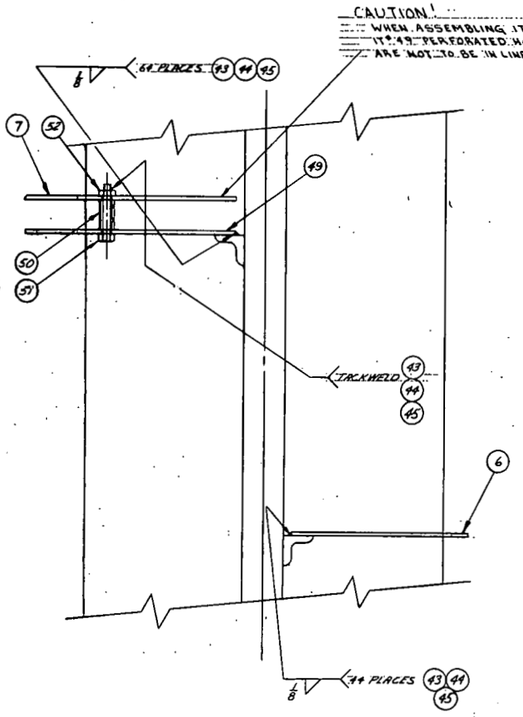

VIEW "J-J"
SCALE 6:12

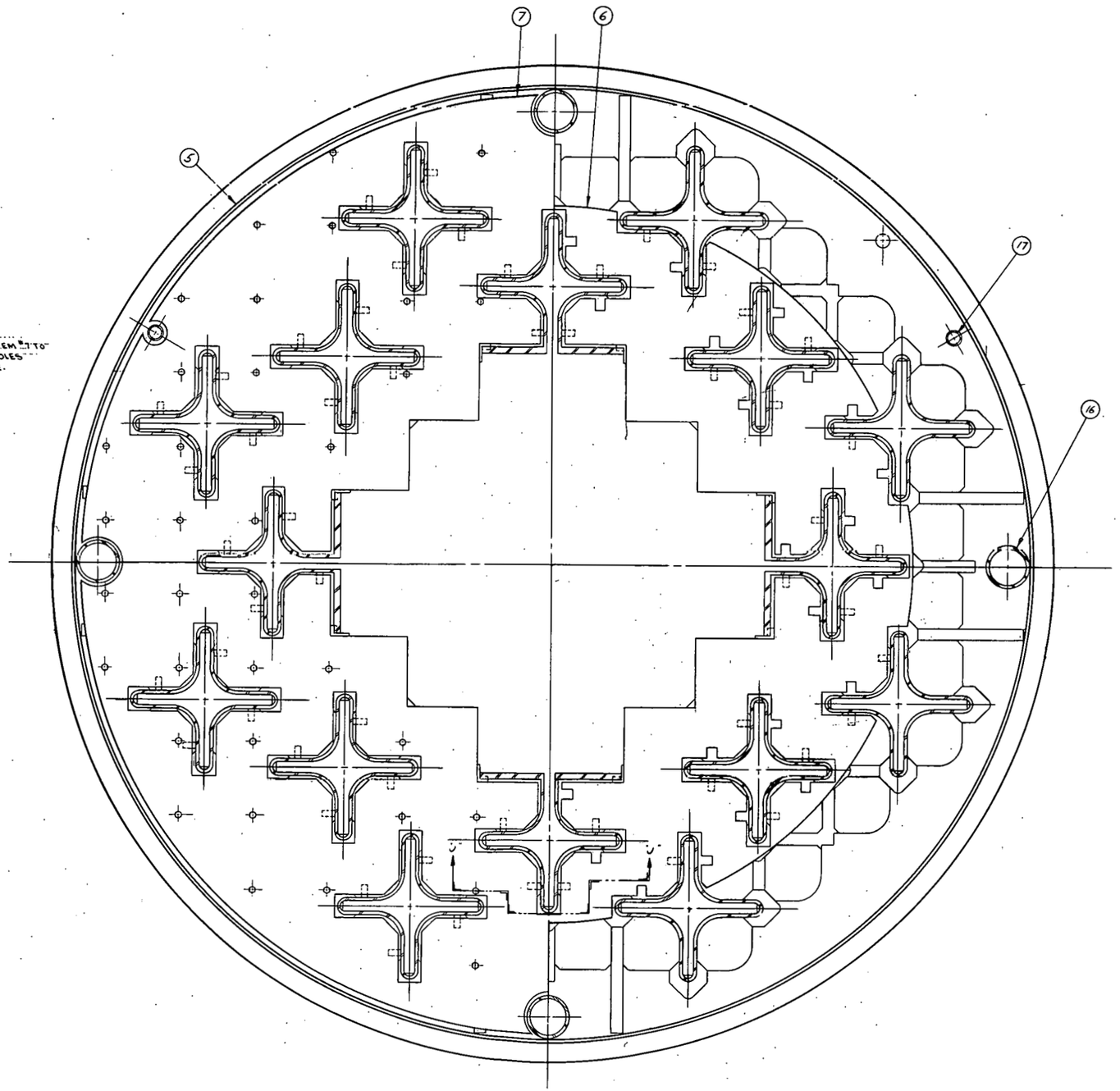

VIEW "H-H"
SCALE 3:12

Figure 4.1 - Fuel Element Hold-Down Assembly (Sheet 4 of 4) (43-500-974)

1. An elastic energy analysis was performed on the lattice plates of the grid structure.
2. An elastic energy analysis was performed on the hold-down flange ring.

Elastic Energy Analysis of Lattice Plates. Each quarter segment of the hold-down assembly is geometrically identical. Also, the loading on each half of a quarter segment is identical. Thus, only a one-eighth segment of the grid structure is analyzed for mechanical stress. The location of the load applied by each fuel element box is shown in Figure 4.2.

In the elastic energy analysis, the following assumptions have been made:

1. Load acting at point 4 is transferred to point 1 as a load and moment.
2. Load acting at point 11 is transferred to point 7 as a load and moment.
3. Load acting at point 12 is transferred to point 8 as a load and moment.
4. Plate between point 4 and point 5 will not restrict the deflection or rotation of the structure at point 5.
5. Plate between point 6 and point 9 will not restrict the deflection or rotation of the structure at point 9.

The grid section shown in Figure 4.3 was analyzed as follows:

Analysis 1 - A vertical auxiliary load F is applied at point C. The

beam is cantilevered off point A.

The elastic-energy equation for the work done by Force F is:

$$F\,\Delta = \int_o^L \frac{m\,M\,dx}{EI} + \int_o^L \frac{t\,T\,dx}{GJ} \tag{4.1}$$

Since the deflection, Δ, at the restraint is zero, the work due to F is zero. Thus:

$$0 = \int_o^x \frac{F\,x\,M\,dx}{EI} + \int_o^y \frac{F\,y\,M\,dy}{EI} - \int_o^y \frac{F\,L_3\,T\,dy}{GJ} \tag{4.2}$$

Performing the necessary integration:

$$0 = \left\{\left(\frac{R_c\,L_3^3}{3}\right) - \left(\frac{M_c\,L_3^2}{2}\right) - \left(\frac{P(L_a + L_b)^2}{2}\left[L_1 + \frac{2(L_a + L_b)}{3}\right]\right)\right.$$

$$\left. - \left(\frac{3P\,L_b^2}{4}\left[L_2 + \frac{2L_b}{3}\right]\right)\right\} + \left\{\left(\frac{L_5^2}{2}\left[T_c - \frac{PL}{2}\right]\right) - \left(\frac{PL\,L_5^2}{2}\right)\right.$$

$$\left. - \left(\frac{2P\,L_5^3}{3}\right) - \left(\frac{L_5^3}{3}\left[\frac{5P}{2} - R_c\right]\right) - \left(\frac{PL_4^2}{2}\left[L_c + \frac{2L_4}{3}\right]\right)\right\}$$

$$- \left\{\frac{EI}{GJ}\,L_3\left[L_5\left(M_c + P\,[L_a + L_b] + \frac{3P\,L_b}{2} - R_c\,L_3\right)\right]\right\} \tag{4.3}$$

Substitution yields:

$$0 = 8655\,R_c - 556\,M_c + 60.5\,T_c - 6{,}233{,}000 \tag{4.4}$$

Analysis 2 - An auxiliary moment m is applied at point C. The beam is cantilevered off point A.

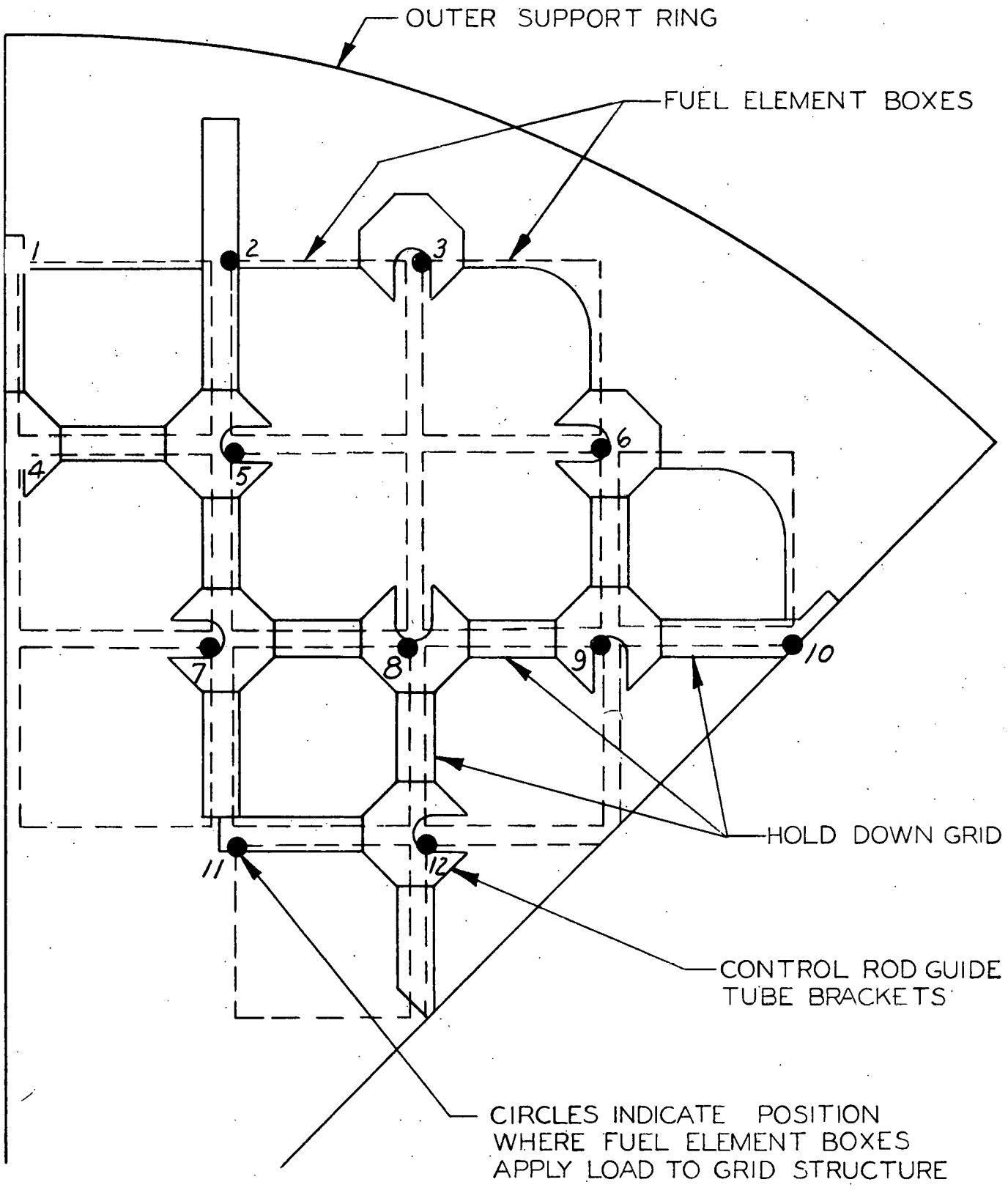

Figure 4.2 - Loading on Fuel Element Hold-Down Grid Structure (43-025-155)

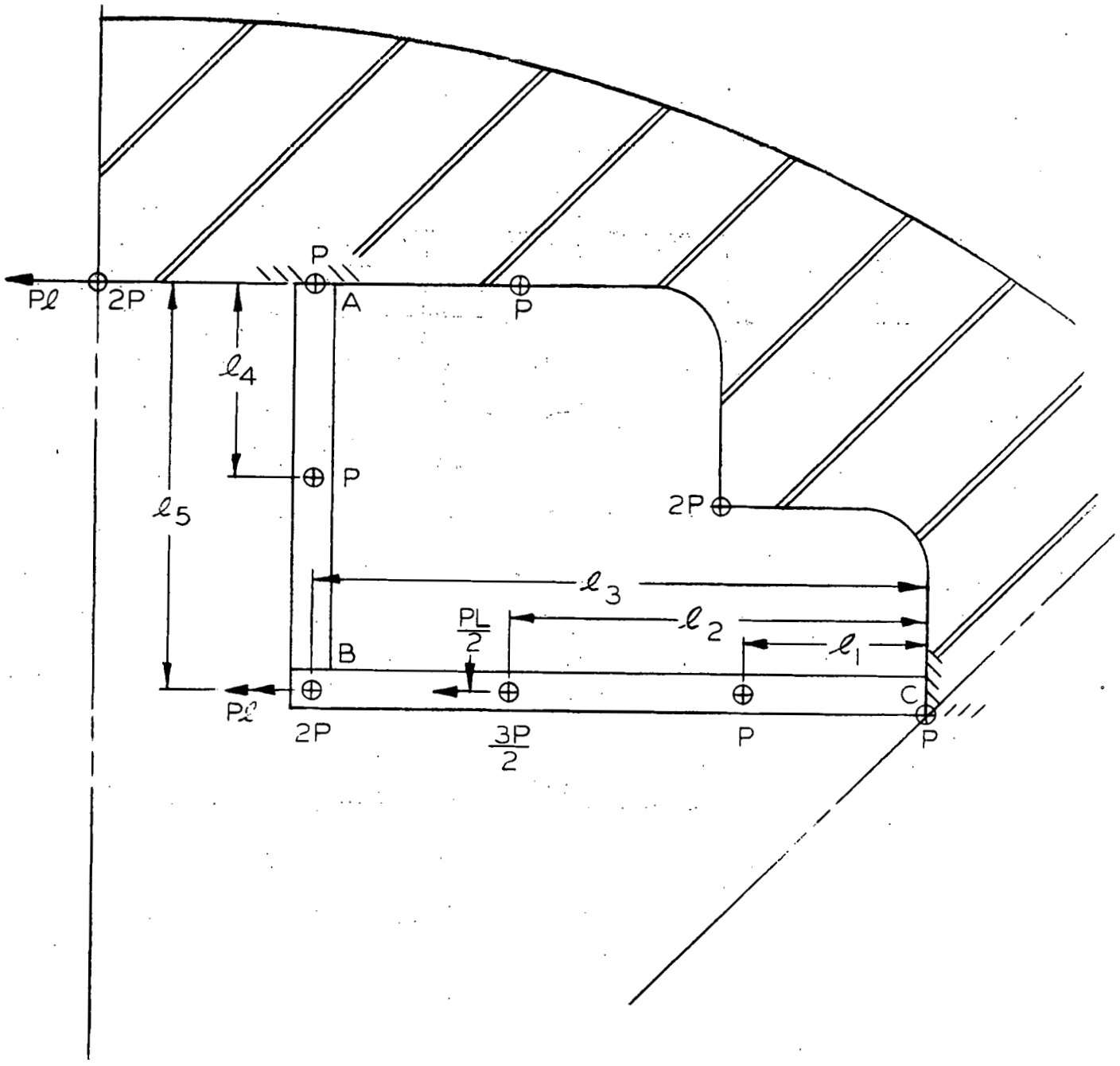

Figure 4.3 - Fuel Element Hold-Down Assembly Grid Section (Sheet 1 of 2)

(43-025-164)

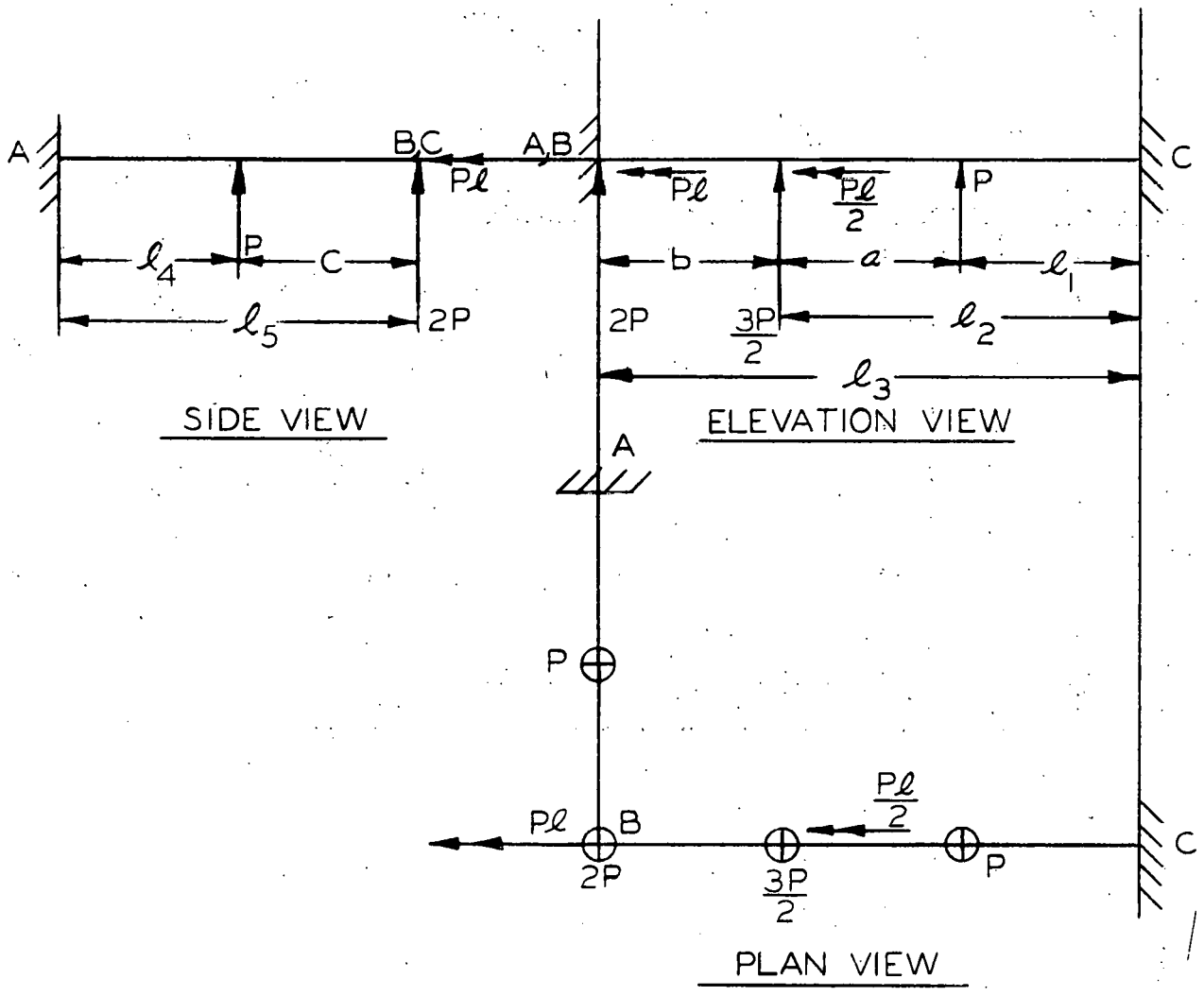

Figure 4.4 - Fuel Element Hold-Down Grid Section (Sheet 2 of 2)

(43-025-165)

The elastic energy equation for the work done by moment m is:

$$m\gamma = \int_o^L \frac{mMds}{EI} + \int_o^L \frac{t\ Tds}{GJ} \tag{4.5}$$

Since the slope, γ at the restraint is zero, the work due to M is zero. Thus:

$$0 = \int_o^x \frac{mMdx}{EI} + \int_o^y \frac{(-t)\ Tdy}{GJ} \tag{4.6}$$

Through integration:

$$0 = \left[\frac{R_c L_3^2}{2} - M_c L_3 - \frac{P(L_a + L_b)^2}{2} - \frac{3P\ L_b^2}{4}\right] - \frac{EI}{GJ}(-T_B L_5) \tag{4.7}$$

Substitution yields:

$$0 = 555\ R_c - 42.7\ M_c - 313{,}510 \tag{4.8}$$

Analysis 3 - An auxiliary torque t, is applied at point C. The beam is cantilevered off point A.

The elastic energy for the work done by the torque t is:

$$t\theta = \int_o^L \frac{mMds}{EI} + \int_o^L \frac{t\ Tds}{GJ} \tag{4.9}$$

Since the angle of twist, θ at the restraint is zero, the work due to t is zero.

By substitution and integration:

$$0 = \frac{EI}{GJ}\left[(T_C L_3) - \frac{(P\ L\ L_b)}{2}\right] + (M_B\ L_5) - (P\ L\ L_5)$$

$$- (P\ L_5^2) - \frac{(R_B\ L_5^2)}{2} - \frac{(P\ L_4^2)}{2} \qquad (4.10)$$

Thus:

$$0 = 49.9\ T_C + 60.5\ R_C - 210{,}350 \qquad (4.11)$$

The desired values for load, moment, and torque at the support points are found by solving equations (4.4), (4.8), and (4.11), simultaneously.

Stress Calculations - The stress due to the maximum bending moment is found by:

$$S_{MAX} = \frac{M(h/2)}{I_x} \qquad (4.12)$$

The stress due to the maximum torsional moment is found by the equation as given by Timoshenko and MacCullough (Ref. 4):

$$S_{MAX} = \frac{T}{\alpha\ bc^2} \qquad (4.13)$$

Where: b = longer side of rectangular cross section
c = shorter side of rectangular cross section
α = numerical factor depending upon the ratio b/c.

The principle stresses are found by:

$$(S_n)_{MAX} = S_B/2 + \sqrt{(S_B/2)^2 + (S_s)^2} \qquad (4.14)$$

$$(S_n)_{MIN} = S_B/2 - \sqrt{(S_B/2)^2 + (S_S)_{AM}^2} \qquad (4.15)$$

Elastic Energy Analysis of Hold-Down Flange Ring - The flange ring is fastened to the boiler core shroud by four bolts, equally spaced around the periphery of the ring. In this analysis, the ring was considered to be rigidly restrained at the four hold-down bolt locations, and free to deflect at any other location. Further more, the load imposed by the fuel element boxes on the hold-down assembly grid structure is considered to be transferred to the flange ring as a uniformly distributed load and edge moment.

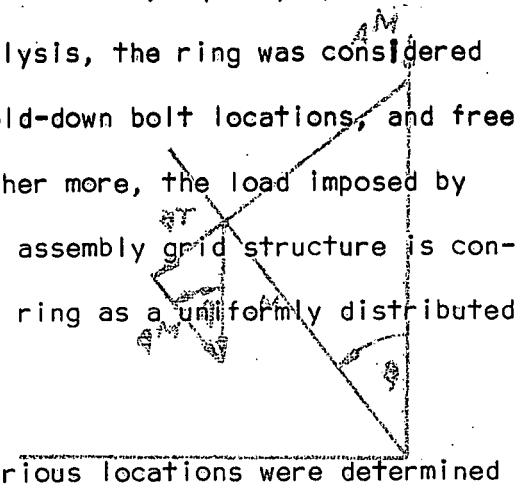

The bending and torsional moments at various locations were determined by the elastic energy methods. Stresses were calculated by considering the flange cross section to be constant. Cross sectional areas equal to the minimum and maximum ring cross sections were used to establish limits of stress at any specific location.

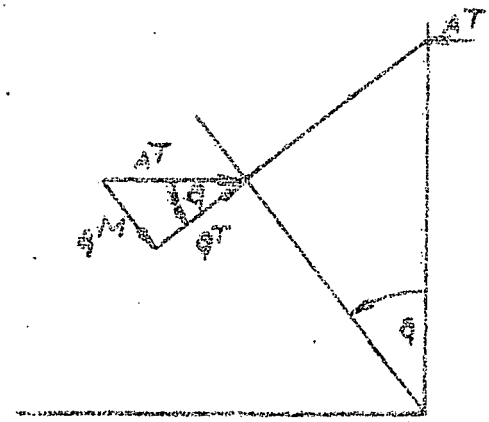

Moment and torque due to M_A

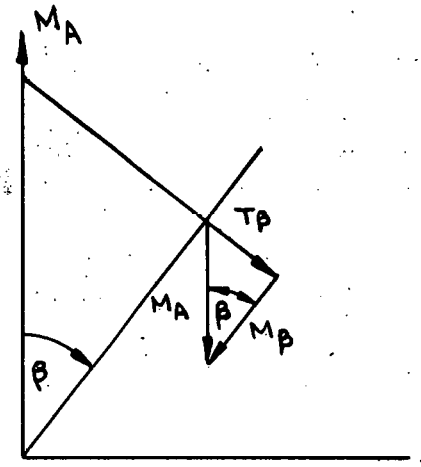

$$(M_\beta)_{M_A} = M_A \cos \beta \qquad (4.16)$$

$$(T_\beta)_{M_A} = + M_A \sin \beta \qquad (4.17)$$

Moment and torque due to T_A

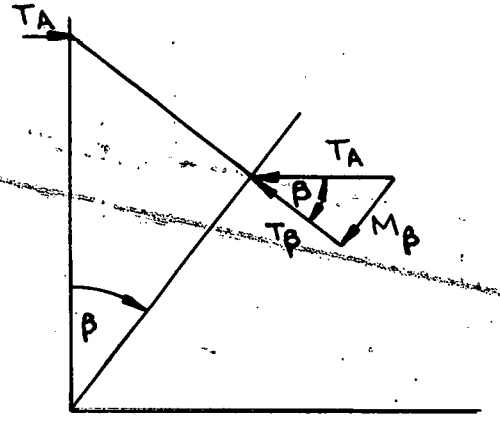

$$(M_\beta)_{T_A} = T_A \sin \beta \qquad (4.18)$$

$$(T_\beta)_{T_A} = - T_A \cos \beta \qquad (4.19)$$

Moment and torque due to vertical reaction at A

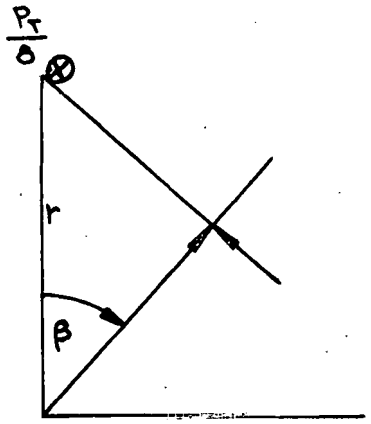

$$(M_\beta)_{\frac{P_T}{8}} = -\frac{P_T}{8} r \, SIN \, \beta \qquad (4.20)$$

$$(T_\beta)_{\frac{P_T}{8}} = -\frac{P_T}{8} r(1 - COS \, \beta) \qquad (4.21)$$

Moment and torque due to M_ϕ

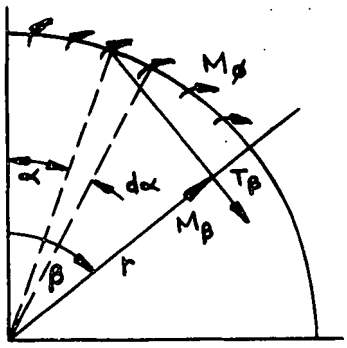

$$(M_\beta)_{M_\phi} = -\left[\int_{\alpha=0}^{\alpha=\beta} M_\phi \, r \, SIN(\beta-\alpha) d\,\alpha\right]$$

$$= -M_\phi \, r(1 - COS \, \beta) \qquad (4.22)$$

Moment and torque due to M_ϕ (Continued)

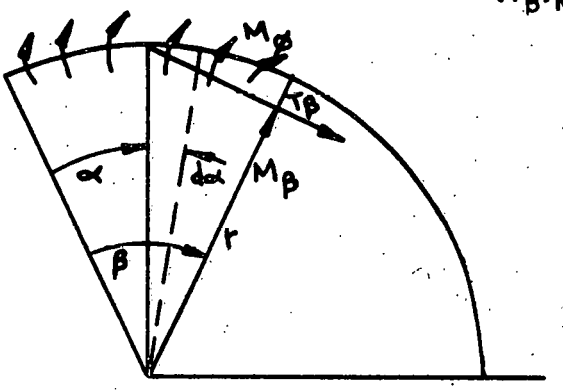

$$(T_\beta)_{M_\phi} = \int_{\alpha=0}^{\alpha=\beta} M_\phi \, r \, \cos(\beta - \alpha) \, d\alpha$$

$$= M_\phi \, r(\sin \beta) \qquad (4.23)$$

Moment and torque due to q

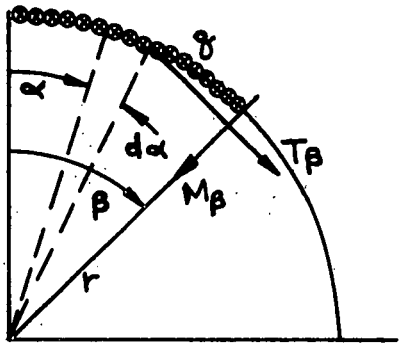

$$(M_\beta)_q = \int_{\alpha=0}^{\alpha=\beta} q \, r \, R \sin(\beta - \alpha) \, d\alpha$$

$$= q \, R^2(1 - \cos \beta) \qquad (4.24)$$

$$(T_\beta)_q = \int_{\alpha=0}^{\alpha=\beta} q \, r[r - r \cos(\beta - \alpha)] \, d\alpha$$

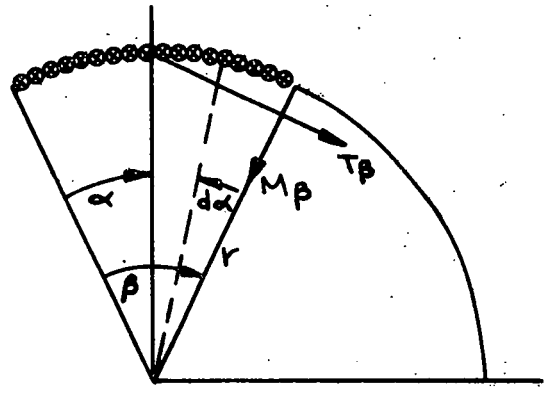

$$= q \, R^2(\beta - \sin \beta) \qquad (4.25)$$

Auxiliary torque and moment due to auxiliary torque t.

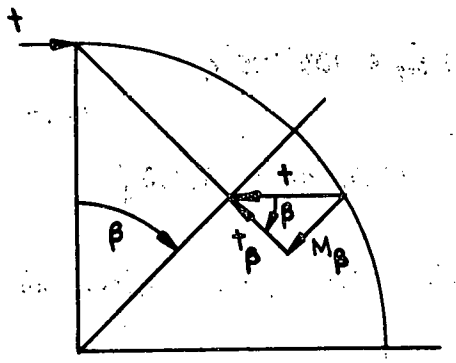

$$(M_\beta)_t = t \text{ SIN } \beta \tag{4.26}$$

$$(t_\beta)_t = - t \text{ COS } \beta \tag{4.27}$$

Bending moment at any angle β

$$M_\beta = M_A \text{ COS } \beta + T_A \text{ SIN } \beta - \frac{P_T}{8} \text{ SIN } \beta \tag{4.28}$$

$$- M_\phi \; r \; (1 - \text{COS } \beta) + qr^2 \; (1 - \text{COS } \beta)$$

Torsional moment at any angle β

$$T_\beta = M_A \text{ SIN } \beta - T_A \text{ COS } \beta - \frac{P_T}{8} r(1 - \text{COS } \beta)$$

$$+ M_\phi \; r \text{ SIN } \beta + qr^2 \; (\beta - \text{SIN } \beta) \tag{4.29}$$

Elastic Energy Equation:

$$t\beta = \int_o^L \frac{m \, M\beta \, ds}{EI} + \int_o^L \frac{t \, T_\beta \, ds}{GJ}$$

$$t\beta = 4 \int_o^{\pi/2} t \text{ SIN } \beta \; \frac{M\beta \; r \; d\beta}{EI} + 4 \int_o^{\pi/2} (-t \text{ COS } \beta) \; \frac{T_\beta \; r \; d\beta}{GJ} \tag{4.30}$$

$t\beta$ equals zero since the flange ring is restrained at the hold down bolt locations.

Substitution for M_B and T_B and integration yields:

$$0 = 0.5\ M_A + 0.785\ T_A - 3.68\ P_T - 18.75\ M_\phi + 703.125\ q$$

$$- \frac{EI}{GJ} [0.5\ M_A - 0.785\ T_A - 1.008\ P_T + 18.75\ M_\phi + 98.438_q] \tag{4.31}$$

As mentioned previously, the stress is determined using the minimum and maximum cross section of the flange ring.

For the maximum ring cross section:

$$\frac{EI}{GJ} = 0.44$$

For the minimum ring cross section:

$$\frac{EI}{GJ} = 1.10$$

The relationship between M_A, T_A, P_T and M_ϕ can be determined from statics by considering the sum of the moments about A.

$$M_A - T_B + \frac{P_T\ r}{8} - \frac{P_T\ r}{2\ \pi} + M_\phi\ r = 0 \tag{4.32}$$

but, $T_B = T_A$

Thus, substitution yields:

$$M_A - T_A = - 8837 \tag{4.33}$$

Substituting the values of EI/GJ, P_T, M_ϕ, and q into Equation (4.31) and solving Equations (4.31) and (4.33) simultaneously:

Maximum cross section

M_A = 45,980 lb-ins

T_A = 54,820 in-lbs

Minimum cross section

M_A = 40,580 lb-ins

T_A = 49,420 in-lbs

Stress Calculations - The bending stress present in the flange ring can be readily calculated using the equation:

$$S_B = \frac{M_C}{I} \tag{4.34}$$

Minimum cross section

S_B = 8650 psi

Maximum cross section

S_B = 4730 psi

The torsional (shear) stress can be determined from the equation as given by Timoshenko, et al (Ref. 4) (Eq. 4.13)

$$S_s = \frac{T}{\alpha\ bc^2}$$

Minimum cross section

S_s = 8350 psi

Maximum cross section

$$S_s = 3750 \text{ psi}$$

The principle stresses can be readily calculated:

$$(Sn) = S_B/2 \pm \sqrt{(S_B/2)^2 + (S_s)^2}$$

Minimum cross section

$$(Sn)_{max} = 13,725 \text{ psi}$$

$$(Sn)_{min} = -5075 \text{ psi}$$

Maximum cross section

$$(Sn)_{max} = 6805 \text{ psi}$$

$$(Sn)_{min} = -2075 \text{ psi}$$

4.2 Deflection Analysis of Grid Structure

The maximum deflection of the grid structure is assumed to occur at point II (Fig. 4.2). The deflection at point II is the resultant of three effects:

1. Deflection of the beam shown in Figure 4.3.
2. Displacement due to rotation of the beam.
3. Deflection of the structure between points 7 and II due to the load acting at point II.

Analysis 1 - With reference to Figure 4.3, an auxiliary load F is applied at point B, with the beam cantilevered off point A.

The work done by the auxiliary load F is:

$$F\,\Delta = \int_o^L \frac{m\,M\,ds}{EI} + \int_o^L \frac{t\,T\,ds}{GJ} \tag{4.35}$$

But: t = zero between C and B, and B and A, therefore:

$$F\,\Delta = \int_o^y (-FY)\ \frac{M}{EI}\,dy \tag{4.36}$$

Integration yields:

$$\Delta = -\frac{1.0}{EI}\left[\frac{M_B L_5^2}{2} - \frac{2\,PL_5^3}{3} - \frac{R_B L_5^3}{3} - \frac{PL_4^2}{2}\left(L_C + \frac{2L_4}{3}\right) + \frac{PL\,L_5^2}{2}\right] \tag{4.37}$$

Substitution yields:

$$\Delta = 0.00133 \text{ in.}$$

Analysis 2 - An auxiliary moment, M, is applied at point B, with the beam cantilevered off point A.

$$M\,\theta = \int_o^L \frac{m\,M\,ds}{EI} + \int_o^L \frac{t\,T\,ds}{GJ} \tag{4.38}$$

but: t = zero between C and B, and B and A

m = zero between C and B

Therefore:

$$m\,\theta = \int_o^y (-m)\,\frac{M}{EI}\,dy \qquad (4.39)$$

Integration yields:

$$\theta = -\frac{1.0}{E\,I}\left[(M_B{}'L_5 - \frac{2\,P\,L_5{}^2}{2} - \frac{R_B\,L_5{}^2}{2} - \frac{P\,L_4{}^2}{2} - P\,L\,L_5)\right] \qquad (4.40)$$

Substitution yields:

θ = 0.00018 radians

Since displacement equals θ L;

Displacement = 0.00097 in.

Analysis 3 - The deflection of the beam between points 7 and 11 can be determined from the equation:

$$\text{Deflection} = \frac{P\,L^3}{3\,EI} \qquad (4.41)$$

$$= 0.00006 \text{ in.}$$

The total deflection is:

$$\delta_{MAX} = \Delta + \theta\,L + \frac{P\,L^3}{3\,EI} \qquad (4.42)$$

$$\delta_{MAX} = 0.00236 \text{ in.}$$

4.3 Experimental Stress Analysis of Grid Structure

In order to facilitate further stress analysis, a quarter-scale model of the hold-down assembly was constructed of Plexiglas II.

In keeping with the assumptions set forth in Section 4, the Grid Structure, only, was experimentally analyzed for stress and deflection. The identical test apparatus used during the experimental analysis of the grid plate was used to analyze the hold-down grid structure. The test apparatus is shown in Figure 2.2.

To determine the direction of the principle stresses, stress-coat ST 12045 was applied to the grid structure according to standard procedures. Strain gages were to be employed to obtain quantitative results.

Thin cellophane sheets were placed over a one-eighth segment of both the upper and lower surfaces of the stress-coated model, and the stress trajectories were traced with pen and ink. These cellophane sheets were used to lay out the strain gage locations and also to check gage orientation after placement.

The size of the model prevented two strain gage rosette placements at many of the points where stress values were desired. Thus, it was decided to place one set of gages in one principle stress direction, load the model, and obtain all strain readings; then remove all gages and place the orthogonal set in the same location and load again to the same value.

The C40-111 and FABX -25-12 gages were bonded to the model with Eastman 910 cement and moisture proofed with Tatnal GW-1 moisture proofing compound.

The model was loaded by pressurizing the inflatable diaphragm until a pressure of 9.25 in. of water was reached. This pressure simulates the actual load of 50,400 lb on the Pathfinder hold-down assembly.

The principle stresses were computed from the measured principle strains by the equation:

$$\sigma_1 = \frac{E}{1 - \mu^2} (\epsilon_1 + \mu\epsilon_2) \qquad (4.43)$$

The corresponding reactor hold-down assembly stresses were calculated by the equation:

$$S = 1/N^2 \quad (P/P_M) \quad (S_M) \qquad (4.44)$$

The predicted location of maximum stress in the Grid Structure was verified. However, the theoretical stress was lower than measurements by about 37 per cent. The major portion of this inconsistancy is probably due to the incorrect assumption concerning the location of some of the loads applied by the fuel element boxes. Relocation of the loads with the deflection information obtained from the model test would eliminate most of the discrepancy.

Upon completion of the stress analysis program, a deflection test was conducted to determine the magnitude and location of maximum vertical deflection. A uniform load was applied to the grid structure with the inflatable diaphragm. Dial indicators were mounted on the structure at nine critical locations. Corresponding reactor hold-down deflections were calculated by the equation:

$$Y = 1/N \ (P/PM) \quad (EM/E) \quad (Y_M) \qquad (4.45)$$

The results of the deflection test program verified the theoretical location of the point of maximum deflection. The magnitudes differ, however, due to the failure of the model to properly simulate the rigidity of the welded interlocking joints.

NOMENCLATURE - FUEL ELEMENT HOLD-DOWN ASSEMBLY

dx = Incremental length

E = Modulus of elasticity, psi

F = Auxiliary load, lb

G = Shear modulus, psi

h = Height of rectangular plates in grid structure, in.

I = Moment in inertia, $in.^4$

J = Polar moment of inertia, $in.^4$

M = Moment due to actual loads, lb-in.

m = Moment due to auxiliary load, lb-in.

N = Length scale

P = Load, lb

q = Distributed load, lb/in.

r = Hold-Down bolt circle radius, in.

S = Stress, psi

T = Torque due to actual loads, in.-lb

t = Torque due to auxiliary loads, in.-lb

Y = Deflection, in.

Δ = Deflection due to auxiliary load, in.

δ = Deflection, in.

θ = Angle of twist due to auxiliary load, radians

γ = Slope due to auxiliary load

Subscripts

M = Model

5. STEAM DRYER ASSEMBLY (See Figure 5.1)

The steam dryer assembly serves six purposes:

1. Supports upper end of the superheater.
2. Supports weight of the upper control rod guide tubes.
3. Contains the mesh type steam dryer.
4. Provides restrainment against lateral vibration of the superheater assembly.
5. Directs steam flow from the boiler core through the steam dryers and into the superheater.
6. Provides final alignment of the boiler core control rods to facilitate latching.

5.1 Steam-Dryer Hold-Down Structure

The steam dryer hold-down structure provides a restaining force against lateral vibratory motion of the superheater assembly. The structure consists of four tapered beams mounted at their bases on a cylinder, and at their periphery to an angle ring.

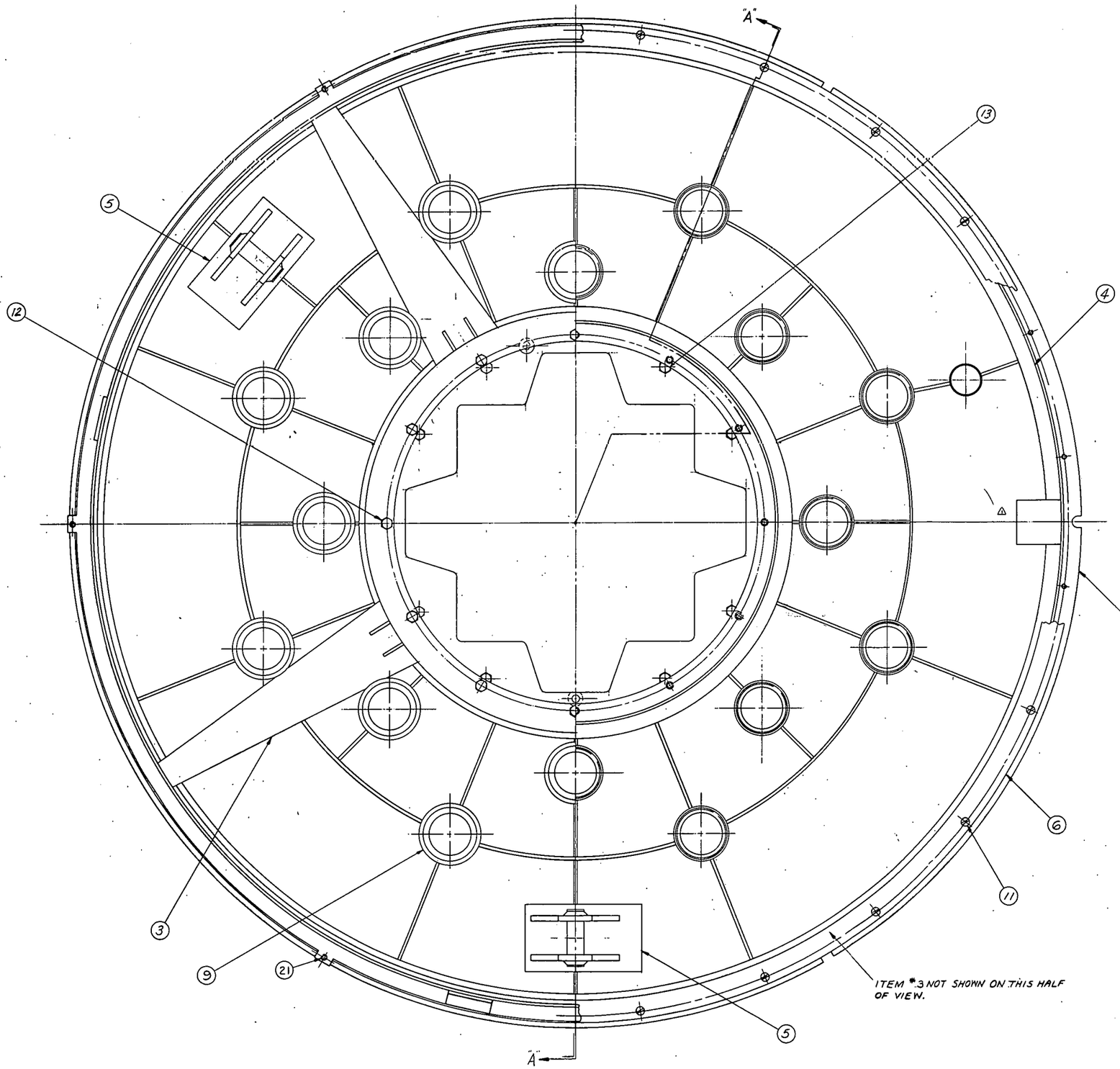

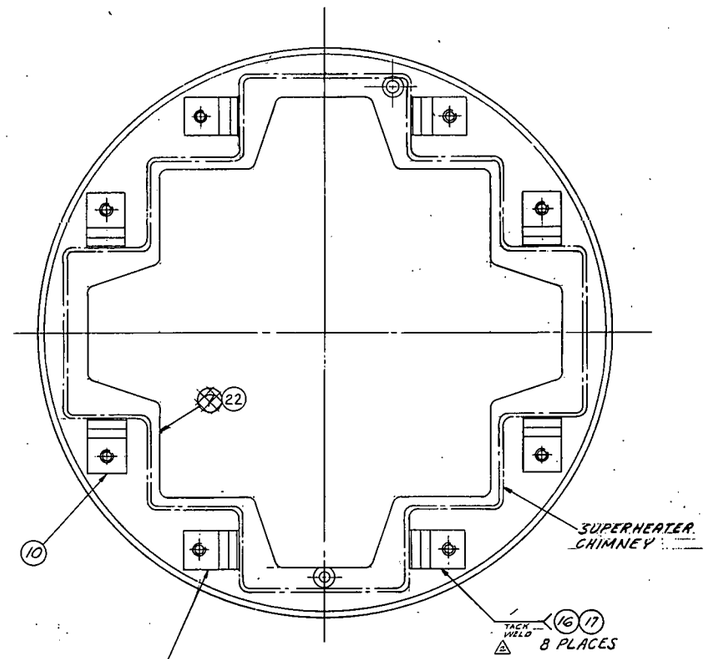

Figure 5.1 - Steam Dryer Final Assembly (Sheet 1 of 2) (43-501-029)

MK SOL REQ	ITEM	DESCRIPTION	MATERIAL	PART NUMBER DRAWING	CLASS	WT.
/	1	STEAM DRIER FINAL ASSEMBLY		43-501-029	501	3600#
1	2	STEAM DRIER SUPPORT ASSEM.		43-501-021	501	
7	3	STEAM DRIER HOLD-DOWN		43-501-019	501	
1	4	STEAM DRIER ASSEMBLY		43-501-022	502	
3	5	LIFTING LUG ASSEMBLY		43-301-821	503	
1	6	RING		43-301-818	502	
~~1~~	~~7~~	~~SHIM~~		~~43-301-845~~	~~502~~	
~~1~~	~~8~~	~~FIELD SHIM~~		~~43-301-799~~	~~502~~	
16	9	REDUCER		43-301-815	501	
8	10	LOCATOR		43-301-805	502	
24	11	3/8-16 UNC-2A X 3/4 LG FLAT HD. MACH. SCREW		43-101-601	403	
12	12	5/8-11 UNC-2A X 1 1/2 LG. HVY. S.F. HEX BOLT		43-101-379	261	
8	13	3/4-10 UNC-2A X 2 3/4 LG. HVY. S.F. HEX BOLT		43-101-379	305	
3	14	1/2-13 UNC-2A X 3 3/4 LG. HVY. S.F. HEX BOLT		43-101-379	193	
3	15	1/2-13 UNC-2B HVY. S.F. HEX NUT		43-101-376	108	
AS REQ	16	WELD ROD. ASTM. A298-SST. CLE 308 ELC. 1/16 DIA		THIS	DWG.	
YES	17	WELD PROCEDURE SPEC		43-101-207	401	
YES	18	FINAL CLEANING SPEC.		43-201-661	402	
YES	19	MANUFACTURING PROCEDURE SPEC.		43-101-216	401	
YES	20	MARKING SPEC.		43-101-282	401	
6	21	STUD		43-202-612	502	
1	22	FIELD SHIM		43-301-799	504	

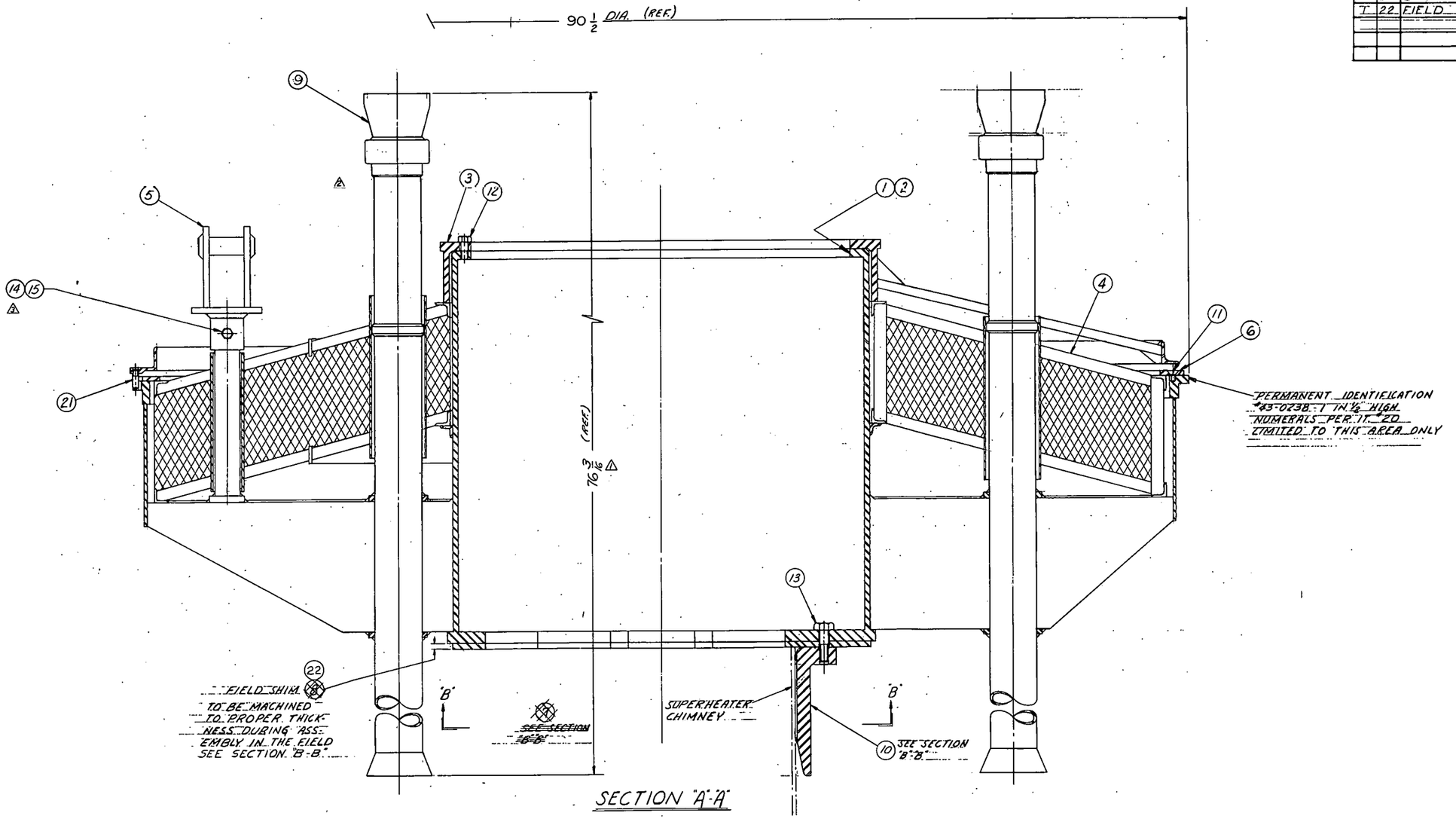

Figure 5.1 - Steam Dryer Final Assembly (Sheet 2 of 2) (43-501-029)

Four surfaces on the angle ring fit flush with the lugs welded to the inside surface of the vessel closure flange. Placement of the vessel closure onto the vessel causes an initial vertical loading in the steam dryer hold-down. Structure differential vertical expansion between the superheater chimney and vessel is absorbed by the flexing of the four tapered beams. This results in an increased vertical force being transmitted onto the dryer assembly by the hold-down structure. The vertical force is sufficient to restrain the steam-dryer assembly against the forces exerted on the assembly due to the steam pressure drop across the dryers.

The friction between the angle ring and lug mating surfaces resists differential radial expansion, thus imposing a radial force on the hold-down structure. The radial force is transmitted by the hold-down structure through the dryer assembly onto the superheater chimney as a force restraining the chimney against lateral vibratory motion. However, due to the necessity of designing the steam dryer hold-down structure with sufficient flexibility to absorb differential, radial, and vertical expansion, the hold-down structure does not present a rigid support to the superheater chimney. Nevertheless, with the hold-down structure having a spring constant of 31,200 lb/in., the support effect is adequate to raise the superheater fundamental frequency to 1129 cpm, sufficiently above forcing frequencies.

The hold-down assembly is attached to the main cylinder by a bolted connection. If it ever becomes necessary to withdraw the mesh assembly

for inspection, the hold-down structure can be easily disconnected and removed.

5.2 Steam Dryer

Separation of steam phase from water phase within the reactor pressure vessel is an economic advantage in a boiling-water reactor. This concept eliminates costly external steam drums and the additional containment-vessel volume and shielding needed to confine the increased energy represented by a reactor with external separation.

The Pathfinder Atomic Power Plant utilizes such internal separation within the reactor pressure vessel. Two stages of separation are employed to achieve steam quality of 99.9 per cent.

1. Primary separation is accomplished by releasing part of the steam at the interface, permitting separation of the phases by natural mechanisms; then separating the rest by forcing the mixture through centrifugal separators.
2. Secondary separation, removing trace amounts of moisture from the steam is accomplished by passing the mixture through impingement-type mechanical dryers.

The Pathfinder dryers consist of a knitted wire mesh modification of an impingement-type dryer. This assembly is fabricated of multiple layers of inconel knitted wire mesh. Inconel was selected to reduce the possibility of stress corrosion cracking which might result in loose pieces of wire in the system. The layers are arranged to provide a maze

of unaligned, non-symmetrical openings with a large wire surface area for impingement targets. In operation, the mixture continually changes direction as it passes through the mesh. The droplets impinge upon the wires where they coalesce. As the droplets combine and grow larger they break away and fall back through the mixture to the two-phase interface.

Selection of impingement type mechanical dryers resulted from an extensive test program involving various types of centrifugal and impingement dryers, particularly knitted wire mesh dryers. Testing of the various type dryers was performed and reported by J. F. Wilson and R. J. Grenda in (Ref. 5). As a result of the above mentioned test program, the Pathfinder steam dryer is fabricated in layers inclined 15 degrees to the horizontal, to facilitate drop drainage, with a mesh density of 5 lb/ft^3, a density yielding maximum permissible steam flow rate.

The entire mesh assembly can be removed to facilitate inspection or replacement of the knitted wire mesh.

5.3 Upper Control Rod Guide Tubes

Sixteen upper control rod guide tubes are supported by braces cantilevered off the inner cylinder. Each guide tube is 76-3/8 in. long with a 3.760 in. I D. The functions of the guide tubes are to protect and guide the control rod rack and latch during normal operation, and, by use of a reducer at the lower end, to facilitate line-up of the control rod and latch during the latching operation.

The upper end fixtures are removable to facilitate replacement or inspection of the mesh dryer assembly. Collars on the guide tubes provide final alignment of the mesh assembly in the dryer support structure.

6.0 STEAM SEPARATOR SUPPORT SHELF (See Figure 6.1)

The separator shelf supports and locates the centrifugal steam separators. The support shelf is composed of three 120 degree shelf segments, each of which supports fifteen steam separators. The shelves are braced along all edges to minimize vertical deflection.

6.1 Theoretical Stress Analysis

A static deflection analysis was performed on the separator shelf by use of a computer program.

In this analysis the shelf was assumed to be a straight beam, 110 in. in length, and supported at three points. The support positions are shown in Figure 6.2. The beam was divided into fifty-five 2 in. segments, and the loading force and moment of inertia calculated for each segment.

Although the computer also indicated the slope, deflection, and shear at each segment, only the calculated moments and support reactions were of interest. The computed deflection of the separator shelf cannot be accepted with any degree of certainty since the shelf is of a configuration which does not lend itself readily to positive analysis. The loading force on each 120 degree segment of the separator

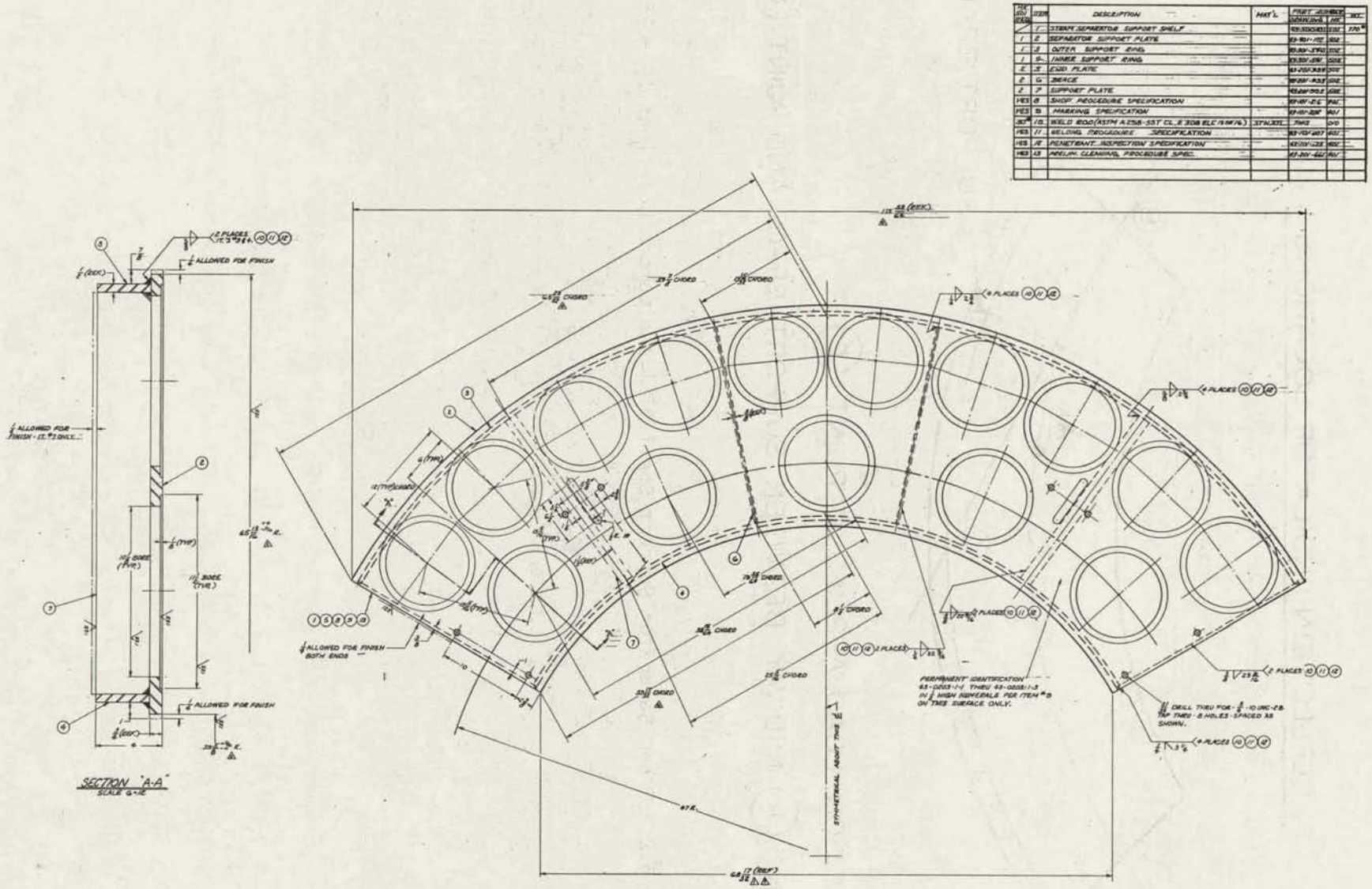

ITEM	DESCRIPTION	MAT'L	PART NUMBER (DRAWING)	REF
1	STEAM SEPARATOR SUPPORT SHELF		43-500-831	330
2	SEPARATOR SUPPORT PLATE		43-101-112	302
3	OUTER SUPPORT RING		43-301-590	302
4	INNER SUPPORT RING		43-301-591	302
5	END PLATE		43-203-389	302
6	BRACE		43-301-903	302
7	SUPPORT PLATE		43-301-903	302
MES	SHOP PROCEDURE SPECIFICATION		43-101-EC	PAC
MES	MARKING SPECIFICATION		43-101-201	401
30	WELD ROD (ASTM A 258-55T CL. E 308 ELECTRODE)	STAINLESS	RWG	010
MES	WELDING PROCEDURE SPECIFICATION		43-101-207	401
MES	PENETRANT INSPECTION SPECIFICATION		43-201-138	402
MES	PRELIM. CLEANING, PROCEDURE SPEC.		43-201-662	401

Figure 6.1 - Steam Separator Support Shelf (43-500-831)

DEFLECTION INDICATOR LOCATIONS

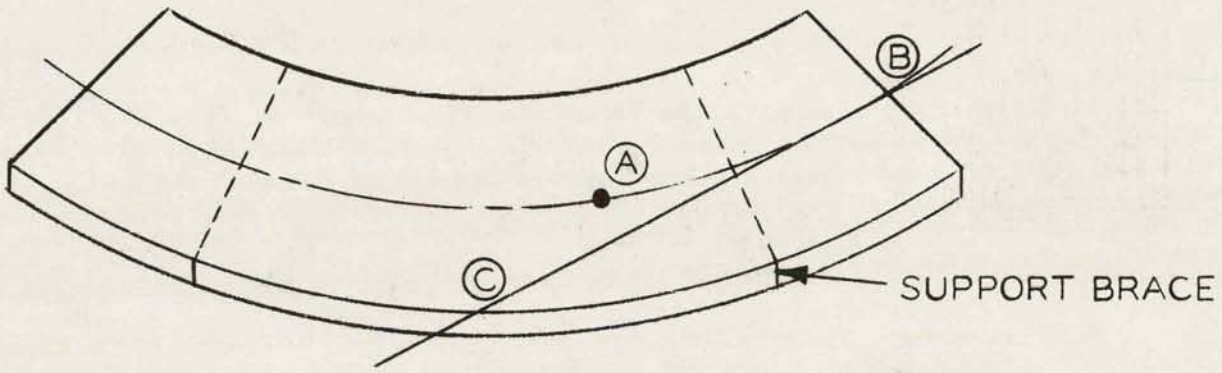

REACTION LOAD APPLIED AT POINT (C)

POINT (A) MIDWAY BETWEEN SUPPORT BRACE AND POINT (C)

Figure 6.2 - Steam Separator Support Shelf Dial Indicators Locations (43-025-166)

shelf is the resultant of three individual forces:

1. Force exerted by the fifteen separators supported by each shelf segment. Each separator weighs 168.7 lbs.
2. Force exerted by the weight of the shelf itself.
3. Force exerted by the pressure drop across the shelf. In this analysis a pressure drop of 3.38 psi (150 per cent rated) is assumed.

The computer predicted the maximum bending moment in the shelf to occur at the outer supports with a magnitude of 28,176 lb-in.

The maximum bending stress was calculated to be 5,100 psi, well within the allowable limits for the stainless steel separator shelf.

The computer calculated the support reactions to be a force of 5306 lb for the end supports, and 2381 lb for the center support. This information was incorporated in the investigation of the support lugs.

6.2 Experimental Stress and Deflection Analysis

In order to calculate the bending stresses present in the separator shelf, certain simplifying assumptions were made. By comparing the calculated support reactions with experimentally determined reactions, the validity of the assumptions can be checked.

The deflection of the separator shelf, however, cannot be calculated with any degree of certainty since the shelf is of a configuration that

does not lend itself readily to analysis. Thus the deflection of the shelf under full load was determined through use of a model.

The model was a quarter scale Plexiglas II representation of a 120 degree segment of the separator shelf. The pertinent model information is listed below:

Scale:	1/4" = 1"
Material:	Plexiglas II
	$E_M = 5 \times 10^5$ psi
	$\mu = 0.35$
Loading:	Uniform on entire length

In order to represent an equally distributed load, rock salt was spread evenly into a shallow paper container having the same shape as the support shelf. The container construction was such that negligible resistance to bending was present in the load container.

The model was supported on two support braces running the full width of the shelf. Deflection indicators were positioned at points A, B and C, as illustrated in Figure 6.2. The model was loaded initially with no central support.

To eliminate the effect of creep in the plastic model, deflection readings were begun 6 minutes after application of the load. Preliminary tests on a sample piece of the model material indicated that creep occurs at a significant rate for the first 6 minutes after load application.

After 6 minutes the creep rate is reduced sufficiently to allow readings to be taken.

Loads were applied in 1000 g increments, except when rated and maximum loads were to be represented. All load and reaction forces were measured on a 2610 kg capacity laboratory scale.

After every load change, upon completion of the deflection measurements, weight was added to a reaction measuring device until point C on the shelf model returned to zero deflection. The deflections at points A and B were then recorded to determine the effect of the support at point C.

By placing a point reaction at point C, the same support conditions as found in the reactor were achieved. In Pathfinder, the shelf is supported on two lugs located near each end of the shelf segment and on a pad located at the midspan. Due to its small size, the pad exerts a reaction only to a small area of the shelf at the vessel wall.

Experimental analysis of the separator shelf indicated that a maximum deflection of 0.032 in. would occur at point A under maximum loading conditions. The deflection is not excessive since the shelf could deflect as much as 0.375 in. without any adverse effects.

The reaction at support point C was determined experimentally to be 2130 lb. The calculated center reaction was 2220 lb. Thus, original assumptions used in calculating the reactions appears to have been

acceptable, and the theoretical bending moments, and related maximum bending stresses, can be considered acceptable. The magnitude of the maximum bending stress, 5100 psi, is well within the allowable stress limits for the stainless steel support shelf.

7.0 NUCLEAR SUPERHEATER (See Figure 7.1)

The nuclear superheater located at the geometrical center of the nuclear boiler core has a cross sectional width of 33.66 in. maximum and an overall length between the parting line of the lower tube sheet flange to the top tube sheet of 15 ft 8 in. (188 in.), excluding the chimney; the chimney above the top tube sheet has a length of 50 ft 1/4 in. The lower tube sheet which supports the superheater is made of 316 stainless steel. The plate consists of a spherical segment, 3/4 in. thick, welded to a flange ring and bolted to the steam-line flange. The seal between the flanges, preventing mixture of water and superheated steam, is obtained by a spiral wound, 316 Stainless Steel, asbestos-filled gasket.

Four baffles, fabricated from 1 in. thick 304 Stainless Steel plate, are spaced between the lower and top tube sheets, and are the radial supports of the tubes. The baffles, located 15-1/2 in., 64 in., and 112-1/2 in. above the lower tube sheet flange parting line are also used to regulate the amount of cooling water and moderator flow passing through the superheater fuel region. Each baffle is perforated with sharp edged orifices centered in the flow channel among the tubes. The

MK. 502 REQ.	MK. 501 REQ.	ITEM	DESCRIPTION	MATERIAL	PART NUMBER DRAWING	MK.	WT.
--	1	25	LOWER BAFFLE		43-401-217	505	
-	1	26	UPPER BAFFLE		43-401-218	505	
-	125*	27	WELD ROD (ASTM A371-53T CL.ER 316 L		THIS	027	
17	--	28	MED. SPRING LOCKWASHER		43-101-553	032	
-	1	29	INTERMEDIATE TUBE SHEET *4		43-500-894	504	
17	-	30	SPACER		43-202-870	502	
1	--	31	TEST PLATE FOR ITEM *3		THIS	031	
1	--	32	TEST PLATE FOR ITEM *4		THIS	032	
1	--	33	TEST PLATE FOR ITEM *20		THIS	033	
1	--	34	TEST PLATE FOR ITEM *29		THIS	034	
1	--	35	TEST PLATE FOR TRANSITION TUBE SHEET		THIS	035	
415	--	36	INNER INSULATING TUBE		43-301-758	501	
52	-	37	INNER INSULATING TUBE		43-301-772	501	

MK. NO. REQ.	MK. NO. REQ.	IT.	DESCRIPTION	MATERIAL	PART NUMBER DRAWING	MK.	WT.
1	/	1	SHELL ASSEMBLY		43-500-918	501	48000
-	1	2	LOWER GRID PLATE & SUPPORT ASSEMBLY		43-500-896	501	
-	1	3	UPPER GRID PLATE		43-500-893	502	
-	1	4	UPPER TUBE SHEET		43-500-894	502	
YES	YES	5	CLEANING SPEC.		43-201-627	001	
YES	YES	6	MARKING SPEC.		43-101-283	001	
-	1	7	CHIMNEY ASSEMBLY		43-401-188	303	
17	-	8	3/8-16 UNC-2B HVY. S.F. HEX. NUT		43-101-368	106	
1	--	9	INVERTED SPACER		43-500-894	501	
-	12	10	TUBE SHEET SHROUD SUPPORT		43-301-609	504	
--	4	11	LOWER BAFFLE QUARTER SECTION		43-401-217	505	
--	4	12	UPPER BAFFLE QUARTER SECTION		43-401-218	505	
/	-	13	SUPERHEATER SHELL ASSEMBLY		43-500-918	502	
-	416	14	SUPERHEATER TUBE (CUT TO SIZE)		43-301-639	501	
YES	YES	15	WELD PROCEDURE SPEC. (RADIOGRAPHIC INSPEC. NOT REQUIRED		43-101-207	001	
25*	25*	16	WELD ROD (ASTM A298-58T GR. C 304 316 CB 9 MO)		THIS	016	
YES	YES	17	FLUID PENETRANT INSPECTION SPEC.		43-101-173	001	
YES	YES	18	FABRICATION PROCEDURE SPEC.		43-101-216	001	
-	52	19	CONTROL ROD GUIDE TUBE		43-301-238	304	
-	1	20	INTERMEDIATE TUBE SHEET *3		43-500-894	503	
YES	YES	21	SHOP ASSEMBLY PROCEDURE		43-101-304	001	
--	8	22	TUBE SHEET SHROUD SUPPORT		43-301-715	504	
--	12	23	TUBE SHEET SHROUD SUPPORT		43-301-609	505	
--	8	24	TUBE SHEET SHROUD SUPPORT		43-301-715	505	

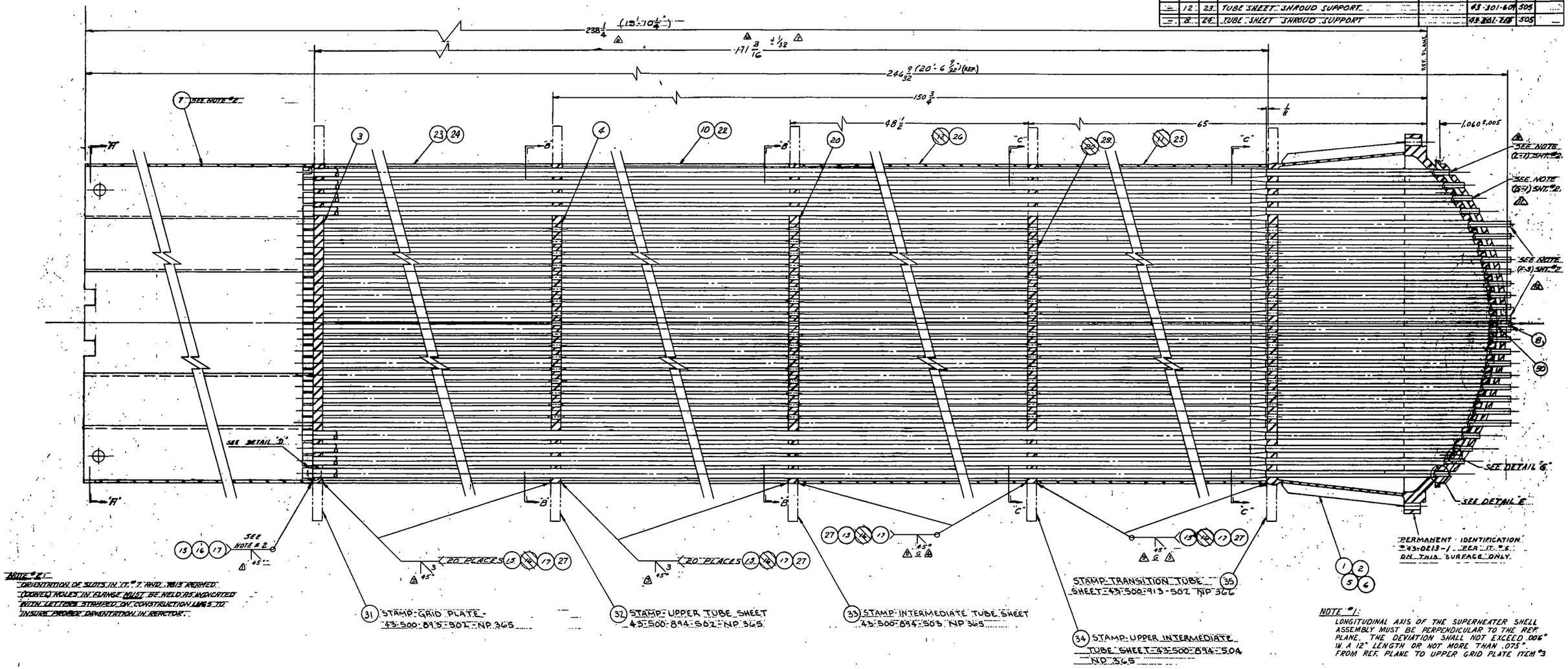

Figure 7.1 - Superheater Shell Assembly (Sheet 1 of 2) (43-500-918)

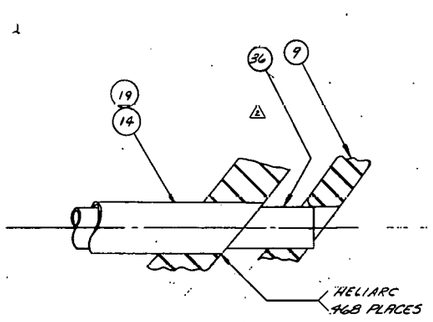

DETAIL "E"
SCALE: 12:12

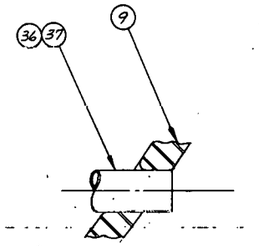

DETAIL "I"
SCALE: 12:12

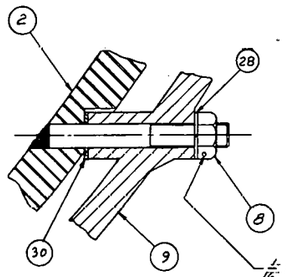

DETAIL "G"
SCALE: 12:12

1/16 DRILL THRU HEX. FOR WIRE LOCKING AT FINAL ASSEMBLY.

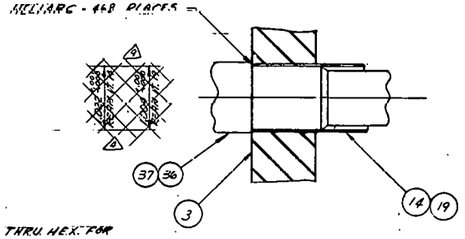

DETAIL "D"
SCALE: 12:12

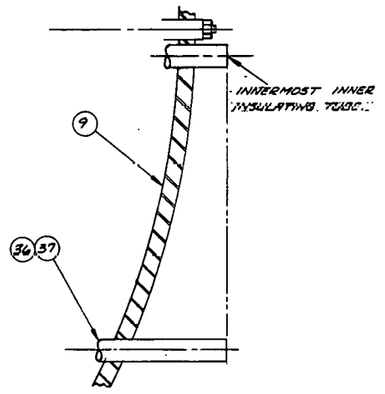

DETAIL "H"
SCALE 6-12

(15) ALL OF ITS. #36 & #37 ON THIS LINE & AREA WITHIN SHALL BE USED AS PURCHASED — (196 3/8 LG.) SEE DETAIL "H".

~~(15) ALL OF ITS. #36 & 37 ON THIS LINE & AREA WITHIN SHALL BE CUT AS SHOWN (SEE DETAIL "I") PER COMMON LENGTH DETERMINED AT ASSEMBLY ±1/4~~

(15) (16) ALL ITS. #36 & 37 OUTSIDE THIS AREA, EXCEPT 8 OUTERMOST ITS. #36, SHALL BE CUT AS SHOWN (SEE DETAIL "I") PER LENGTH DETERMINED AT ASSEMBLY ±1/4

(16) 415 PLACES (36) (16)

(37) (19) 52 PLACES AS SHOWN

(15) DRILL & REAM .7813 +.0005 -.0000 DIA. 4 HOLES LOCATED PER DWG. 43-500-966 AFTER ALL WELDING IS COMPLETED SEE NOTE 2 (SHT. #1)

(16) THE 8 OUTERMOST OF ITS. #36 SHALL BE CUT AS SHOWN (SEE DETAIL "G") PER LENGTH DETERMINED AT ASSEMBLY ±1/32.

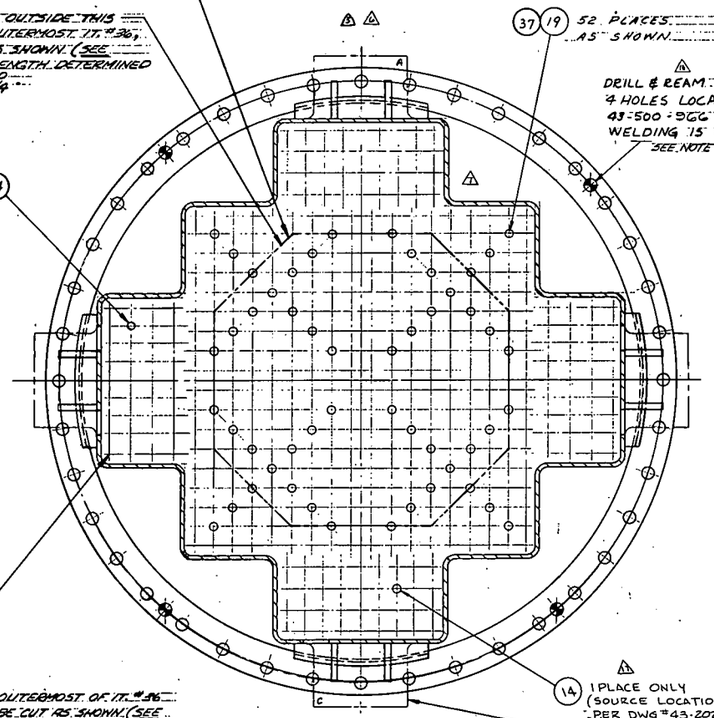

SECTION "A-A"
SCALE: 3:12

(14) 1 PLACE ONLY (SOURCE LOCATION 3:21 PER DWG #43-202-174)

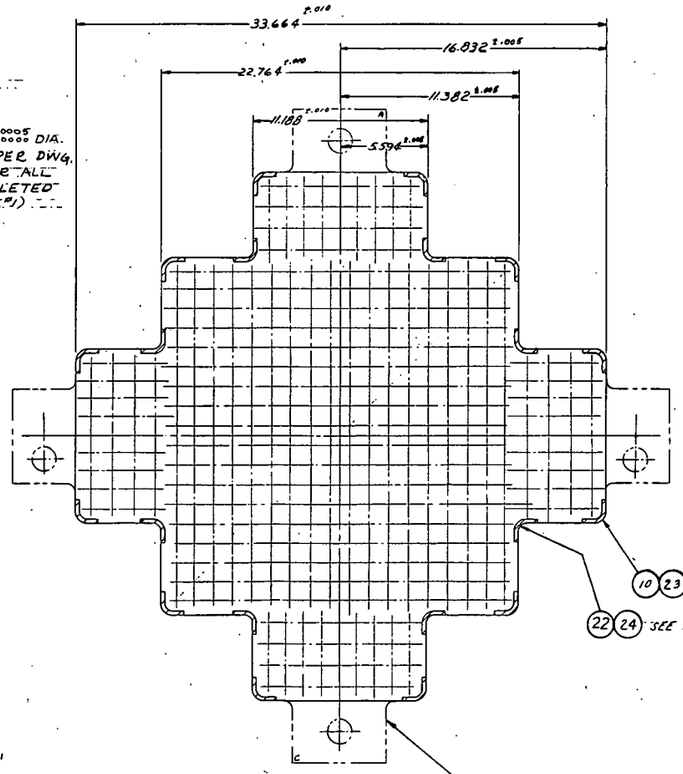

SECTION "B-B"
SCALE: 3:12

(13) LUGS FOR CONSTRUCTION PURPOSES ONLY. TO BE REMOVED AFTER ASSEMBLY IS COMPLETE & TESTED. CARE MUST BE TAKEN NOT TO GET CHIPS IN ASSEMBLY. SEE NOTE #2.

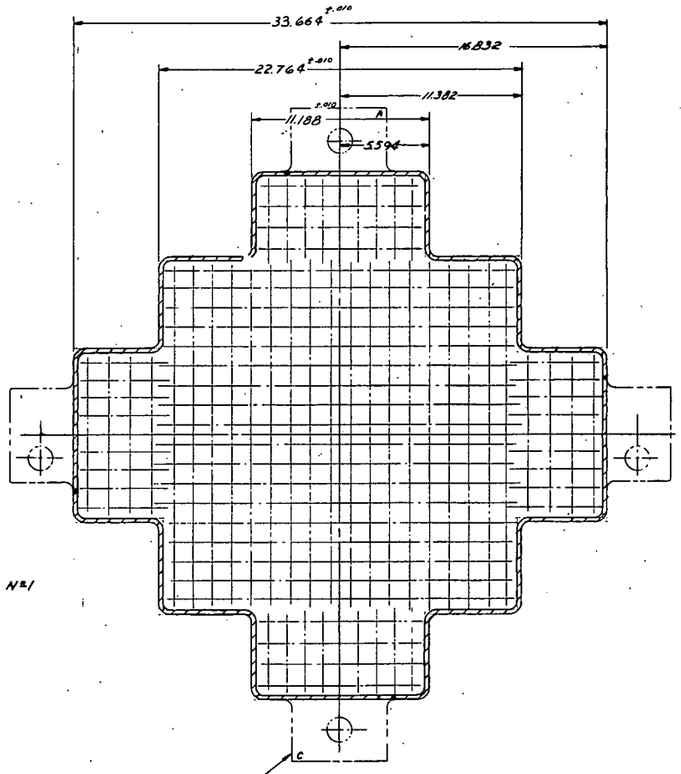

SECTION "C-C"
SCALE: 3:12

Figure 7.1 - Superheater Shell Assembly (Sheet 2 of 2) (43-500-918)

shroud is made in two sections over the length of the fuel and is made watertight in order to separate the moderator flow in the superheater from that in the boiler. The shroud also serves as the structural support of the superheater assembly. The lower section is made of 1/4 in. thick 316L Stainless Steel plate. To improve the nuclear characteristics of the core, the upper half of the shroud is made of 1/8 in. thick 316L Stainless Steel plate. This reduces the amount of stainless steel to a more optimum amount in the upper region of the superheater.

Above and below the fuel region, the shroud is replaced by 316 Stainless Steel structural supporting members welded to each baffle above the fuel and to the baffle and tube sheet below the fuel. Additional structural support is provided by 468 outer container tubes.

The thermal shield located below the lower tube sheet provides a 1/2 in. space of stagnant steam between the shield and tube sheet, thus limiting the thermal gradient across the tube sheet to a minimum value. The thermal shield is constructed of 1/2 in. thick 405 Stainless Steel plate. The shield, provided with adequate spacers, is bolted to the lower tube sheet.

The chimney, and the top tube sheet form a watertight seal preventing the cooling water from flowing inside of the superheater tubes in the event of an abnormal increase of liquid level. The chimney, 1/4 in. thick 304 Stainless Steel plate, open at the top, is of watertight constuction along its periphery and is welded to the 1-1/8 in. thick 304 Stainless Steel top tube sheet.

Superheater control is accomplished by four control rods and drive units. Each superheater control rod assembly consists of twelve 3/4 in. diameter stainless steel rods containing 2% natural boron, suspended on a cruciform shaped rack. Each control assembly can be inserted and removed as a single unit. The rack can also be removed and each of the twelve fingers handled separately. It is not intended that these rods should be SCRAMMED. They will be RUN IN, under power, by the drive unit.

7.1 Tubes

The superheater consists of 468 outer container tubes, insulating tubes, and fuel tubes. The 468 outer container tubes are weld drawn 316 Stainless Steel, 1.076 in. o.d. swaged at one end to 0.800 in. o.d. Each tube is fusion welded, with a flush type weld, to the top tube sheet and bottom tube sheet, thus separating the moderator water from the steam. The tubes are integral parts of the mechanical structure of the superheater. 415 of the tubes have a wall thickness of 0.026 in. and contain fuel elements. One of the remaining 53 tubes contains the neutron source. The remaining 52 tubes, with a wall thickness of 0.035 in., are used as control rod guides. During operation, the steam passing through the superheater creates a pressure drop that subjects the outer container tubes to external pressure and end loading. At normal operating conditions, the pressure drop is 65 psi.

During an assumed transient state caused by a malfunction in the control system, the turbine throttle valve and dump valve could be simultaneously opened causing a maximum differential pressure of about 200 psi.

The insulating tubes are made of 304L Stainless Steel, 0.967 in. o.d. x 0.015 in. wall tapered at the lower section of 0.640 in. o.d. The tubes are inserted in the container tubes and control rod guide tubes. This arrangement provides an insulating gap of stagnant steam between the tubes. The insulating tubes are kept concentric in the container tubes by ribs 120 degrees apart over the entire length of the insulating tubes. The insulating tubes are free to expand axially in the downward direction.

The insulating gap is sealed at the top tube sheet. The joint is formed by insert pieces fusion welded to the insulating tubes and expanded in the container tubes. The joints provide a seal for saturated steam, and can be disassembled by pulling upward on the insulating tubes.

The superheater fuel element assembly consists of two concentric fuel bearing tubes, a central burnable poison rod, spacers and end fittings.

The fuel tubes and poison rod are fastened together by a spacer and support fitting at the lower end. Radial spacers over the whole length of the fuel tubes maintain concentricity of the components. The fuel tubes are free to expand axially. The steam flow channels formed by the tubes assured proper coolant flow for optimum heat transfer. The superheater fuel assembly is about 6-1/2 ft long with an active fuel length of 72 in. It is inserted in the insulating tubes and rests on the transition section of the tubes. The bottom of the active fuel is located 34-1/2 in. above the bottom tube sheet flange parting line.

Collapsing Pressure. For design calculations, the allowable external pressure on the outer container tube was based on the Pressure Vessel Code "External Pressure on Thin Wall Tubing" (U.P.V.; 1959, UG-31). The minimum collapsing pressure was based on the test described in paragraph 7.1.1.

Buckling Load. In calculating the buckling load, it was assumed that the entire load due to the maximum differential pressure across the superheater is resisted by the outer container tubes, neglecting the reinforcing effect of the outer shell (shrouds and legs).

7.1.1 Tube Collapsing-Pressure Test

Tests were conducted to determine the collapsing pressure of the thin-walled tubes that are used for the superheater outer container tubes.

A circular tube can collapse owing to external pressure at stresses far below the elastic limit of the material. The pressure at which the circular tube becomes unstable and buckling occurs is referred to as the collapsing pressure, Pc, in this test.

Test Set-Up. A 5 in. diameter pipe, closed with welded cap at one end and blind flange at the other end, was used as the containment vessel. The tube specimens, 40 in. long, sealed at both ends with either rubber or welded plugs, were placed in the containment vessel. The pressure was supplied by a hand pump and read on a calibrated gage.

A rack was made to support three tube speciments. The rack was designed to:

1. Support the tubes at both ends.
2. Axially load the tube with a compressive spring (250 lb-in.) in addition to end loading due to pressure.
3. Apply a concentrated bending load between the supports so as to cause a deflection in the tube of 0.125 in. at the mid-point.
4. Apply end moments on the tubes so as to cause a deflection of 0.125 in. at the mid-point. The unsupported length of the tube in the rack was 32-1/2 in.

Collapsing Pressure. Several tube samples were tested for each of the conditions described below. Each tube sample (1.080 in. O.D.)) was within a diametral tolerance for roundness of $\pm$ 0.002in. Tubes with wall thicknesses of 0.020 in. and 0.025 in. were pressurized in the containment vessel.

The collapsing pressure of tubes with 0.020 in. thick walls was 390 psi, and for tubes with 0.025 in. thick walls was 790 psi.

Effect of Out-of-Roundness on Collapsing Pressures. Several tube specimens were flattened to an elliptical shape and tested. Results were as follows:

For tubes with 0.020 in. thick wall and with out-of-roundness of 0.010 in., 0.025 in., and 0.030 in. the collapsing pressure was

375 psi, 325 psi, and 300 psi, respectively. For tubes with a 0.025 in. thick wall and with out-of-roundness of 0.025 in., 0.030 in., and 0.135 in., the collapsing pressure was 630 psi, 580 psi, and 275 psi, respectively.

Effect of Dents. Several tube specimens of 1.080 in. I.D. were dented to various depths with a 1/8 in. diameter pin. Except for the dented area, the tubes out-of-roundness were within a $\pm$ 0.002 in. For tubes with 0.020 in. thick walls and with dent depths of 0.070 in. and 0.050 in. the collapsing pressure was 375 psi and 380 psi, respectively. For tubes with 0.025 in. thick walls and with dent depths of 0.050 in., 0.080 in., and 0.205 in., the collapsing pressure was 775 psi, 500 psi, and 385 psi, respectively. A typical collapsed tube is shown in Figure 7.2. A dent localized in a small area and equal in depth to the wall thickness does not affect the collapsing pressure of the tube by a measurable amount provided the tube roundness is within the diametral tolerance specified.

Effect of Inner Container and Fuel Tubes on Collapsing Pressure. A mock-up of the fuel assembly was made. The mock-up consisted of the following:

Outer container tube	1.080" O.D. x 0.020" wall
Insulating tube	0.926" O.D. x 0.020" wall
Outer fuel tube	0.790" O.D. x 0.027" wall
Inner fuel tube	0.600" O.D. x 0.027" wall

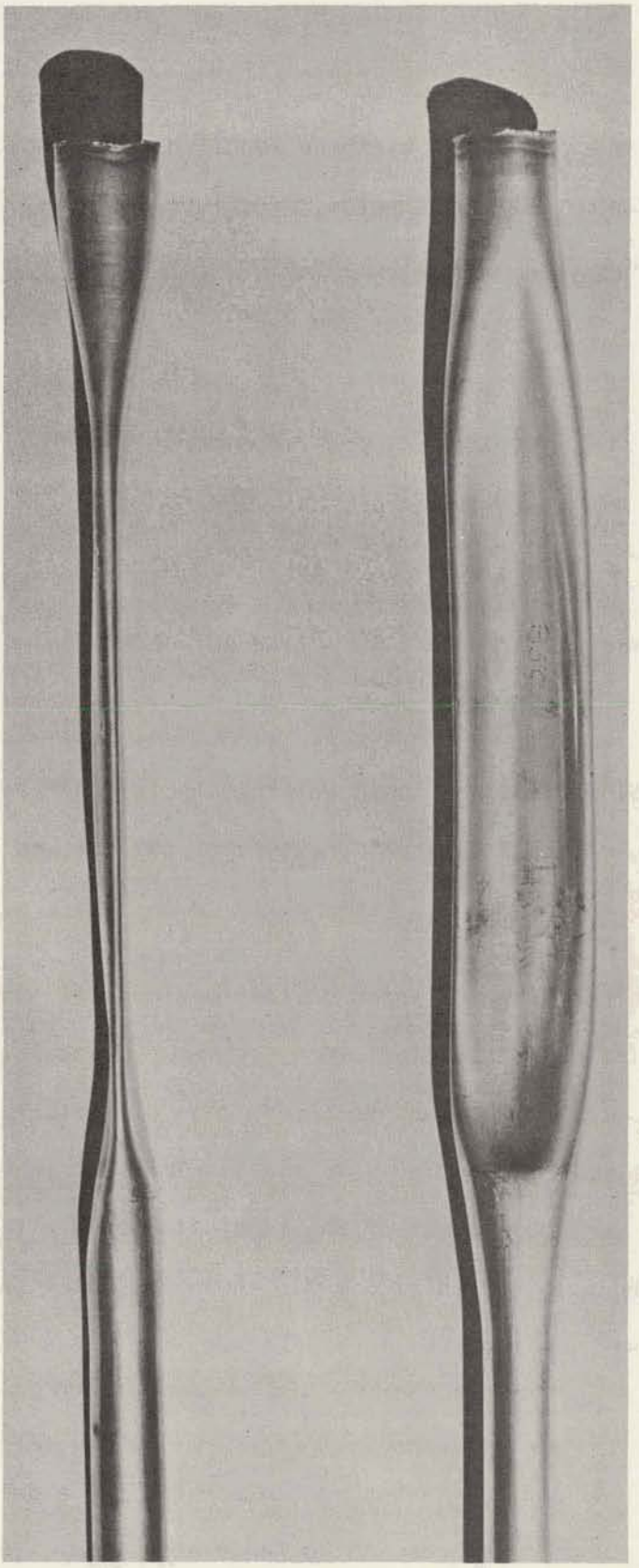

Figure 7.2 - Collapsed Unsupported Superheater Container Tube (Typical)

(211999)

Each tube was held concentric by three longitudinal wires spaced 120 degrees apart in a given annulus. The tube assembly, plugged at both ends, was inserted in the containment vessel and pressurized. The support rack was not used for the test.

The outer container tube collapsed with an external pressure of 390 psi to an elliptical shape (1.270 in. OD max., 0.955 in. O D min.). The insulating tube did not collapse but deformed to an elliptical shape (0.950 in. O D max., 0.893 in. O D min.). The fuel tubes were not deformed and were readily pulled out of the outer container tube.

The outer container tube was replaced; the insulating tube and fuel tubes were reused. External pressure of 390 psi was applied and maintained.

The outer container tube collapsed uniformly along its longitudinal axis to an elliptical shape (1.37 in. O D max., 0.962 in. O D min.). The insulating tube was deformed to an elliptical shape (0.955 in. O D max., 0.866 in. O D min.). The fuel tubes did not deform and were pulled out of the insulating tube without difficulty. The assembly in Figure 7.3 shows the outer and insulating tubes with the fuel tubes removed, and shows the degree of deformation

Outer, insulating, and fuel tubes were assembled. The external pressure was increased in order to collapse each tube. The outer,

insulating, and outer fuel tubes collapsed at 390 psi, 425 psi, and 620 psi, respectively. The inner fuel tube did not collapse completely but showed signs of deformation when the external pressure reached 900 psi. The middle section in Figure 7.3, is the collapsed assembly.

In order to simulate the actual superheater condition, a tube assembly consisting of the following was made:

1. Outer container tube with 1.080 in. O D × 0.025 in. wall with one end swaged to 0.800 in. O D
2. Insulating tube with 0.926 in. O D × 0.020 in. wall over the whole length of the 1.080 in. O D tube up to the swaged section.
3. Fuel tube of 0.790 in. O D × 0.027 in. wall and fuel tube of 0.600 in. O D × 0.027 in. wall.

Both fuel tubes extended the whole length of the 1.080 in. o.d. tube up to 7-1/2 in. from the swaged section.

The outer container and insulating tubes collapsed completely at 800 psi over the 7-1/2 in. length unsupported by the fuel tubes. The section supported by the fuel tubes did not collapse. However, near the end of the fuel tubes, the outer container and the insulating tubes were deformed over 1 ft lengths, then tapered to their original shape. The fuel tubes did not deform, except at the end where the outer container tubes collapsed. The fuel

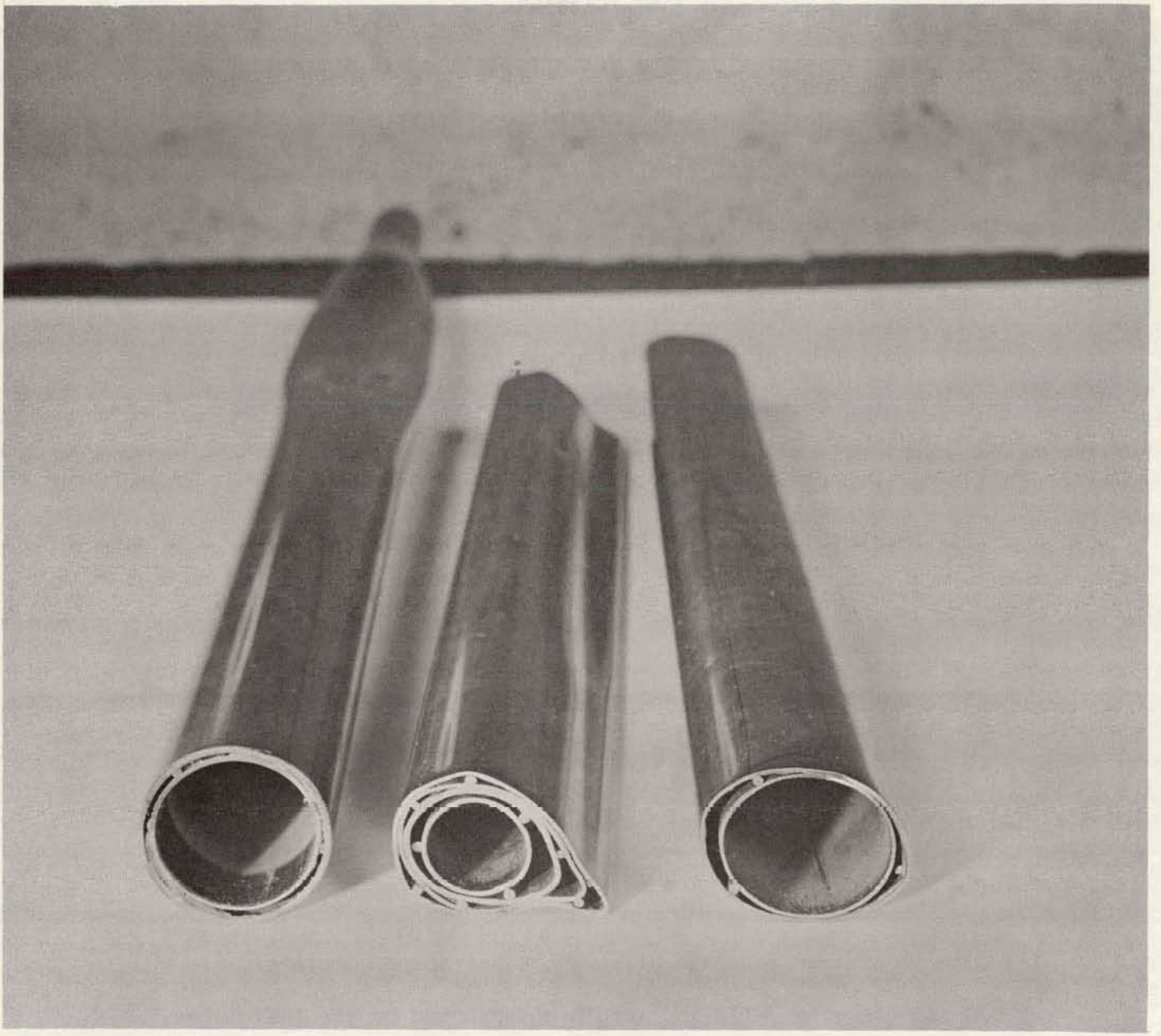

Figure 7.3 - Collapsed Mock-Up of Superheater Assemblies (211666)

tubes were pulled out without difficulty. The left section in Figure 7.3, is the collapsed assembly.

Discussion. All tests were conducted at room temperature. Elevated temperature testing would result in the same collapsing configuration as shown in Figure 7.3, but would lower the collapsing pressure in direct ratio to the change in Young's Modulus as shown in Equation (7.2).

The out-of-roundness appears to be the greatest cause of tube collapse due to external pressure. The axis of collapse is always coincident with the minor axis of out-of-roundness.

A bending stress on the tube due to mechanical loading within the elastic limit of the material does not affect the collapsing pressure appreciably, if the tube roundness is within the ovality tolerance of $\pm$ 0.002 in. for the tube considered (thickness-to-diameter ratio).

In the test conducted, pressure was applied on the ends as well as the sides of the tubes. The end load, W, due to the pressure was as follows:

$$W = \pi/4 \times D^2 \times P \qquad (7.1)$$

(Where, P was the pressure applied to collapse the tubes).

Due to this end load, the measured collapsing pressures are somewhat lower than for a tube with side loading only, which would more closely simulate Pathfinder conditions. However, the test set-up was not designed to obtain side loading only

R. G. Sturm has reported a semi-empirical formula (Ref. 6) for determining the collapsing pressure of thin-walled tubes:

$$P_c = K\ E\ (t/D)^3 \qquad (7.2)$$

Where: P_c = Collapsing pressure

D = Outside diameter, in.

E = Modulus of elasticity

t = Wall thickness, in.

K = Constant, f (2L/D and D/t)

L = Length of tube, in.

For long thin-walled tubes where 2L/D and D/t are greater than 20 and with pressure on sides only, K is about 2.2. For the case when the ends as well as the sides are loaded, K differs. The effect of end loads due to pressure is to reduce slightly the collapsing pressure, as is shown in Figure 7.4

In the case where the outer container tube is assembled with the insulating tube and fuel tubes, the external pressure at which the outer and insulating tubes reached elastic instability is the same as if they were not supported by the inner tubes.

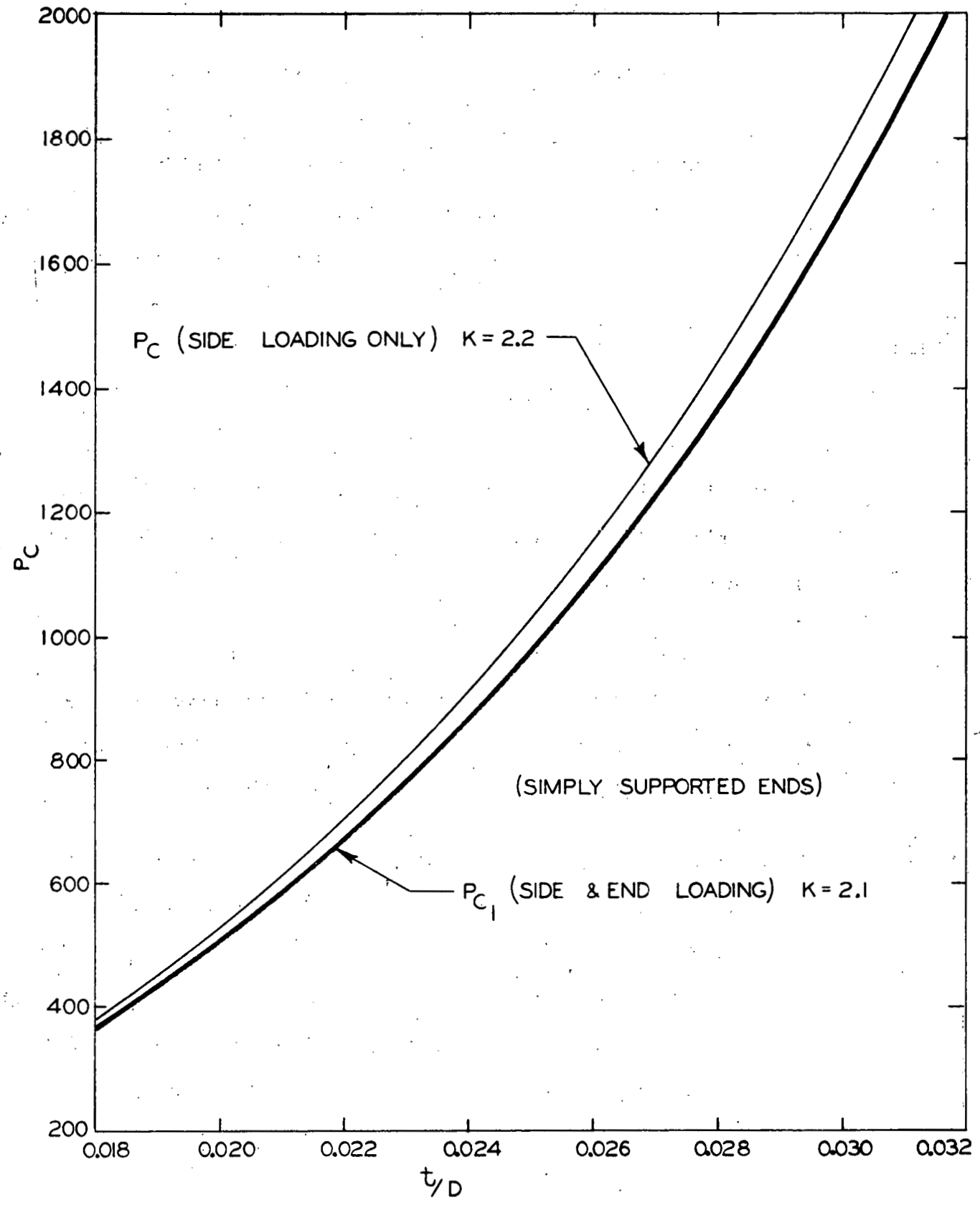

Figure 7.4 - Collapsing Pressure of Tubes with Side and End Loading as a Function of Wall-thickness to Diameter Ratios (43-024-426)

However, the outer and insulating tubes did not collapse completely, but became elliptical with the minor axis of the insulating tube and about equal to the outside diameter of the outer fuel tube. From the several assemblies tested, the reduction of the gap area between the insulating and outer fuel tubes is 10 to 15 per cent.

7.2 Superheater Lower Tube Sheet

The lower tube sheet, which supports the superheater, is 316 Stainless Steel. The plate consists of a spherical head segment welded to a flange ring. The spherical portion is perforated by 468 holes with diameters of about 0.80 in.

The spherical tube sheet was selected instead of a flat tube sheet, because the thickness of the flat plate that would have been required for the several operating conditions would have resulted in large temperature gradients and excessive thermal stresses.

Abnormal operation conditions that were considered are as follows:

1. Simultaneous opening of all four safety-relief valves
2. Opening of the dump valve with the turbine throttle valve still open. (This could be caused by a control-signal loss). A pressure differential of up to 200 psi can be expected as a result of these conditions.

7.2.1 Mechanical Stress Calculations

Analysis of stresses due to mechanical loading was done using conventional methods. An outline of the calculation method is shown below. A deflection efficiency of 50 per cent was used for the perforated plate. Deflection efficiency is defined as the ratio between the deflection of a perforated plate and a solid plate of the same configuration under the same load. This value was based on experimental tests of perforated plates performed at Allis-Chalmers and other laboratories.

Analysis Outline (See Figure 7.5).

Flange

Angular Rotation (Ref. 2, p. 231)

$$\theta = \frac{R_m M_t}{2 \pi E I} \tag{7.3}$$

Radial Displacement (Ref. 7, p. 10)

$$\delta = \left(F - H\right)\left(\frac{R_m}{2 \pi A E}\right) - \theta d \tag{7.4}$$

Hemispherical Head

Angular Rotation (Ref. 8, p. 474)

$$\theta = \frac{2\lambda^3 M_o}{\pi R E t K_1 R s} - \frac{\lambda^2 \sin \varphi F}{\pi R E t K_1} \tag{7.5}$$

FREE BODY DIAGRAM

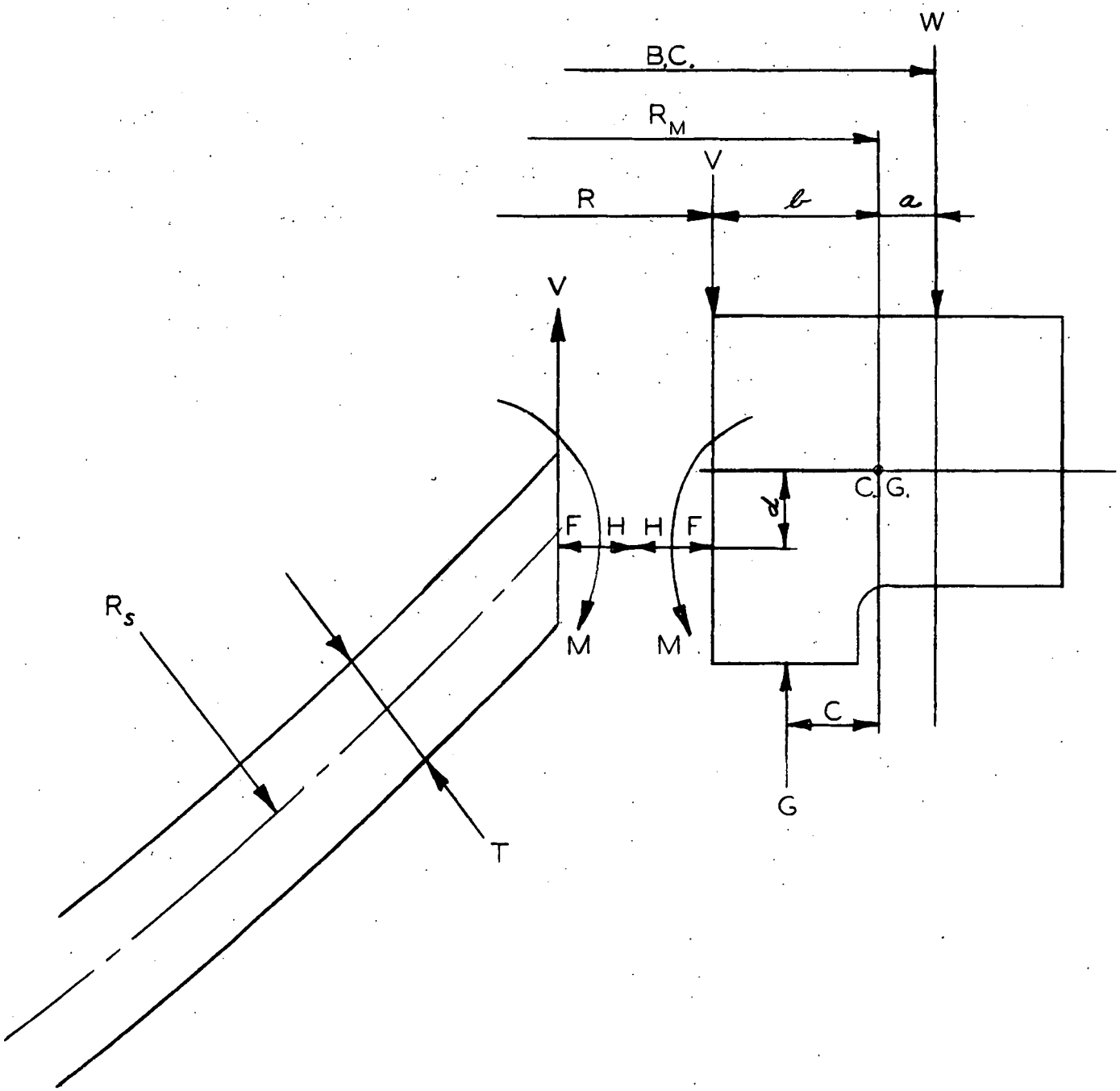

Figure 7.5 - Spherical Grid Plate - Free Body Diagram (43-025-168)

Radial Displacement (Ref. 8, pp. 407, 474)

$$\delta = \frac{PR_s^2 (1 - \mu) \sin \varphi}{2 E t} + \frac{\lambda^2 \sin \varphi M_o}{\pi R E t K_1}$$

$$- \frac{\lambda R_s \sin^2 \varphi}{2 \pi R E t} (K_2 + \frac{1}{K_1}) F \qquad (7.6)$$

The influence coefficients for the angular rotation and the radial displacement become:

$$\begin{bmatrix} \theta \\ \theta \\ \delta \\ \delta \end{bmatrix} = \begin{bmatrix} \frac{R_M M_T}{2 \pi EI} \\ \frac{2\lambda^3 M_o}{\pi R E t K_1 R_s} - \frac{\lambda^2 \sin \varphi F}{\pi R E t K_1} \\ \left(F - H\right)\left(\frac{R_M}{2 \pi AE}\right) - \theta d \\ \frac{PR_s^2 (1 - \mu) \sin \varphi}{2 E t} + \frac{\lambda^2 \sin \varphi M_o}{\pi R E t K_1} \\ - \frac{\lambda R_s \sin^2 \varphi}{2 \pi R E t} (K_2 + \frac{1}{K_1}) F \end{bmatrix}$$

General Equations for Inside Hemispherical Head Stress

1. Tensile stress due to pressure (Ref. 9, p. 53)

$$S_p = \frac{P}{2}\left[\frac{Y^3 + 2}{Y^3 - 1}\right] \tag{7.7}$$

$$\text{where } Y = \frac{R_s + t}{R_s} \tag{7.8}$$

2. Tensile stress due to discontinuity force T_p (Ref. 8, p. 470)

$$S_d = \frac{T_p}{2\pi R_M t} \tag{7.9}$$

$$T_p = Q_p \cot \beta \tag{7.10}$$

$$Q_p = \frac{2}{R_p}\lambda e^{-\lambda\Psi}(\text{SIN } \lambda \Psi) M_o - \sqrt{2}\, e^{-\lambda\Psi}(\text{SIN } \lambda \Psi - \tfrac{\pi}{4}) Q_o \tag{7.11}$$

$$Q_o = F \text{ SIN } \varphi \quad (\text{AT } \varphi) \tag{7.12}$$

(Discontinuity Shear Force)

3. Bending stress due to discontinuity moment M_o at any point on the Hemispherical head (Ref. 8, p. 45)

$$S_{bg} = \frac{3 M_p}{\pi R_p t^2} \tag{7.13}$$

Where:

$$M_P = \sqrt{2}\, e^{-\lambda\Psi} \cdot \text{SIN}\,(\lambda\Psi + \pi/4)\, M_o$$

$$- \frac{R_s}{\lambda} \cdot e^{-\lambda\Psi}\,(\text{SIN}\,\lambda\Psi)\, Q_o \qquad (7.14)$$

(Ref. 8, p. 470)

General Equations for Outside Hemispherical Head Stress (See Fig. 7.6)

1. Tensile stress due to pressure (Ref. 9, p. 53)

$$S_P = 3\,P/2\left[\frac{1}{\gamma^3 - 1}\right] \qquad (7.15)$$

Where:

$$\gamma = \frac{R_s + t}{R_s} \qquad (7.16)$$

2. Tensile stress due to discontinuity force, T_P, is obtained by Equation (7.9).

3. Bending stress due to discontinuity momen, M_o, is obtained by Equation (7.13).

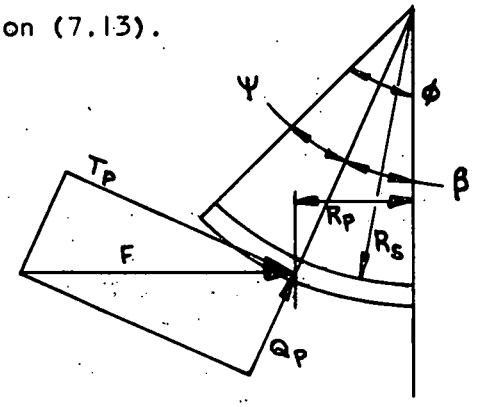

Figure 7.6 - Representative Section of Spherical Grid Plate

NOMENCLATURE - SUPERHEATER TUBE SHEET

F = Discontinuity force at edge.

G = Gasket reaction.

H = Horizontal component force of V.

M_o = Discontinuity moment at edge.

M_p = Discontinuity moment at point considered on head.

M_t = Total moment about flange center of gravity.

$$(M_t = Wa - Vb + Gc - Fd + Hd - M_o)$$

Q_o = Discontinuity shear force at edge.

T_p = Discontinuity force at point considered on head.

V = Hydrostatic force.

W = Bolt loading.

Constants

$\lambda = 1.285\sqrt{R_s/t}$

$K_1 = 1 - \text{Cot}\varphi/5.0\,\lambda$ $\qquad$ $K_2 = 1 - \text{Cot}\varphi/1.25\,\lambda$

μ = Poisson's Ratio

7.2.2 Thermal Gradient Calculations

The spherical tube sheet, with the concave side in contact with the moderator fluid at 489 F and the convex side in contact with the superheated steam at 825 F average temperature, was analyzed.

The thermal shield placed on the convex side of the tube sheet provides an insulating space of stagnant superheated steam. A similar thermal insulation is provided by superheated steam between the inner and outer container tube.

The film coefficients due to radiation and conduction between the thermal shield and between the inner and outer container tube have been determined. The calculations were based on the assumption of steady-state conditions. The effect of gamma heating was not included, since it was not significant.

To determine the thermal gradient across the 3/4 in. thick plate, a typical three-dimensional section of the grid plate was chosen. The temperature distribution was determined using the A-C Thermal Analyzer Program*, for the IBM-704 computer.

The maximum thermal gradient across a 3/4 in. thick plate was found to be 45.5 F, (Figure 7.7). However, due to the curvature of the plate, the thickness near the edge, measured on the vertical plane is about 1 in.; the maximum thermal gradient for this condition is increased by 50 per cent or 68.5 F (Figure 7.8).

*A computer program developed by Allis-Chalmers to handle steady-state and transient heat transfer problems.

Assuming the edge of the plate is clamped, so that angular deflection but not radial expansion, is prevented, the resulting bending stresses may be approximately expressed as follows:

$$S_b = \frac{E\alpha\,(T_{ave} - T)}{1 - \mu} \qquad (7.17)$$

Where: E = Young's Modulus

μ = Poisson's Ratio

α = Coefficient of thermal expansion

T_{ave} = Average temperature through plate thickness

T = Temperature at point under consideration

The results of the mechanical and thermal stress analyses are presented in Figure 7.9 and 7.10. Stresses at the inner and outer surfaces of the spherical tube sheet are given by Figures 7.9 and 7.10, respectively. The apparent discontinuities in the stress distributions shown are the results of the deflection efficiency applied because of the presence of the perforations. Stress concentration factors were not applied at the perforations nor at the edges of the tube sheet.

In the analysis, the following sets of conditions were assumed:

1. Bolted-down condition, no pressure or temperature differential.
2. Normal operation condition (85 psi pressure differential).
3. Abnormal condition (250 psi pressure differential).

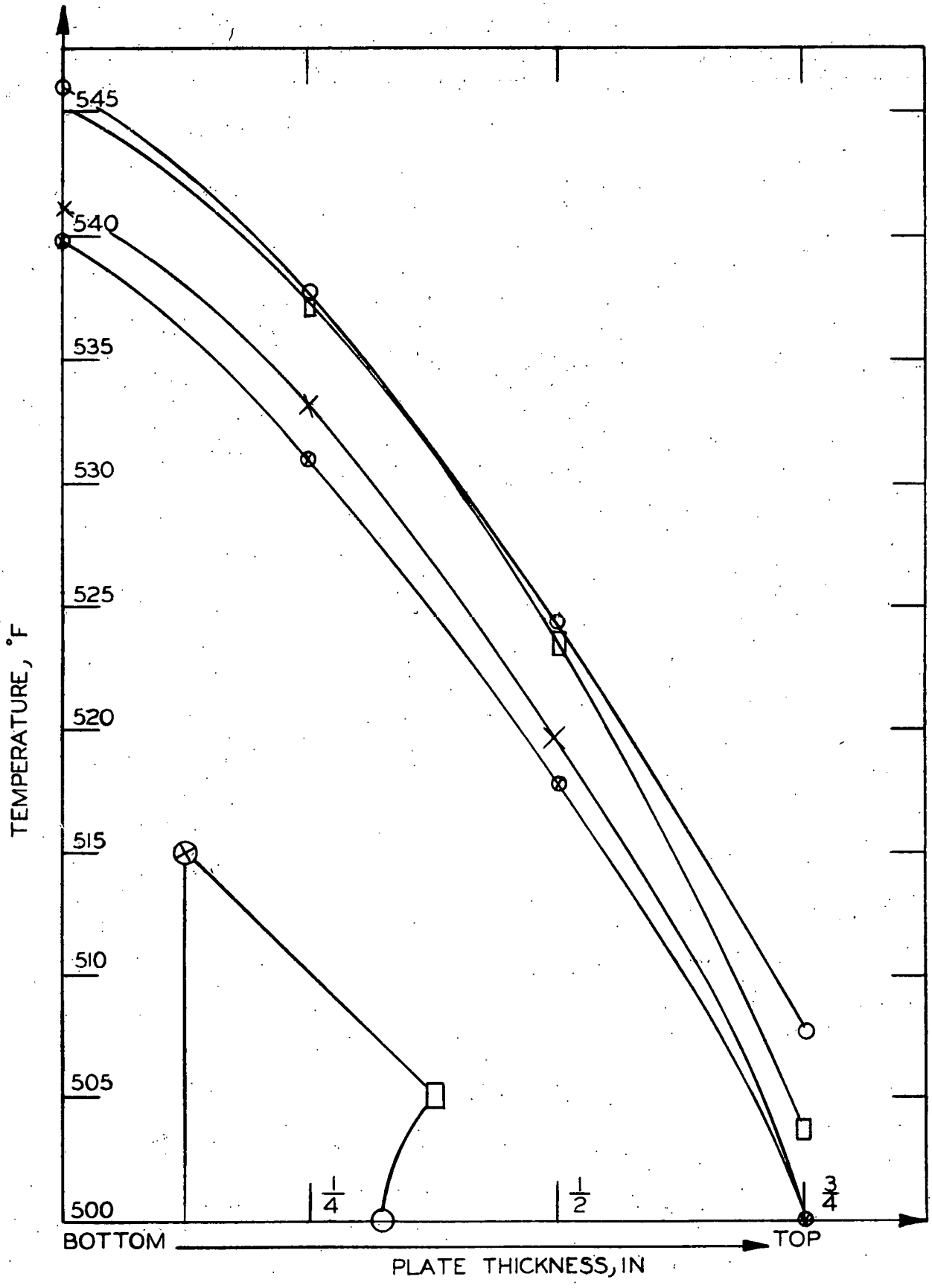

Figure 7.7 - Temperature Gradient 3/4 in. thick Section Plate (43-025-170)

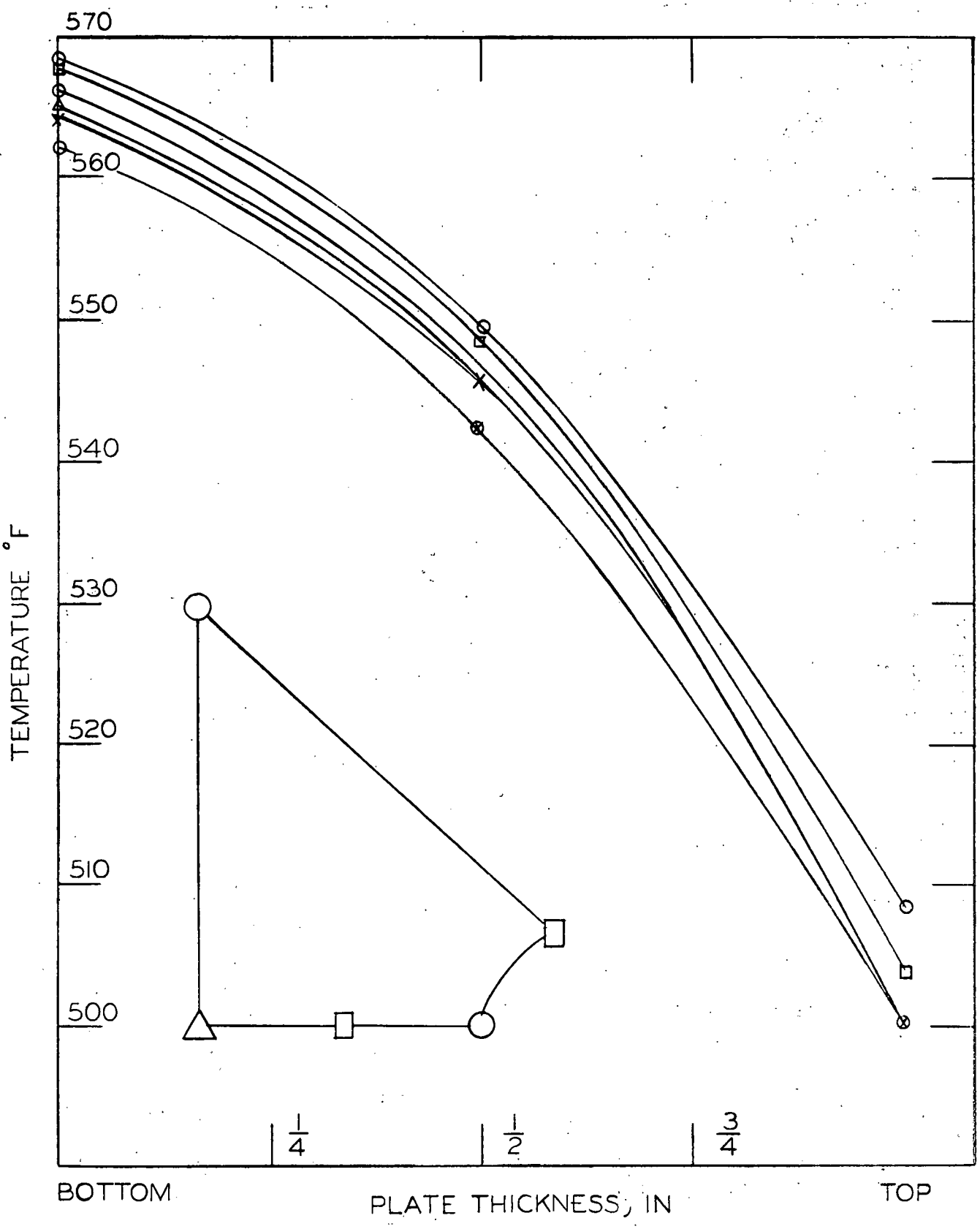

Figure 7.8 - Temperature Gradient 1 in. Thick Section Plate (43-025-172)

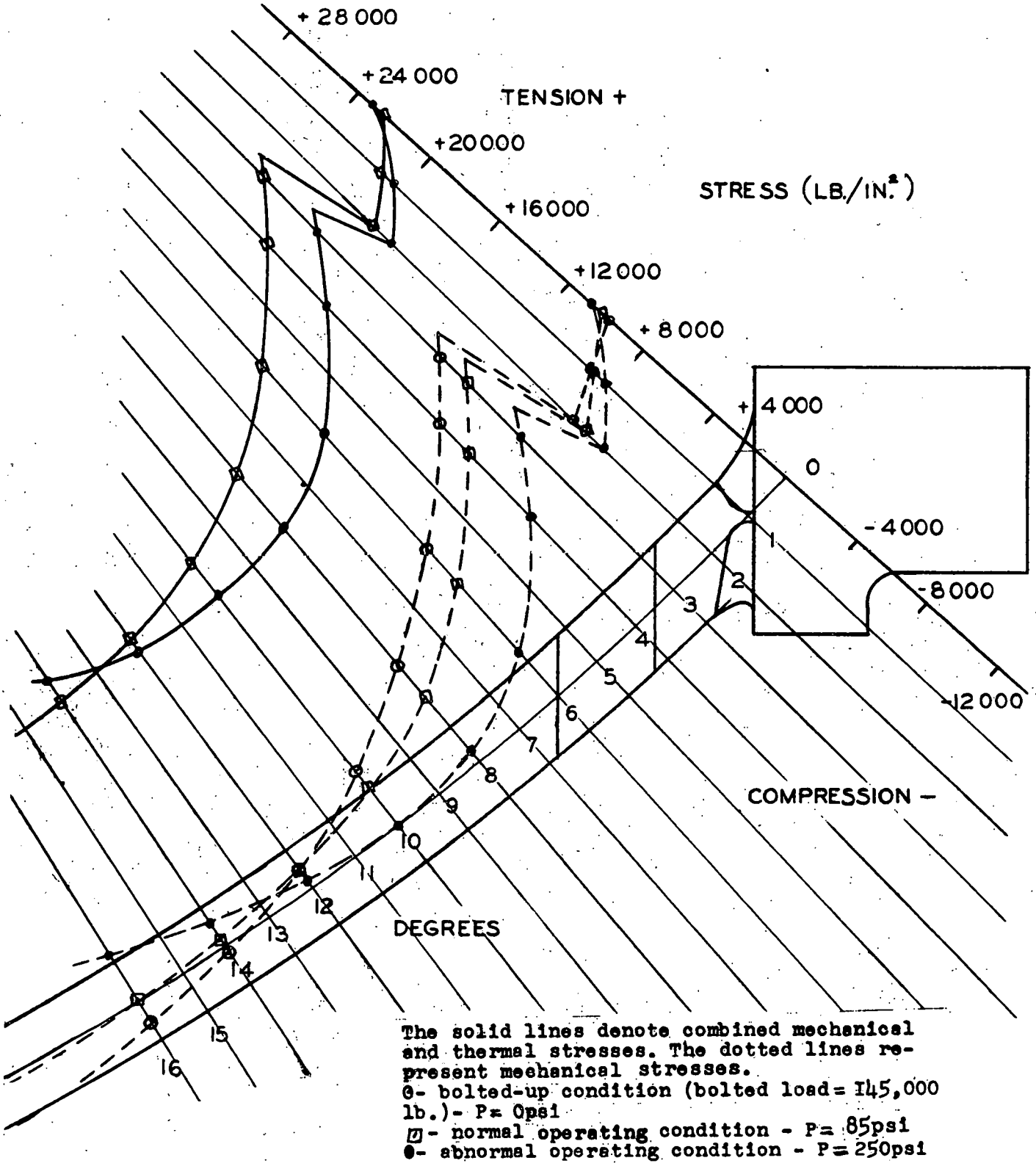

Figure 7.9 - Stress Distribution on Inside Surface of Superheater Grid Plate (43-024-286)

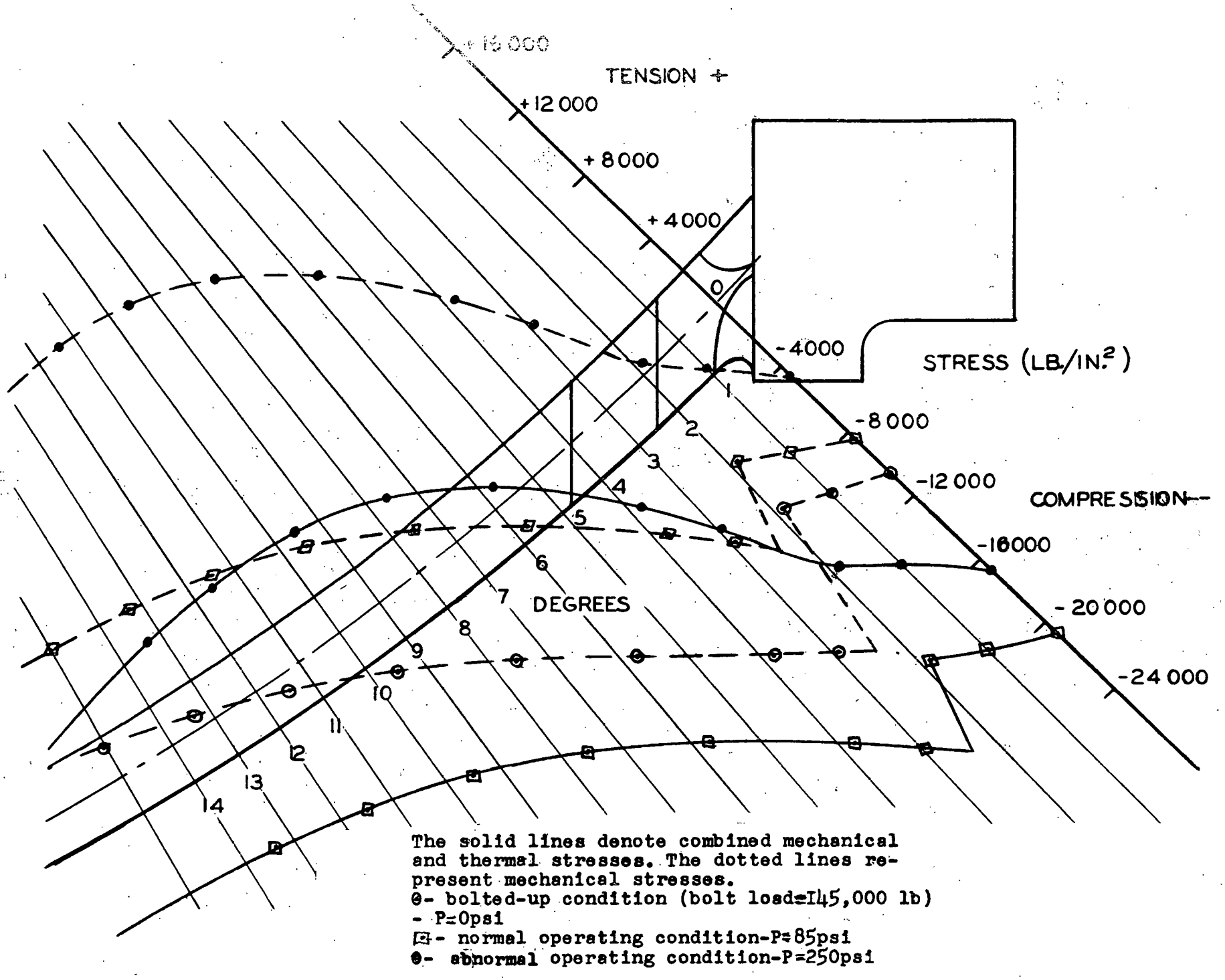

The solid lines denote combined mechanical and thermal stresses. The dotted lines represent mechanical stresses.
⊙- bolted-up condition (bolt load=145,000 lb)
- P=0psi
⊡- normal operating condition-P=85psi
●- abnormal operating condition-P=250psi

Figure 7.10 - Stress Distribution on Outside Surface of Superheater Grid

Plate (43-024-285)

7.3 Superheater Shrouds

Water moderator is directed through the superheater region by an enclosing 316L Stainless Steel shroud between the superheater and boiler regions.

The upper shrouds, 1/8 in. thick, and the lower shroud, 1/4 in. thick, are welded at the top and bottom to the baffles. Both shrouds are subjected to internal pressure during normal operation of the reactor.

The maximum differential pressure exerted on the shrouds by the moderator water within the baffles has been determined from flow calculations. Several methods have been investigated in order to determine the stress and deflection caused by the internal pressure. However, due to the end conditions and the relatively complex geometry, the stress and deflection are not easily calculated.

Since the space between the superheater and the boiler regions is restricted, a test was conducted to determine the maximum deflection of the shrouds when subjected to the maximum possible internal pressure that could occur during reactor operation.

7.3.1 Theoretical Stress Analysis.

Since the superheater is geometrically symmetric, only one-quarter of the baffle need be analyzed. The free body diagram of the section under consideration (Figure 7.11) is given in Figure 7.12.

Through statics, the following relationships can be readily derived:

$$M_B = M_A - PL^2/18$$
$$M_C = M_A + 2\,PL^2/9$$
$$M_D = M_A + PL^2/18$$
$$M_E = M_A + 2\,PL^2/9$$
$$M_F = M_A - PL^2/18$$
$$M_G = M_A$$

By Castigliano's strain energy theorem:

$$\Delta\,\theta = \int_o^{L_1} \frac{Mds}{EI} \qquad (7.18)$$

Since the angle of rotation, θ, is the same at points A and G, the differential angle is zero.

$$0 = \int_o^{L_1} \frac{Mds}{EI}$$

Integration yields:

$$0 = 1/EI \quad (\text{Moment Area}) \; {}_o^{L_1}$$

Summation of the moment areas in the section under consideration and substitution in terms of M_A yields:

$$M_A = -\frac{12}{162}\,PL^2 \qquad (7.19)$$

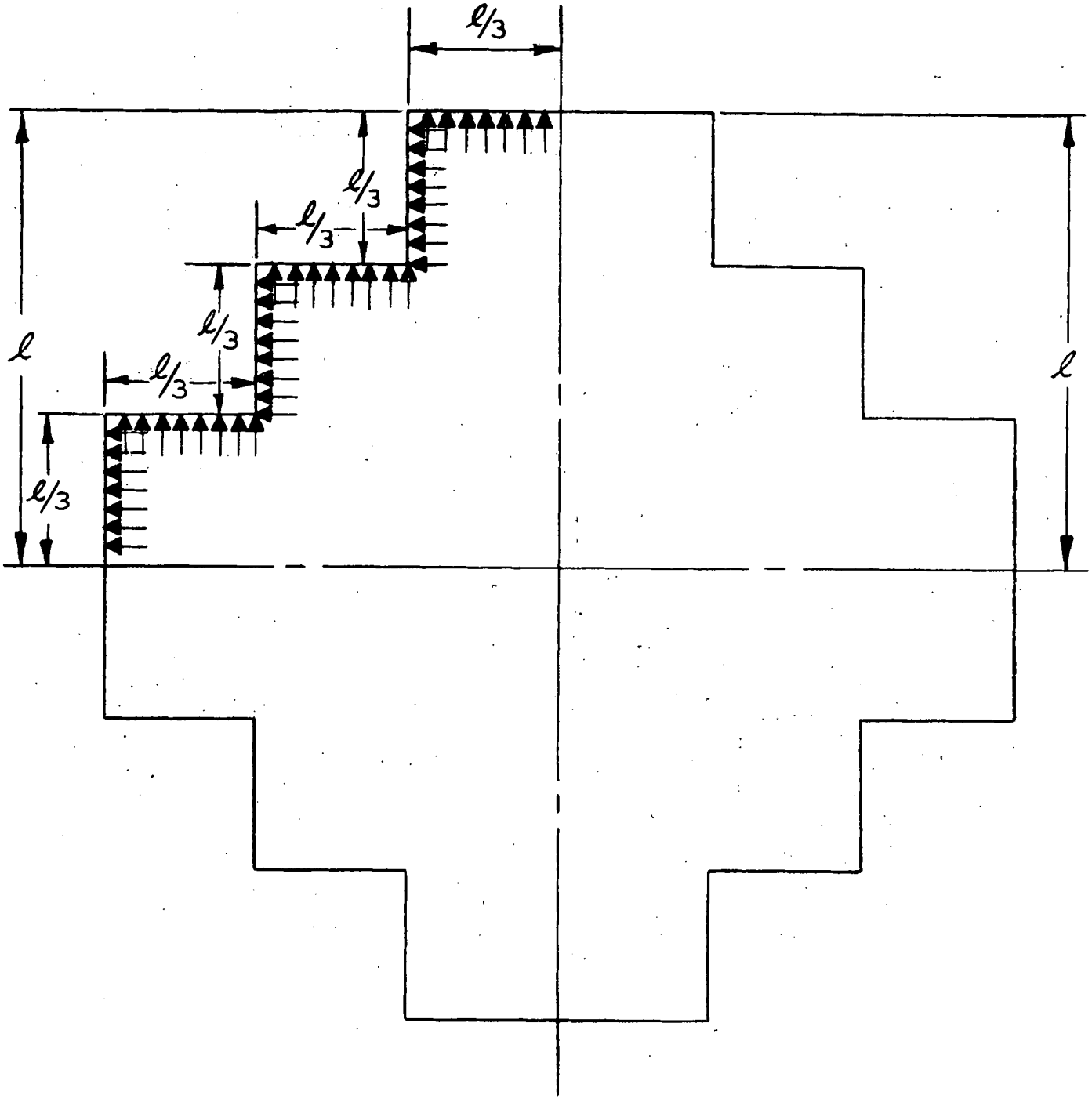

Figure 7.11 - Superheater Baffle Energy Method Analysis (43-025-173)

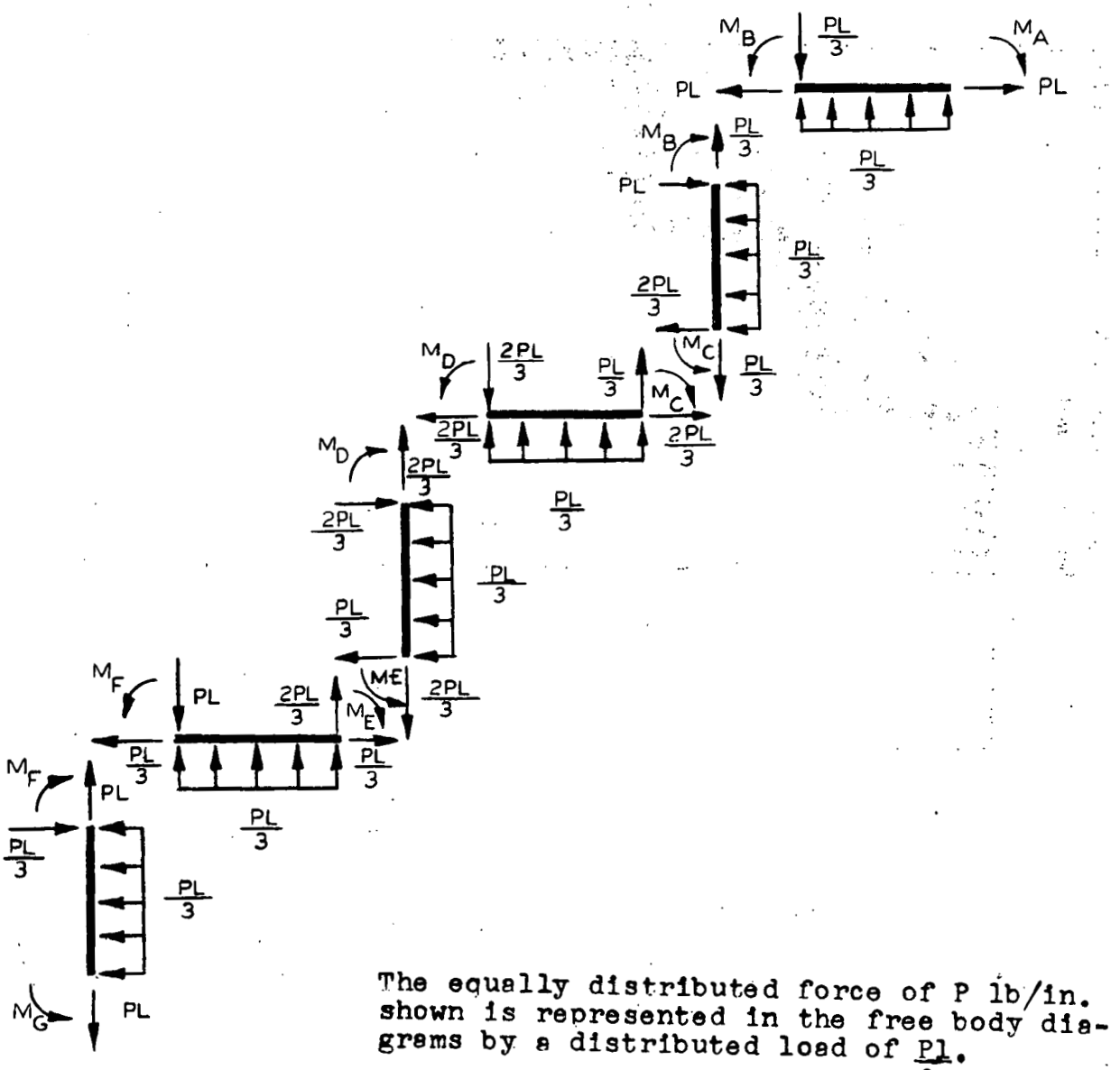

Figure 7.12 - Stress and Deflection Loading Diagrams (Sheet 1 of 3) (43-025-174)

DEFLECTION ANALYSIS

AUXILIARY LOADING DIAGRAM #1

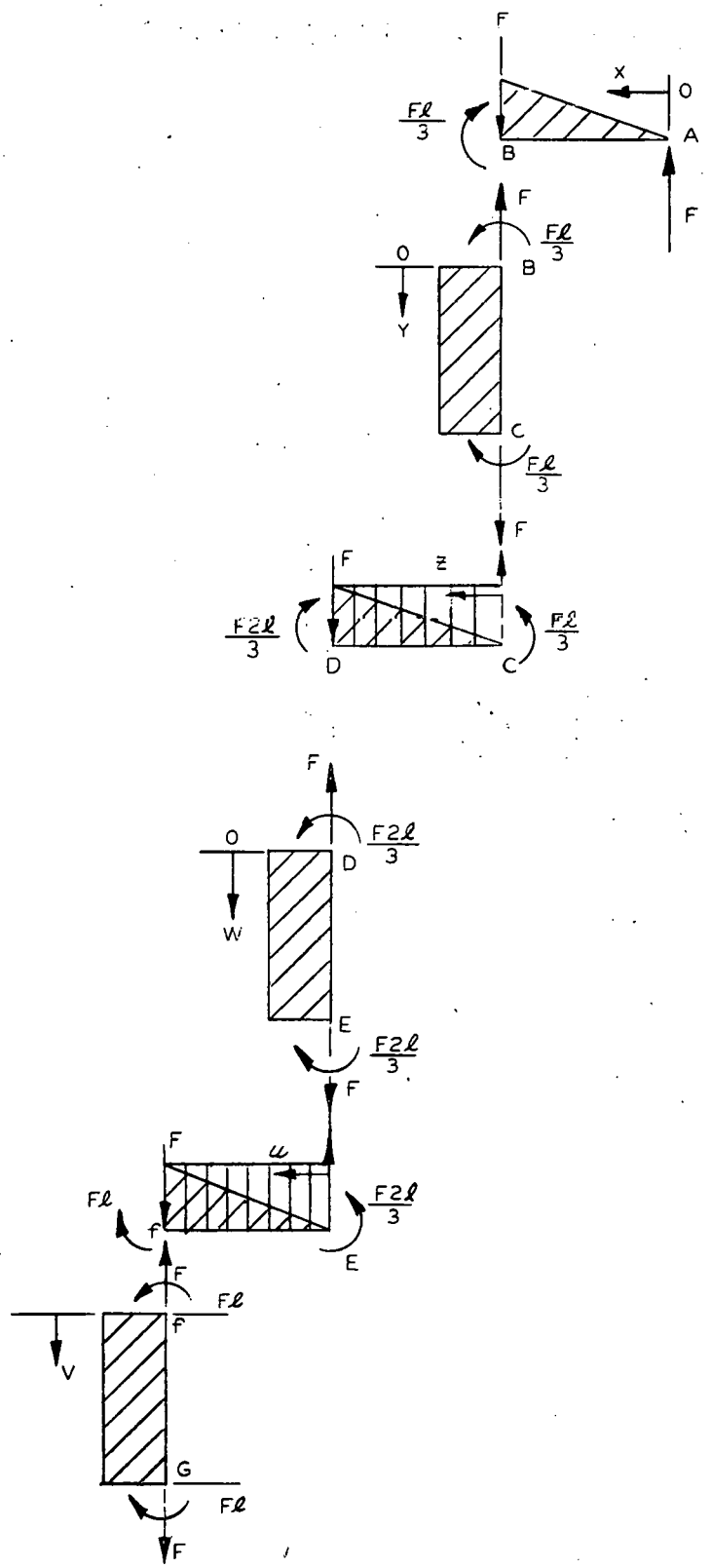

Figure 7.12 - Stress and Deflection Loading Diagrams (Sheet 2 of 3) (43-025-174)

DEFLECTION ANALYSIS

AUXILIARY LOADING DIAGRAM #2

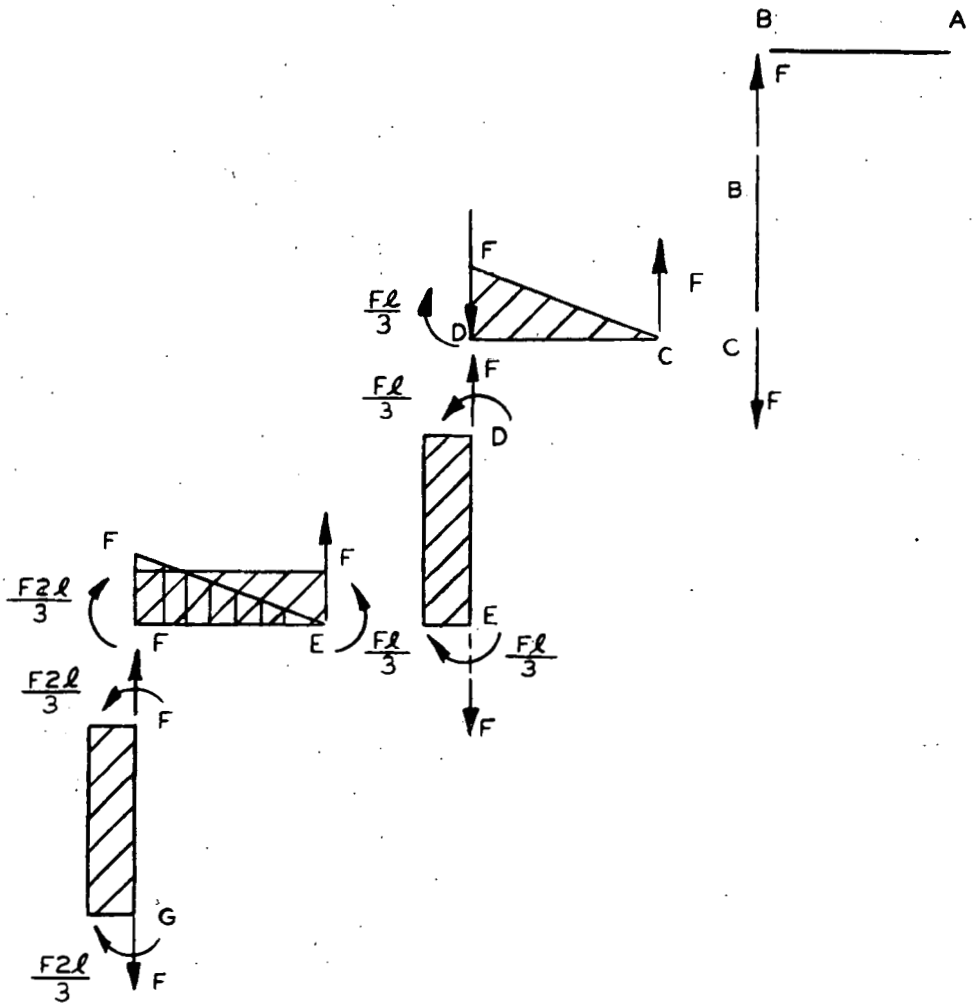

Figure 7.12 - Stress and Deflection Loading Diagram (Sheet 3 of 3) (43-025-174)

Re-substitution yields:

$$M_A = -0.074\ PL^2$$

$$M_B = -0.130\ PL^2$$

$$M_C = +0.148\ PL^2$$

$$M_D = -0.185\ PL^2$$

$$M_E = +0.148\ PL^2$$

$$M_F = -0.13\ PL^2$$

$$M_G = -0.074\ PL^2$$

The maximum stress in the shroud occurs at points C and E.

For A unit length:

$$S = 6\ M/t^2 + F/A \qquad (7.20)$$

Thus, at C and E:

$$S = \frac{0.888\ PL^2}{t^2} + PL/3t \qquad (7.21)$$

7.3.2 Deflection Analysis

Certain simplifying loading conditions are assumed for the section being studied; a section of unit thickness, midway between the end supports.

The effects of the end restraints of this section are considered negligible. (Later tests with an actual shroud proved this assumption wrong.)

An elastic energy analysis was performed on the section shown above (Figure 7.12 sheet 2).

The elastic energy equation for the work done by the force F is:

$$F\,\Delta_A = \int_o^{L1} \frac{Mmds}{EI} \tag{7.22}$$

$$F\,\Delta_A = -\int_A^B Fx\,\frac{Mdx}{EI} - \int_B^C \frac{FL}{3}\,\frac{Mdy}{EI} - \int_C^D \frac{FL}{3}\,\frac{Mdz}{EI}$$

$$-\int_C^D Fz\,\frac{Mdz}{EI} - \int_D^E \frac{2FL}{3}\,\frac{Mdw}{EI} - \int_E^F \frac{2FL}{3}\,\frac{Mdv}{EI}$$

$$-\int_F^G FL\,\frac{Mdv}{EI} - \int_E^F Fv\,\frac{Mdv}{EI} \tag{7.23}$$

Performing the required operations:

$$\Delta_A = \frac{1.0}{EI}\left(\frac{9}{1944}PL^4\right) \tag{7.24}$$

A similar analysis can be performed on point B.

Auxiliary Loading Diagram #2 (Figure 7.12 sheet 3).

The elastic energy equation for the work done by the force F is:

$$F\,\Delta_B = \int_o^{L_1} \frac{Mmds}{EI}$$

$$F\,\Delta_B = -\int_C^D Fz\,\frac{Mdz}{EI} - \int_D^E \frac{FL}{3}\,\frac{Mdw}{EI} - \int_E^F \frac{FuMdw}{EI}$$

$$-\int_E^F \frac{FL}{3}\,\frac{Mdu}{EI} - \int_F^G \frac{2FL}{3}\,\frac{Mdu}{EI} \qquad (7.25)$$

Performing the required operations:

$$\Delta_B = \frac{1.0}{EI}\left(\frac{18}{1944}\,PL^4\right) \qquad (7.26)$$

7.4 Superheater Upper Shroud

Water moderator is directed through the Pathfinder superheater region by a closed stainless steel shroud located between the superheater and the boiler regions. The pressure exerted by the water moderator within the shroud causes deflection of the shroud. Since the space between the baffle and the boiler fuel boxes is restricted, assurance is necessary that the maximum deflection that occurs during the most severe conditions is not excessive. Shroud deflections were determined by experimental techniques since they were not amenable to DIRECT calculation due to the complex geometry.

7.4.1 Deflection Test

A test was conducted to determine the maximum deflection of the superheater shroud when subjected to the maximum conceivable internal pressure. The test was performed with the upper half of the shroud since it represents the thinnest and hence the more critical section.

Test Set-Up (See Figure 7.13). The shroud was set up vertically and was closed at the ends by two flanges. The seals between the flanges, at the top and bottom of the shroud were provided by two rubber gaskets. The gaskets were compressed by four bolts between the two flanges.

The deflection was measured with dial indicators mounted at the various points at mid-elevation on the shroud. Compressed air, controlled with a pressure regulator, was supplied to the closed shroud. The pressure was read on a calibrated gage and a manometer.

Test 1 The top and bottom edges of the shroud were free to expand in the radial direction, since the reaction of the gaskets was negligible.

Run 1

1. Each dial indicator was set at zero for zero pressure.
2. The pressure was increased at 0.5 psi increments up to 1.5 psig.

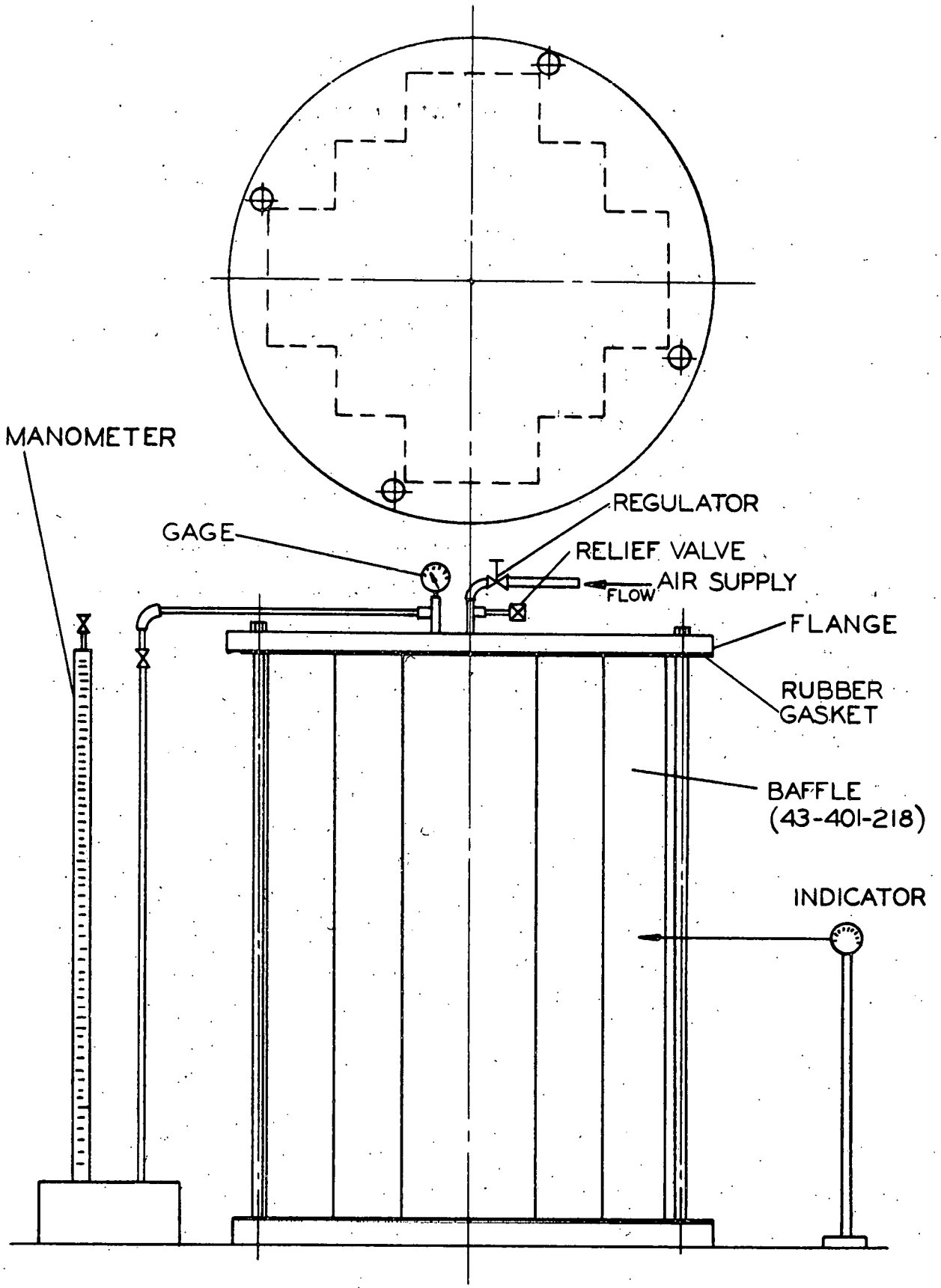

Figure 7.13 - Test Set-Up for Baffle Pressure Test (43-025-178)

3. The pressure and dial indicator readings were recorded.
4. The pressure was dropped to zero and dial indicator readings recorded.

Run 2

5. The dial indicators were reset at zero for zero pressure.
6. The pressure was increased at 0.5 psig increments up to 1.5 psig.
7. The pressure and dial indicator readings were recorded.

Discussion of Test I Results. Test results are given in Figure 7.14. The test results for the first run indicated that local yielding occurs at pressures between 1.0 and 1.5 psig. The permanent offset was about 0.025 in. During the second run, the deflection was a straight line function of pressure (δ (f) P); this function had the same slope as run I before yielding occurred.

The maximum deflection occurs at the four corners labeled 6; the radial displacement was nearly the same over the whole length of the shroud from top to bottom.

Test 2 In order to reproduce more closely the end conditions that are encountered when the shroud is welded to the baffles at the top and bottom edges, additional supports were provided.

The top and bottom edges were held in 16 places at locations 1, 4, 6, and 8 (Figure 7.15) to prevent radial displacement at the ends, but the ends were free to rotate, being simply supported at the edges.

The radial supports were provided by bolts screwed into nuts that were clamped to the flanges. Dial indicators were mounted at the top and bottom edges, near the supported points, in order to control the pre-compression in the shroud when the radial supporting bolts were installed. The pre-compression was limited to about 0.002 to 0.004 in. when the shroud and the radial supporting bolts were in contact at zero pressure.

1. The dial indicators at the top and bottom edges were set at zero for zero pressure.
2. The pressure was increased from zero to 0.5 psig; then the dial indicators located at mid-elevation of the shroud were set at zero, thus insuring an equal contact force at each supported point. The dial indicators at the top and bottom edges were not reset; the readings for the above conditions were basically zero.
3. The pressure was increased from 0.5 to 2.5 psig. The readings of the dial indicators at mid-elevation were recorded.
4. The pressure was decreased from 2.5 to 0.5 psig; the readings of the dial indicators at mid-elevation were recorded.

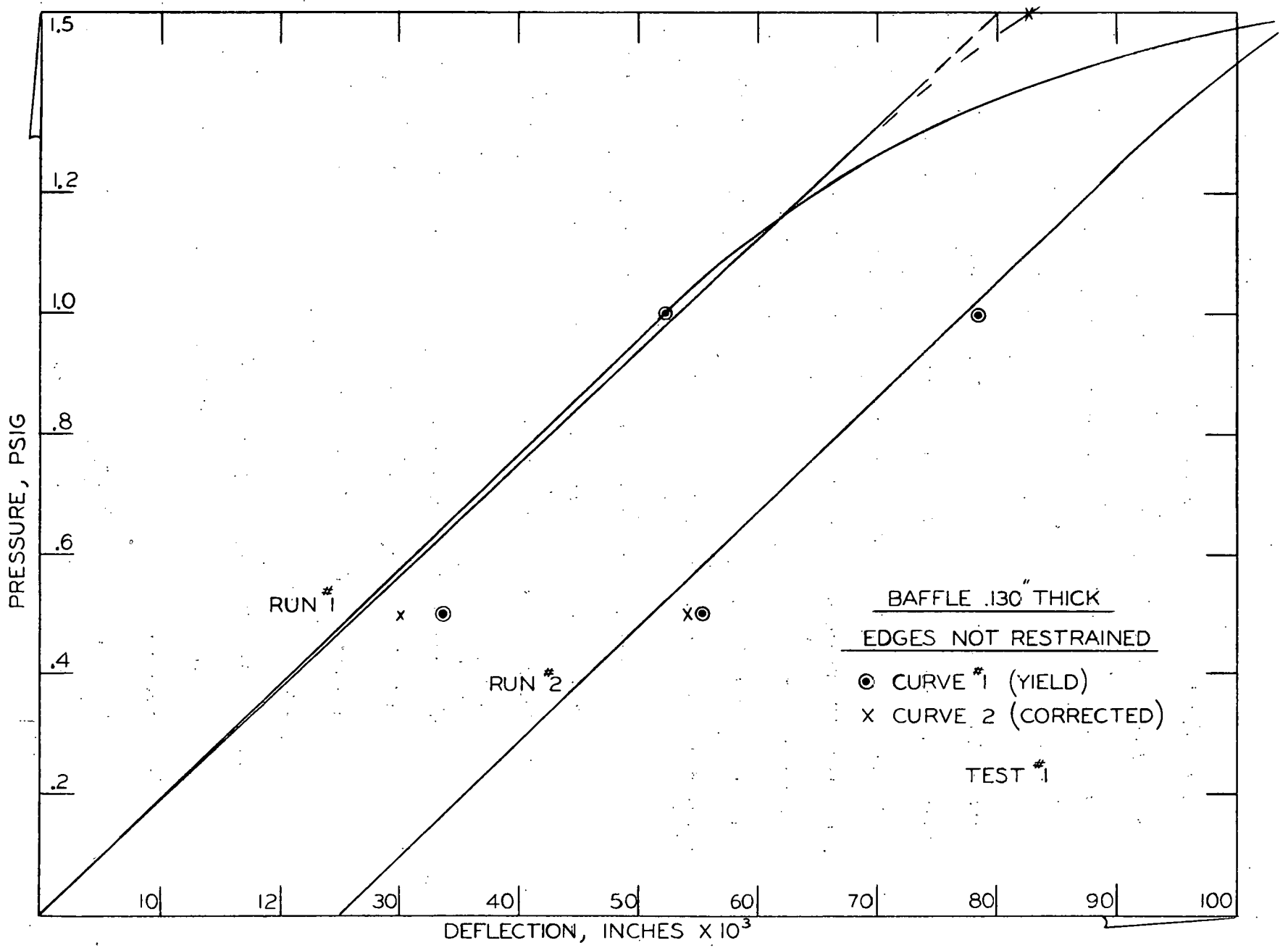

Figure 7.14 - Plot of Baffle Deflection vs Internal Pressure Edges not Restrained (43-025-179)

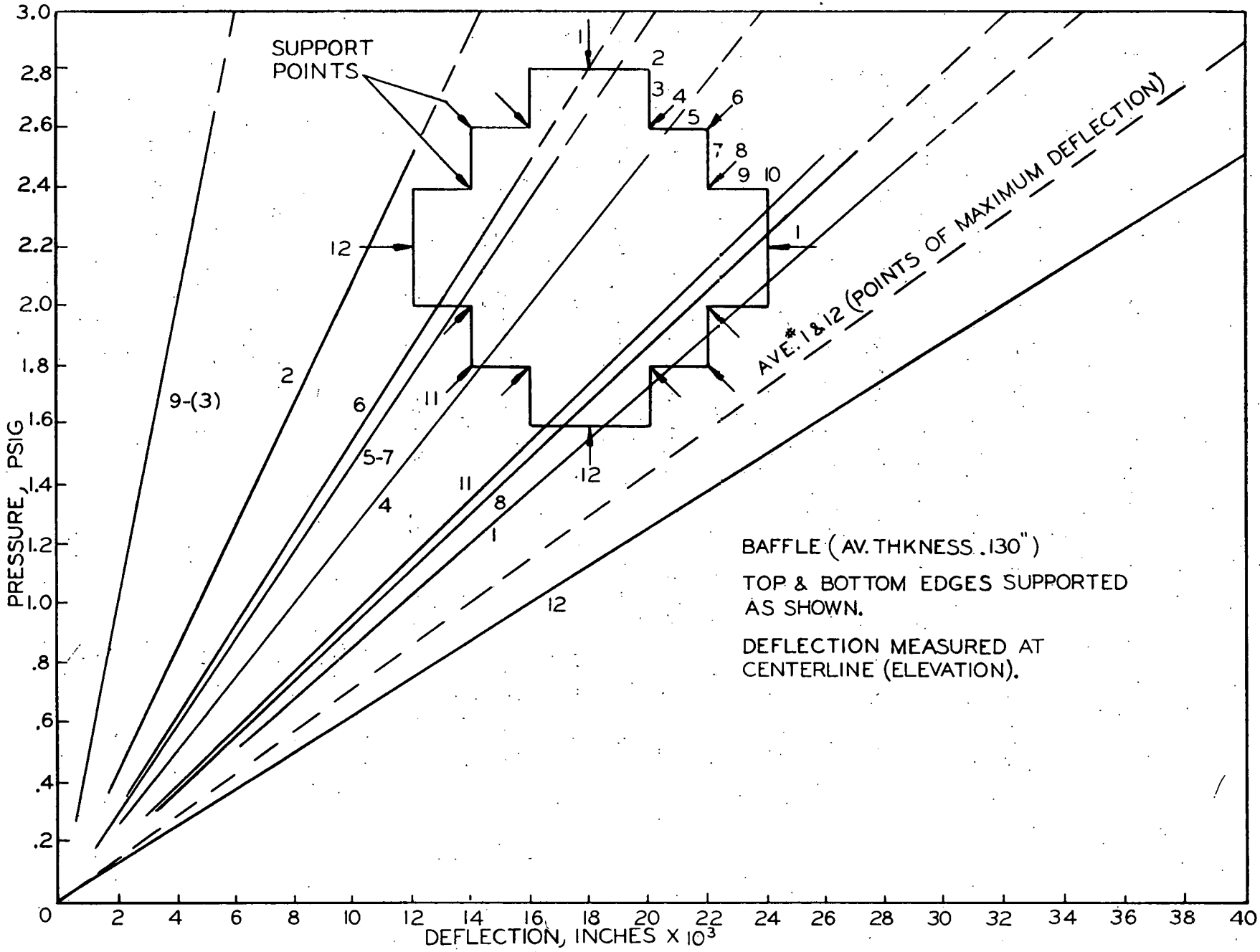

Figure 7.15 - Plot of Baffle Deflection vs Internal Pressure Edges

Restrained at Sixteen Locations (43-025-18C)

5. The pressure was decreased from 0.5 to 0 psig; the readings of the dial indicators at mid-elevation were recorded.

Discussion of Test 2 Results. The test results are given in Figure 7.15; pressure cycles from 0.5 to 2.5 psig were made several times; at 0.5 psig, the dial indicators readings were consistently near the original setting of zero. At the edges, the radial displacement was zero at the supported points, then increased to a maximum at mid-elevation.

The maximum deflection was measured at mid-elevation of points 1 and 12. A radial displacement of about 0.005 in. of the whole shroud was observed during the pressure testing, which accounts for the deflection difference between points 1 and 12.

Since the dial indicators at mid-elevation were set at zero for 0.5 psig, the deflection readings at 2.5 psig were increased by the compression readings observed at zero pressure as shown below:

EXAMPLE:

	Pressure (psig)	Deflection (in.)
Point 1	2.5	0.022
	0.5	0.000
	0	-0.007
Total Deflection at 2.5 psig		0.029

Conclusion. From the preceeding tests, it has been shown that the end conditions of the structure influences greatly the shape and magnitude of the radial deformation. In the reactor, when the shroud is in place in the superheater, the top and bottom edges are welded to the baffles, thus the edges are built in reducing the deflection at the mid-elevation of the shroud.

The tests conducted did not exactly duplicate the actual case since the edges were simply supported at various points, as indicated in Figure 7.15, instead of being built in. The maximum deflection measured at the mid-elevation of the shroud is 0.028 in., at maximum expected pressure of 2 psig, and is satisfactory to avoid interference of the reactor internal parts during operational conditions.

7.5 Steam Line and Superheater Support

The superheater vertical support within the reactor vessel is provided by the double-walled steam line header. The steam line, made of 304L Stainless Steel, 1/2 in. thick, is welded to the reactor vessel penetration sleeve and guided at the superheater flange elevation by eight radial supports (Fig. 7.16).

The inner liner sleeve, made of 304L Stainless Steel, is welded at the top to a ring attached to the steam line, and guided at the bottom with 4 radial supports. The liner cone, made of 304L Stainless Steel, is welded at the bottom to the same ring to which the liner sleeve

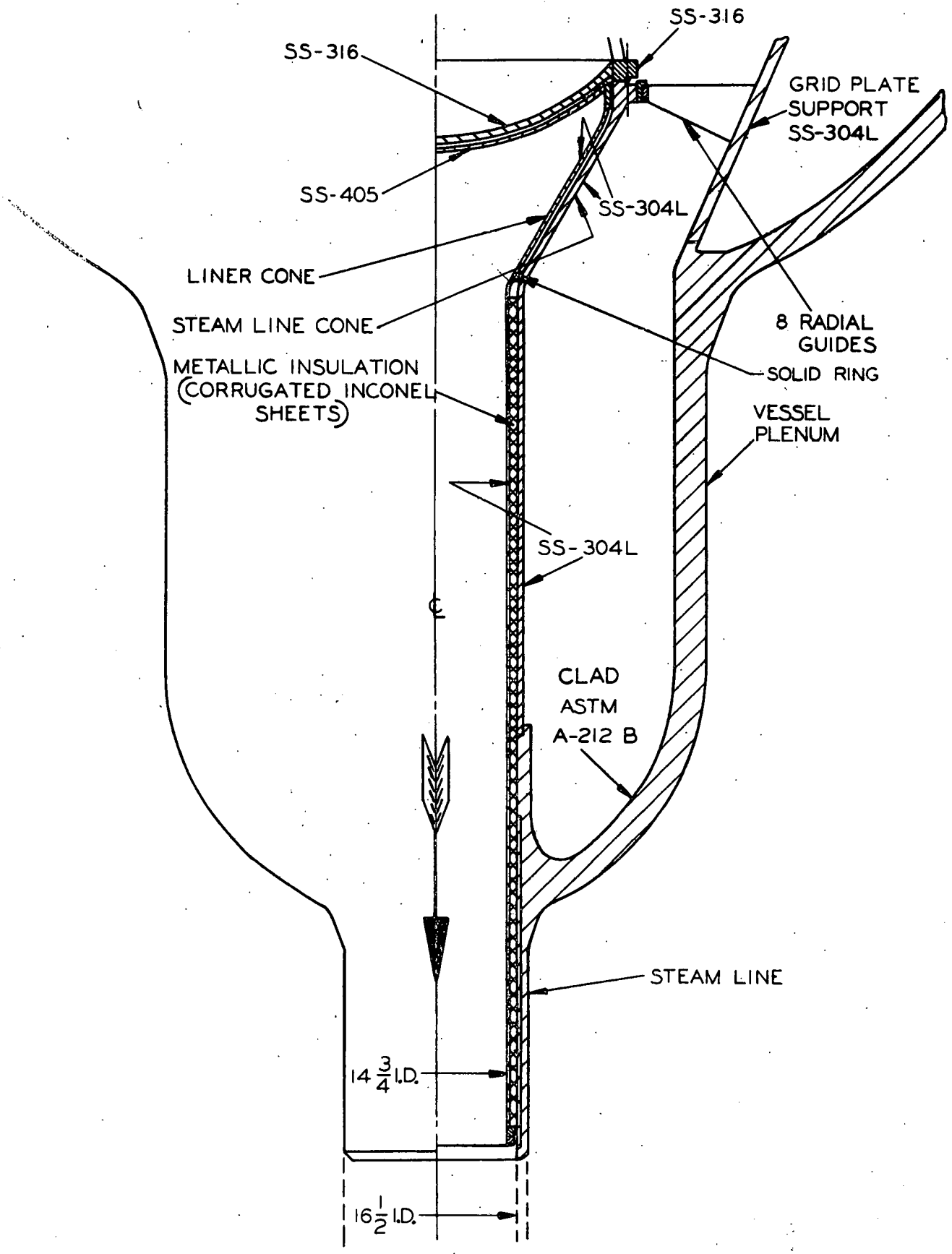

Figure 7.16 - Pathfinder Superheater Design Steam Line (43-025-184)

top is welded. The solid ring separates the two gaps formed by the liner cone and sleeve, thus preventing heat transfer by forced convection.

A metallic insulation made of corrugated Inconel sheets (thermal conductivity one Btu/hr-ft^2 ^oF/in.) was installed between the liner and the steam line over the whole length of the sleeve and at the upper cylindrical portion of the cone near the flange as shown in Figure 7.16.

Approximate calculations have been made to determine the heat transfer losses across the double-walled steam line header. The heat flux has been plotted versus the steam gap thickness between the liner and the steam line, with and without insulation. (Fig. 7.17).

7.6 Superheater Natural Frequencies

The superheater assembly and its support (steam line within the reactor plenum) was analyzed as a vertical beam 306 in. long having variable cross sections along its longitudinal axis.

The internal parts of the superheater, such as insulating tubes and fuel tube assemblies, were assumed to increase the mass but would not contribute to the rigidity of the superheater; the mass of the water in and around the tubes was neglected.

The system was divided into 78 sections; the weight, and the smallest geometrical moment of inertia in respect to the neutral axis of the system were calculated for each section. The system was programmed

to determine the first three natural frequencies of each of the three cases below using the IBM-704 digital computer.

The bottom section, where the steam line penetrates the reactor vessel, was assumed as built in. Thus the deflection and the rotation at this section is equal to zero. The superheater and steam line flanges 66 in. from the bottom were simply supported, preventing the lateral deflection but not the rotation. The upper end was supported as indicated in the following three cases:

1. Top end free

1st frequency	749 cpm
2nd frequency	3638 cpm
3rd frequency	10724 cpm

2. Top end simply supported

1st frequency	2323 cpm
2nd frequency	8079 cpm
3rd frequency	18135 cpm

3. Top end - flexible support (See Figure 7.18) (Spring constant 31,200 lb/in.)

1st frequency	1129 cpm
2nd frequency	5960 cpm
3rd frequency	14758 cpm

The third case is retained since it represents the actual superheater fixity condition. The flexible support at the chimney is provided by

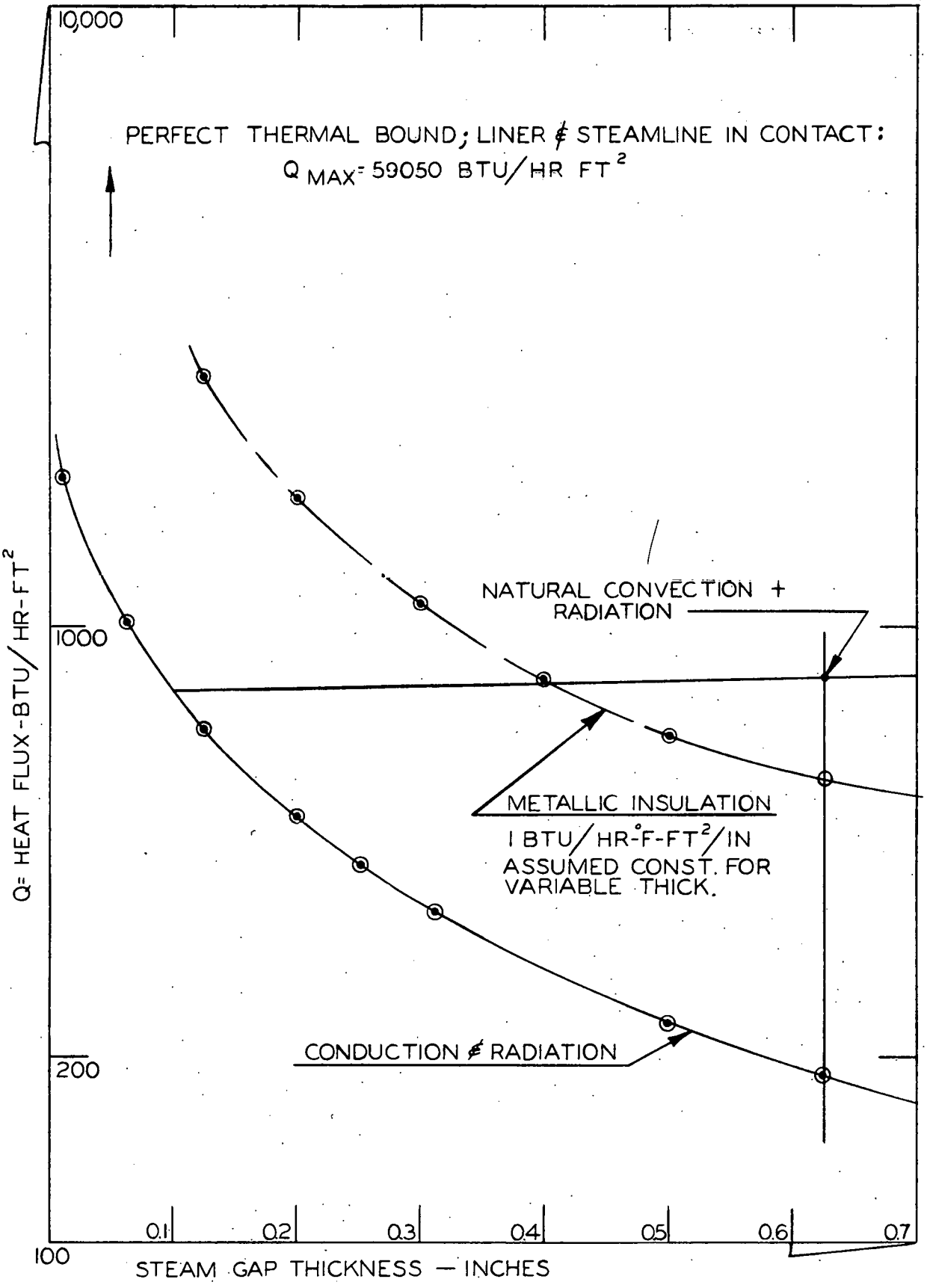

Figure 7.17 - Plot of Heat Flux vs Steam Gap Thickness for Steam Line Header (43-025-182)

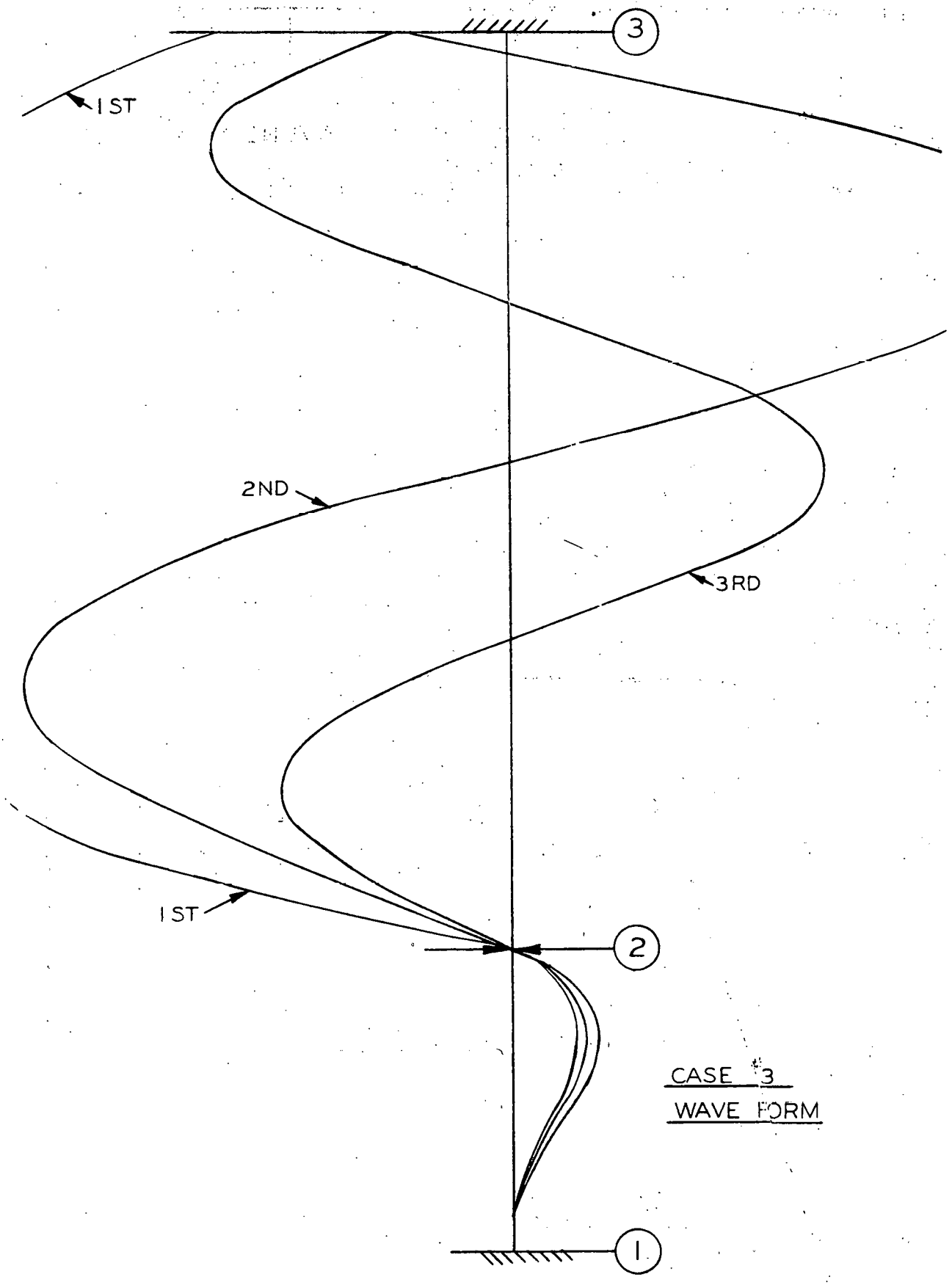

Figure 7.18 - Superheater Vibration Analysis Forms (43-025-183)

the attachments to the steam dryer, for which the spring constant has been determined analytically.

The forcing frequencies which are inherent in the recirculation system are that of the pump rotational speed, 585 cpm, and that of the 5 impeller blades X the rotational speed, or 2925 cpm.

Although, the natural frequencies of the superheater are near an even integer of the forcing frequencies it is improbably that a state of resonance could exist, because of the high turbulence of the water within the reactor plenum.

7.7 Superheater Tube Vibration Test

The purpose of this test was to determine the frequency and magnitude of vibrations of the superheater outer container tubes due to cross and parallel, single and two-phase flow between tubes at various flow velocities.

Test Section (Figure 7.19) was designed to reproduce the geometry and end fixity of the Pathfinder superheater container tubes. The test lattice (Figure 7.20) consisted of a vertical bundle of sixteen tubes rigidly attached to an upper and lower tube sheet and spaced between the tube sheets by four baffles. The lattice was enclosed in a box 4-15/16 in. x 4-15/16 in. inside cross section and 16 ft long. One side of the box was removable, so that the lattice could be inserted.

The sixteen tubes of 304 Stainless Steel were disposed on a square pitch of 1.234 in. the tubes were 192 in. long, 1.080 in. O D with 0.020 in. thick wall except for a 20 in. length at the bottom. The bottom 20 in. was tapered to 0.800 in. O D with 0.023 in. thick wall. At the upper part of the lattice, the tubes were rigidly attached to the 1.0 in. thick tube sheet by fusion welding; the tube sheet was bolted to the end of the box, thus closing the end of the test section. At the bottom, where the tubes were 0.800 in. O D, shoulder type plugs were welded to the tubes; these plugs were threaded in the section that passed through the tube sheet. Nuts were tightened until the tube sheet rested against the shoulder of the plug, providing a semi-rigid end fixity for the tubes. The baffles located between the tube sheets were simply supported in the box. In each baffle, nine sharp-edged orifices on a square pitch spacing of 1.234 in. were centered over the flow channel between the tubes. Each baffle was removable and its elevation could be changed. The transition, intermediate, and upper baffles were also used to regulate the amount of water passing through the tube bundle.

The inlet section was formed by an 8 in. diameter enclosing two sides of the box over a 26 in. length. Two openings 90 degrees apart were cut in the box, thus forcing the water into the tube bundle horizontally.

The channel formed by the box flange and the inside diameter of the 8 in. pipe was such that the velocity at the throat of the plenum duplicated the water velocity at the Pathfinder superheater steam line flange. The discharge section was formed by a 10 in. pipe enclosing three sides of

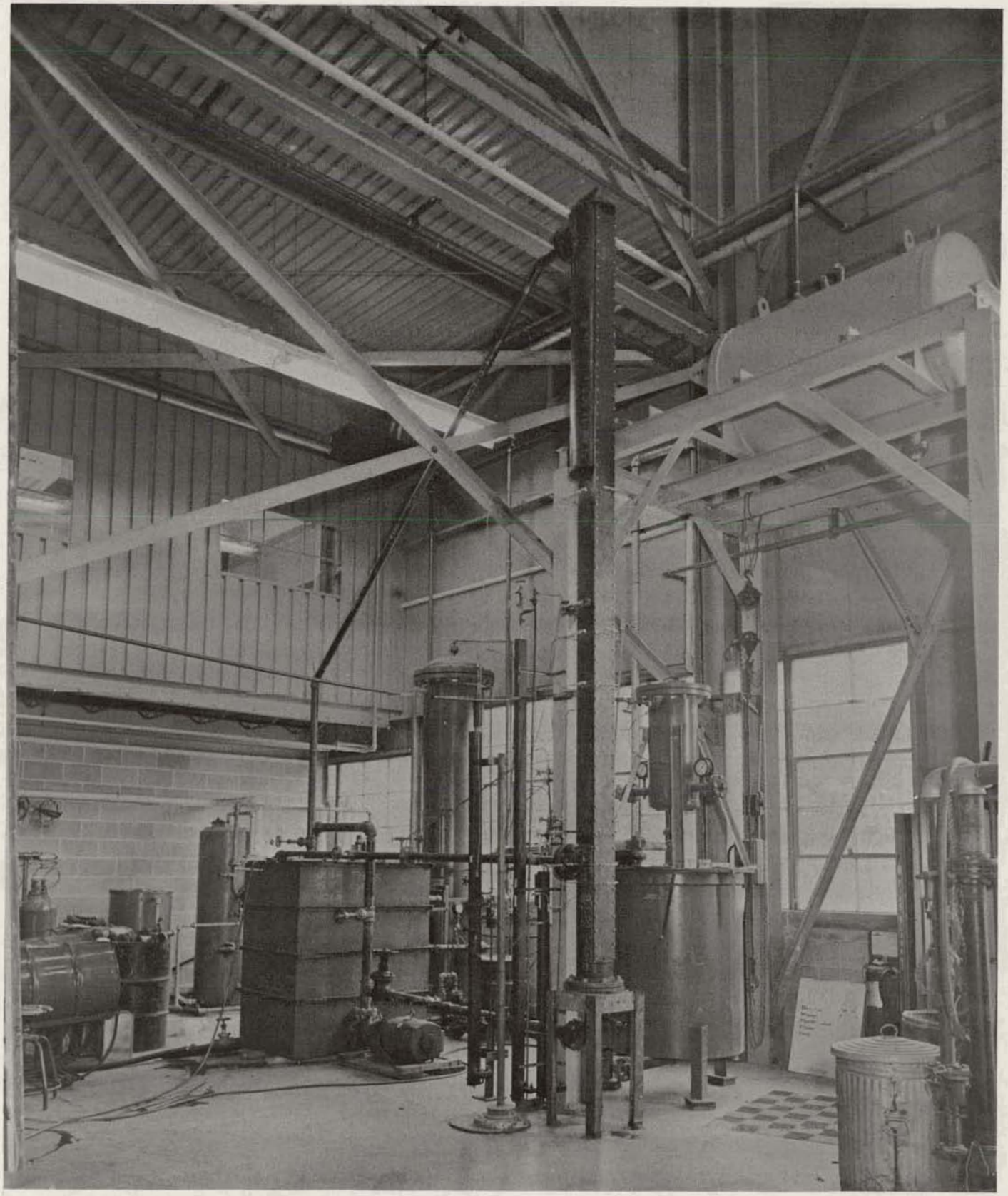

Figure 7.19 - Superheater Tube Vibration Test Loop (210764)

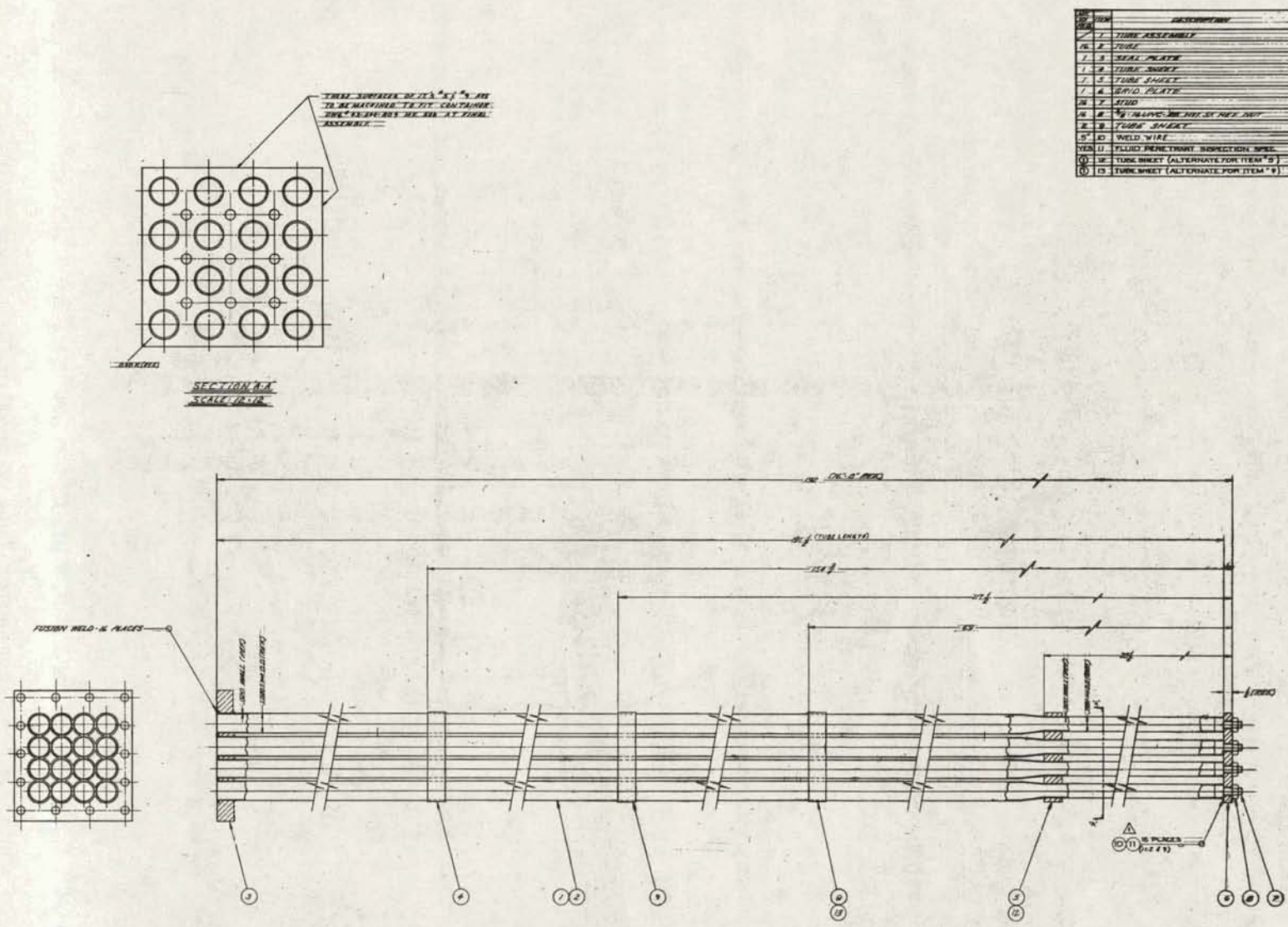

Figure 7.20 - Superheater Vibration Test Section (43-500-794)

the box over a 69 in. length; sixteen openings were cut in two sides of the box 90 degrees apart thus forcing the water out horizontally.

At the intermediate and upper baffles where the tubes were 1.080 in. O.D, the net channel area was 9.73 sq. in.; the equivalent diameter, De, was 0.715 in.

At the transition baffle where the tubes were 0.800 in. o.d., the net channel area was 16.36 sq in.; the equivalent diameter, De, was 1.625 in.

Test Set-up. The test section was placed in a calibrated closed loop constructed of 2-1/2 in. standard pipe with bolted flange connections. The water was recirculated from a suction discharge tank of 500 gal capacity through the loop and test section with an Allis-Chalmers centrifugal pump, Model C-3, size 3 in. x 2-1/2 in. rated at 240 gpm, 150 ft head.

The water flow was measured by reading the pressure differential across a calibrated orifice plate with radius taps connected to a mercury differential manometer. The orifice plate was inserted between two flanges on the 2-1/2 in. pipe connecting the pump to the test section. The water flow was controlled with a by-pass valve inserted between the pump discharge and the orifice plate, and a throttling valve inserted in the test section discharge pipe.

Instrumentation. A novel technique was developed to install the strain gages inside the tubes. This eliminated the necessity for waterproofing. The leads were taken out the open upper end of the tube. The gages were located 147 in. from the upper tube sheet (midway between the transition and intermediate baffles). The unsupported length between the two baffles was 47-1/2 in.

The natural frequency of vibration of the tubes was detected by two strain gages arranged in a Wheatstone bridge circuit. The vibration signal was fed to an amplifier and strain gage indicator, and then through a decade amplifier that was connected to an oscilloscope.

To measure the amplitudes of vibration, the signal was fed to the oscilloscope through an amplifier. A static deflection calibration of the oscilloscope was made.

A calibration of the strain versus deflection was made by measuring the tube deflection with a dial indicator and recording the strain on the strain gage indicator. The amplitides of vibration were also recorded with a pen recorder. The output signal of the bridge was amplified and fed to the recorder.

Test Procedure and Results. Measurements were taken to determine the natural frequency of the test section in air under three conditions:

1. With the tube lattice suspended,
2. With the tube lattice inserted in the box but without the cover, thus providing lateral support to tube sheets and

baffles on three sides.

3. With the tube lattice installed in the containment box with the cover bolted in place providing lateral support of all baffles on all sides.

Vibrations were induced by sharply striking baffles or containment box. The oscilloscope responses for the three cases are shown in Figure 7.21, 7.22 and 7.23. The natural frequency of the tube lattice suspended in air was 25 cps; the frequency of the lattice in air supported on three sides was 68 cps; the frequency in air supported on four sides was 70 cps.

Attempts were made to determine the natural frequency in water by striking the box with a hammer, but the amplitudes of vibration were so dampened that the oscilloscope showed no signal.

Tests were conducted to determine the frequency of vibration due to a single-phase flow and due to two-phase (air and water) flow. For single-phase tests, the water flow was varied from 95 to 190 gpm through the test section. For two-phase tests, the flow varied from 120 to 204 gpm of air included. The oscilloscope response for these tests are shown in Figures 7.24, 7.25, 7.26 and 7.27. The frequency in all cases was 60 cps.

Tests were conducted to determine the interference frequency. The magnification of the vertical vernier was decreased. With the pump running but no water circulating in the test section, the frequency was 60 cps.

Under the same conditions with 190 gpm of water passing through the test section, the frequency was 60 cps. Oscilloscope responses for these cases are shown in Figure 7.28 and 7.29.

A test was conducted to determine the natural frequency of the tube lattice in air with the intermediate baffle removed and with the lattice supported in the box. This arrangement provided an unsupported tube length between the transition and upper baffle of 94 in. The natural frequency in air was 22.5 cps. Oscilloscope response is shown in Figure 7.30.

Tests to determine the natural frequency in water were not successful. Tests to determine the vibration frequency with single- and two-phase flow were also unsuccessful because of a 60 cps interference frequency.

The dynamic deflection of tubes during vibration was based on a static deflection where 1 cm on the oscilloscope screen is equal to 0.027 in. deflection. With no flow, the width of the beam on the oscilloscope screen, e_1, was 0.11 cm (Figure 7.31). The dynamic deflection,

$$\delta_x = \frac{e_x - e_1}{2} \times 0.027 \qquad (7.27)$$

where,

e_x = beam width at flow, Q_x

e_1 = beam width at zero flow

Oscilloscope responses for all tests with the intermediate baffle in place are shown in Figures 7.32 through 7.35. Response for tests with intermediate baffle removed are shown in Figures 7.36 through 7.38.

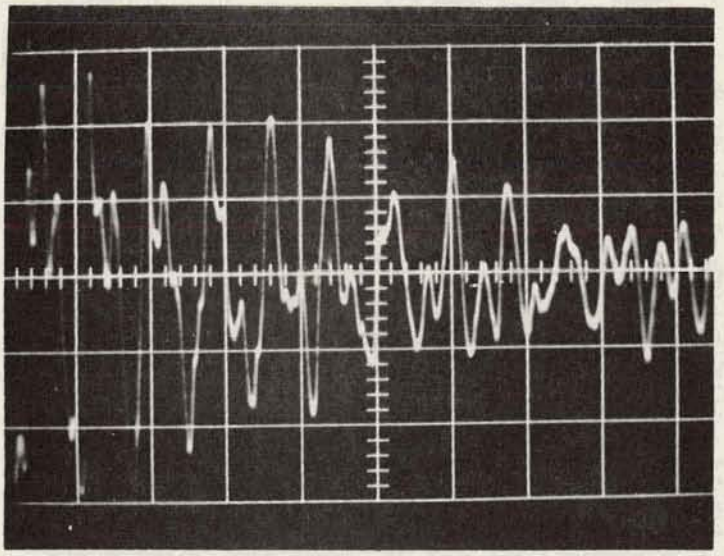

Figure 7.21 - Vibration of Tube Bundle Suspended in Air 2cm = 0.1 f_n = 25 cps

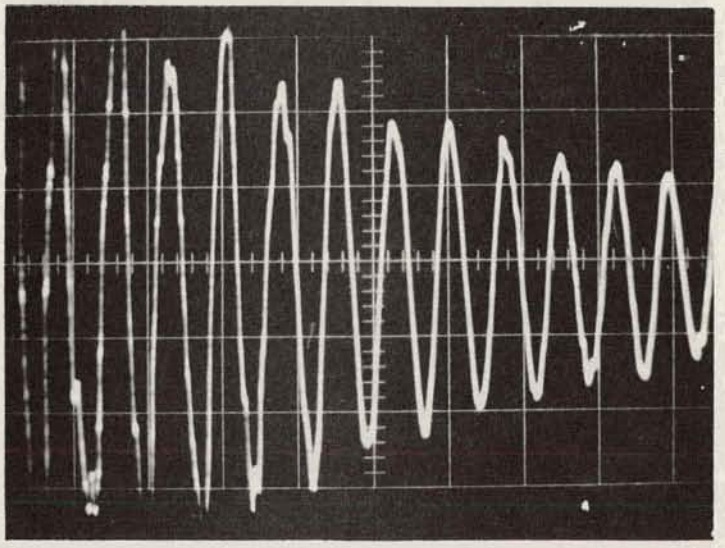

Figure 7.22 - Vibration of Tube Bundle in Air with Tube Sheets Guided on Three Sides 5 cm = 0.1 sec., f_n = 68 cps.

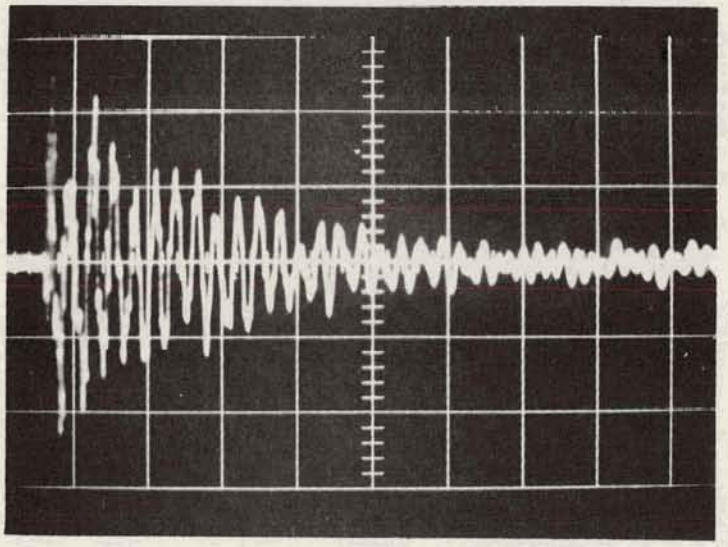

Figure 7.23 - Vibration of Tube Bundle in Air with Tube Sheets Guided on Four Sides 2 cm = 0.1 sec f_n = 70 cps

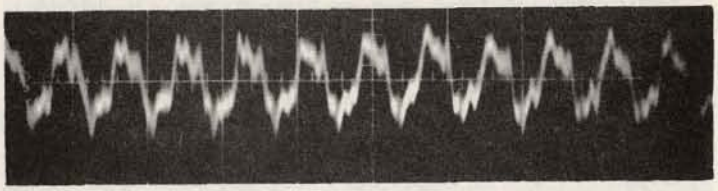

Figure 7.24 - Tube Vibration with 69 GPM and 3.15 FPS Water Flow
5 cm = 0.1 sec f_n = 60 cps

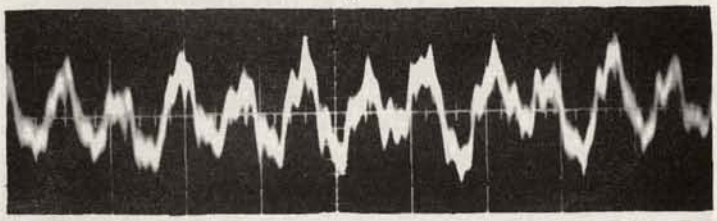

Figure 7.25 - Tube Vibration with 190 GPM and 6.30 FPS Water Flow
5 cm = 0.1 sec f_n = 60 cps

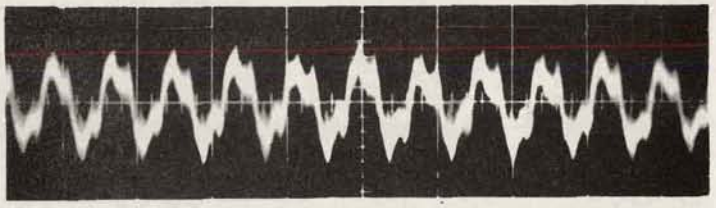

Figure 7.26 - Tube Vibration with 96 GPM and 4 FPS Water Flow and 24 GPM Air Flow
5 cm = 0.1 sec f_n = 60 cps

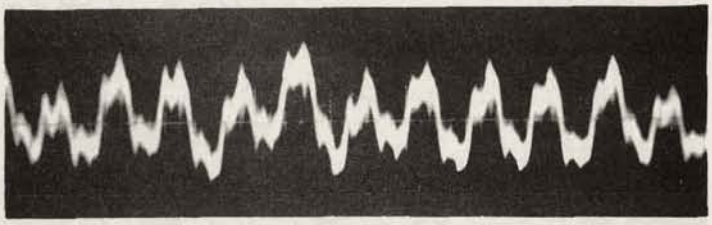

Figure 7.27 - Tube Vibration with 180 GPM and 6.75 FPS Water Flow and 24 GPM Air Flow
5 cm = 0.1 sec f_n = 60 cps

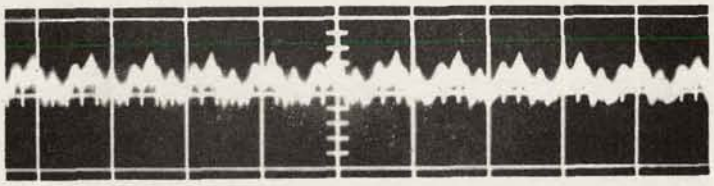

Figure 7.28 - Interface Frequency. 5 cm - 0.1 sec f_i = 60 cps

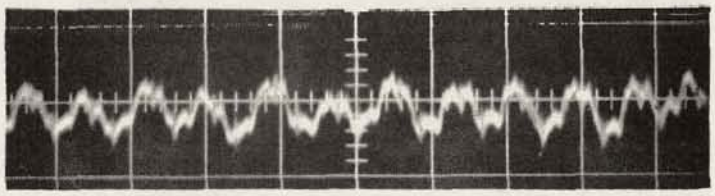

Figure 7.29 - Interference Frequency with 190 GPM Water Flow
5 cm = 0.1 sec f_i = 60 cps

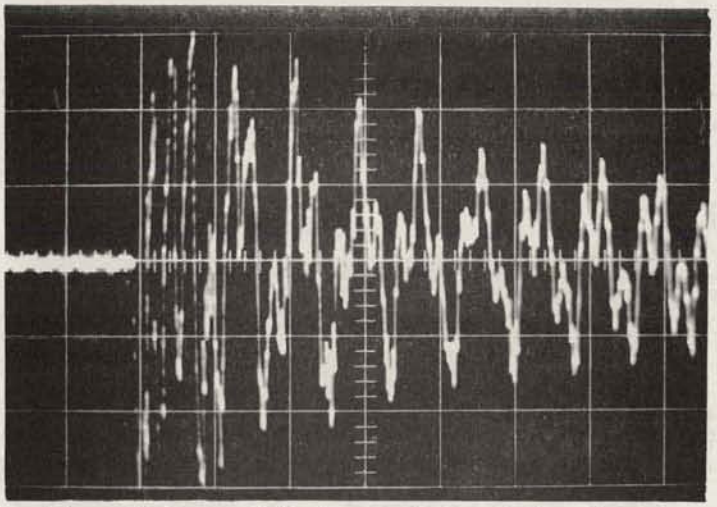

Figure 7.30 - Vibration of Tube (94 in. Between Tube Sheets) Suspended in Air
2 cm = 0.1 sec f_n = 22.5 cps

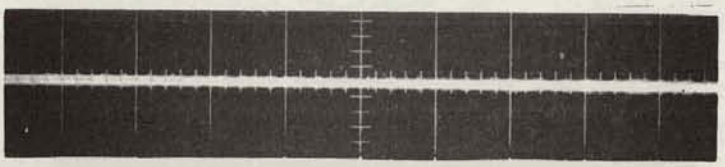

Figure 7.31 - Calibration Beam. 2 cm = 0.027 in. Deflection
el = 0.11 cm δ = 0

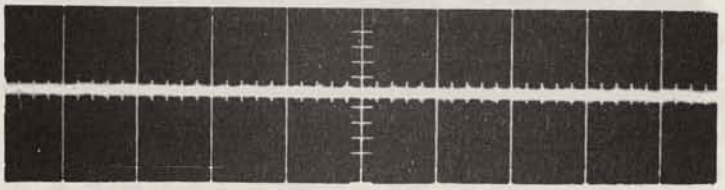

Figure 7.32 - Deflection with Single Phase Flow 96 GPM and 3.15 FPS
e_x = 0.13 cm δ = 0.00027 in.

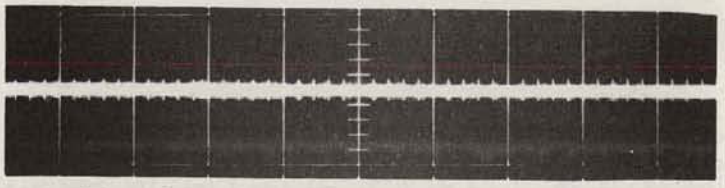

Figure 7.33 - Deflection with Single Phase Flow 190 GPM and 6.3 FPS
e_x = 0.15 cm δ = 0.000054 in.

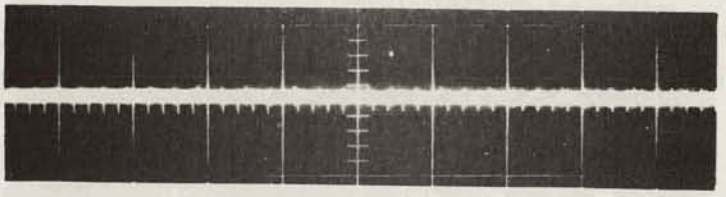

Figure 7.34 - Deflection with Two-Phase Flow 96 GPM Water 24 GPM Air and 4 FPS
e_x = 0.2 cm δ = 0.00121 in.

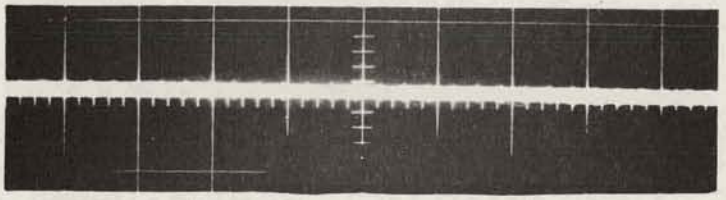

Figure 7.35 - Deflection with Two-Phase Flow 180 GPM Water 24 GPM Air and 6.75 FPS
e_x = 0.22 cm δ = 0.00149 in.

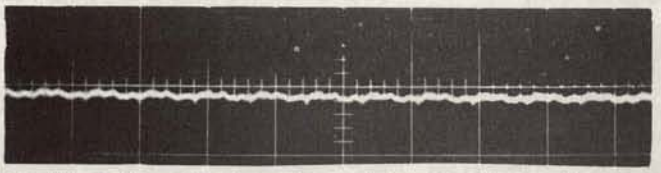

Figure 7.36 - Calibration Beam for 94 in. Span Tube Section at Zero Flow 0.1 cm = 0.025 in. Deflection e_x = 0.11 cm δ = 0

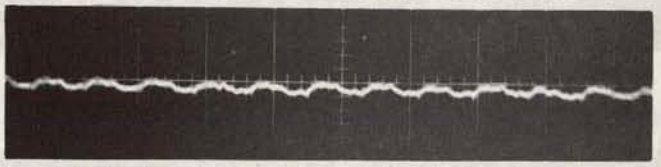

Figure 7.37 - Deflection of 94 in. Span-Tube with Single Phase Flow 190 GPM and 6.3 FPS e_x = 0.2 cm δ = 0.0112 in.

Figure 7.38 - Deflection of 94 in. Tube with Two-Phase Flow 190 GPM Water, 24 GPM Air 7.1 FPS e_x = 0.23 cm δ = 0.0150 in.

The same measurements of dynamic deflection were recorded with the pen recorder. Results for the single-phase flow tests are shown in Figures 7.39 and 7.40.

Discussion. The natural frequency of vibration of tubes when the lattice was suspended in air was not well defined. It appears that the lattice vibrates as a whole at about 25 cps (Fig. 7.2). In such a case; the tubes have many degrees of freedom corresponding to various possible modes of vibration. Of these, all but the fundamental mode were disregarded since large amounts of energy would have been required to cause the tube to vibrate with significant amplitude at higher modes.

Due to the small gage output, the natural frequency and amplitude of vibrations of the tube could not be determined with accuracy when the lattice was submerged in water. The frequency of 60 cps recorded for various flow conditions does not necessarily indicate the actual frequency of the tube, because for these conditions, an interference frequency of 60 cps was prevalent in the system (Fig. 7.28). However, the natural frequency of the tubes in air with the baffles and tube sheets guided laterally was 68 cps. The natural frequency of the tubes in water can be expected to be somewhat lower than in air due to the added mass of water surrounding the tubes. Therefore, the 60 cps observed was assumed to be the natural frequency of the tubes in water.

Measurements of the dynamic deflection of the tubes due to vibrations was difficult since 0.002 in. deflection would appear on the oscilloscope

screen as an increase of beam thickness of 0.148 cm. The dynamic deflection observed on Figure 7.34 and 7.35 were smaller than 0.002 in.

Conclusion. The type of vibrations observed during the test with water flowing around the tubes was of the self-excited variety. In each of the tests with single- and two-phase flow, the tubes vibrate at their natural frequency at all flow velocities. Because of the small output of the strain gages, an accurate measurement of the deflection was difficult to obtain. However, the objective of the tests was to determine if excessive amplitudes of vibration would occur at maximum flow conditions. Excessive amplitudes were considered those greater than 0.002 in.

In making the evaluation, reference is made to Table 7.1, which compares the test and Pathfinder parameters. Since the tubes are very comarable and the test tube vibrations were negligible, less than 0.002 in., it can be concluded that the Pathfinder superheater tubes will operate satisfactorily and tube vibrations will not be a problem during operation.

TABLE 7.1 COMPARISON OF TEST AND PATHFINDER PARAMETERS

Parameter	Unit	Pathfinder	Test
Water velocity at max. flow	fps	4.7	6.5
Unsupported length	in.	47-1/2	47-1/2
Weight per unit length	lb/in	0.0245	0.0190
EI	$lb\text{-}in^2$	2.9×10^5	2.82×10^5
Natural frequency	cps	62	68
Hydraulic diameter	in.	0.753	0.71

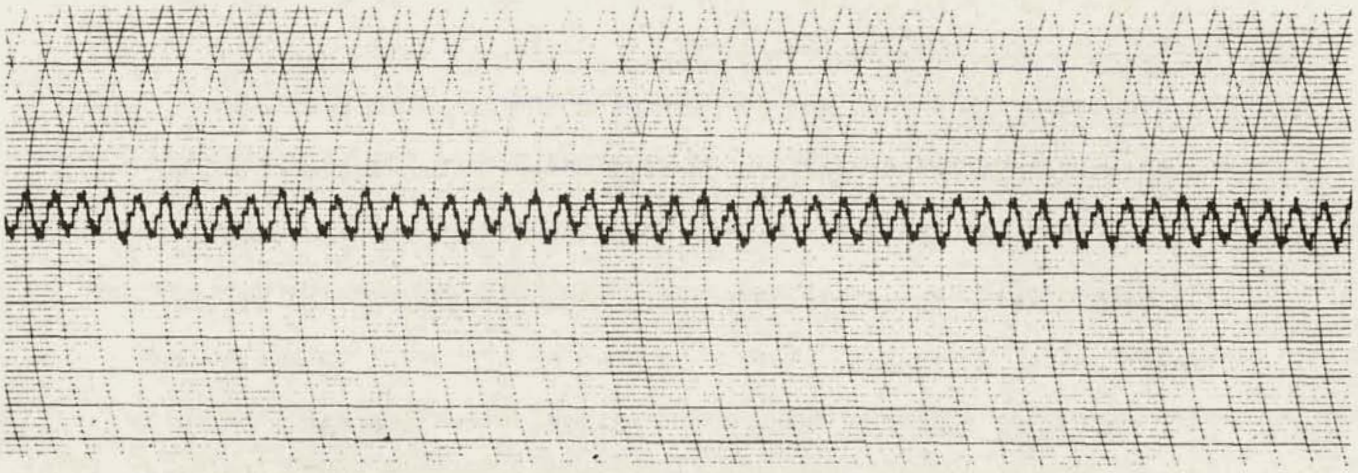

Figure 7.39 - Dynamic Deflection Calibration Curve at Zero Flow
1 cm = 20 μ in/in, f_n = 60 cps, Q = oδ = 0

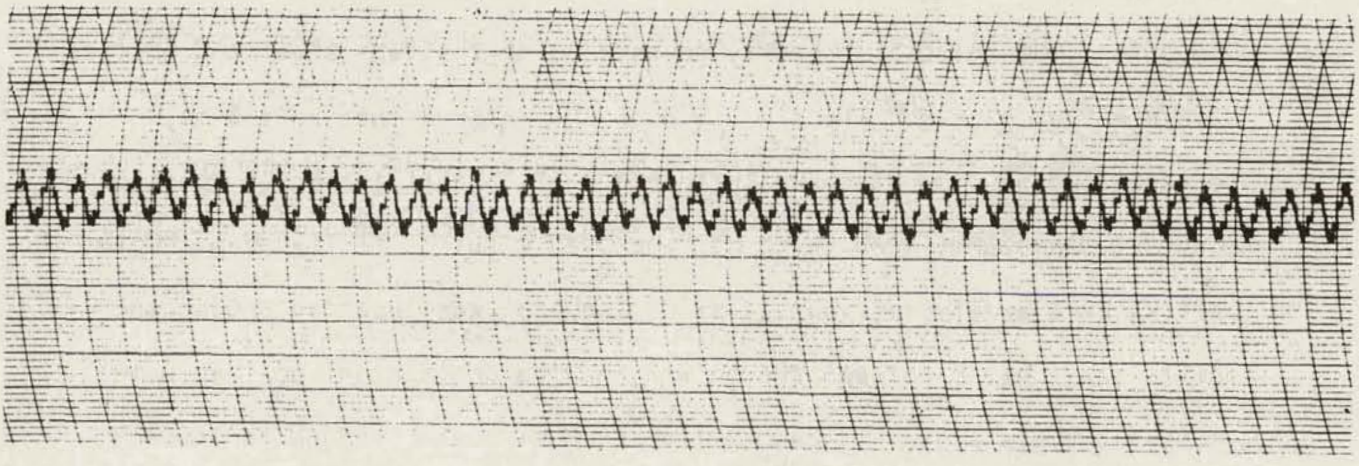

Figure 7.40 - Dynamic Deflection with 190 GPM, 6.3 FPS Water Flow
1 cm = 20 μ in/in f_n = 60 cps, 100 μ in/in strain = 0.031 in.
Deflection. δ = 0.000465 in.

7.8 Superheater Orifice Flow Test

The purpose of this test was to determine the pressure drop across the transition and intermediate baffles with various sized orifices. The loop that was designed for the tube vibration test was used in this test. Refer to Section 7.7 for a detailed description of the vibration test equipment.

Test Set-up. (See Figure 7.41) - The test lattice is shown in Figure 7.20, and was other wise previously described in (Sec. 7.7). The flow through the transition baffle may be described as flow discharging from a multichannel formed by several tubes of 0.800 in. O.D into a multichannel formed by several tubes over a 1-1/2 in. length from 0.800 to 1.080 in. O.D. directly downstream of the tube sheet and enclosed within a finite area. The flow through the intermediate baffle may be described as flow discharging from a multichannel formed by tubes of constant diameter (1.080 in. O.D) enclosed within a finite area. Both baffles were easily removable. An O-ring seal was inserted around each baffle and located between the baffle and the containment box walls to prevent by-pass flow. In each baffle were nine sharp-edged orifices on a pitch spacing of 1.234 in. centered between the tubes.

Test Procedure. The permanent pressure drop across the transition and intermediate baffles was determined experimentally for various sized sharp-edged reamed orifices under various flow conditions.

The permanent pressure drop across the transition baffle was measured with pressure taps located, 4 in. and 8 in. upstream and downstream, respectively, of the baffle. The flow was varied and readings were made on the differential mercury manometer No. 3. Tests were run for each of the following sets of orifices in the transition baffle: 0.318 in., 0.340 in., 0.360 in., 0.381 in., 0.395 in., 0.411 in., 0.438 in., and 0.480 in. diameter.

The permanent pressure drop across the intermediate baffle was measured with the pressure taps located 4 in. and 8 in. upstream and downstream, respectively, of the tube sheet. The flow was varied and readings were made on the differential mercury manometer No. 4. Tests were run for each of the following sets of orifices in the intermediate baffle: 0.330 in., 0.395 in., 0.460 in., 0.490 in., and 0.510 in. diameter.

The permanent pressure drop across the transition and intermediate baffle was recorded, and is presented as a function of flow in Figure 7.42 and 7.43.

The parallel friction loss along the tubes was measured with pressure taps located 97 in. apart, from 4 in. below the transition tube sheet to 4 in. below the upper tube sheet. The total pressure loss of the transition, and intermediate baffle and the friction loss was read on the differential manometer No. 5.

The friction loss, which would have been a difference, could not be determined because the scatter in data was equal or greater than the expected friction loss.

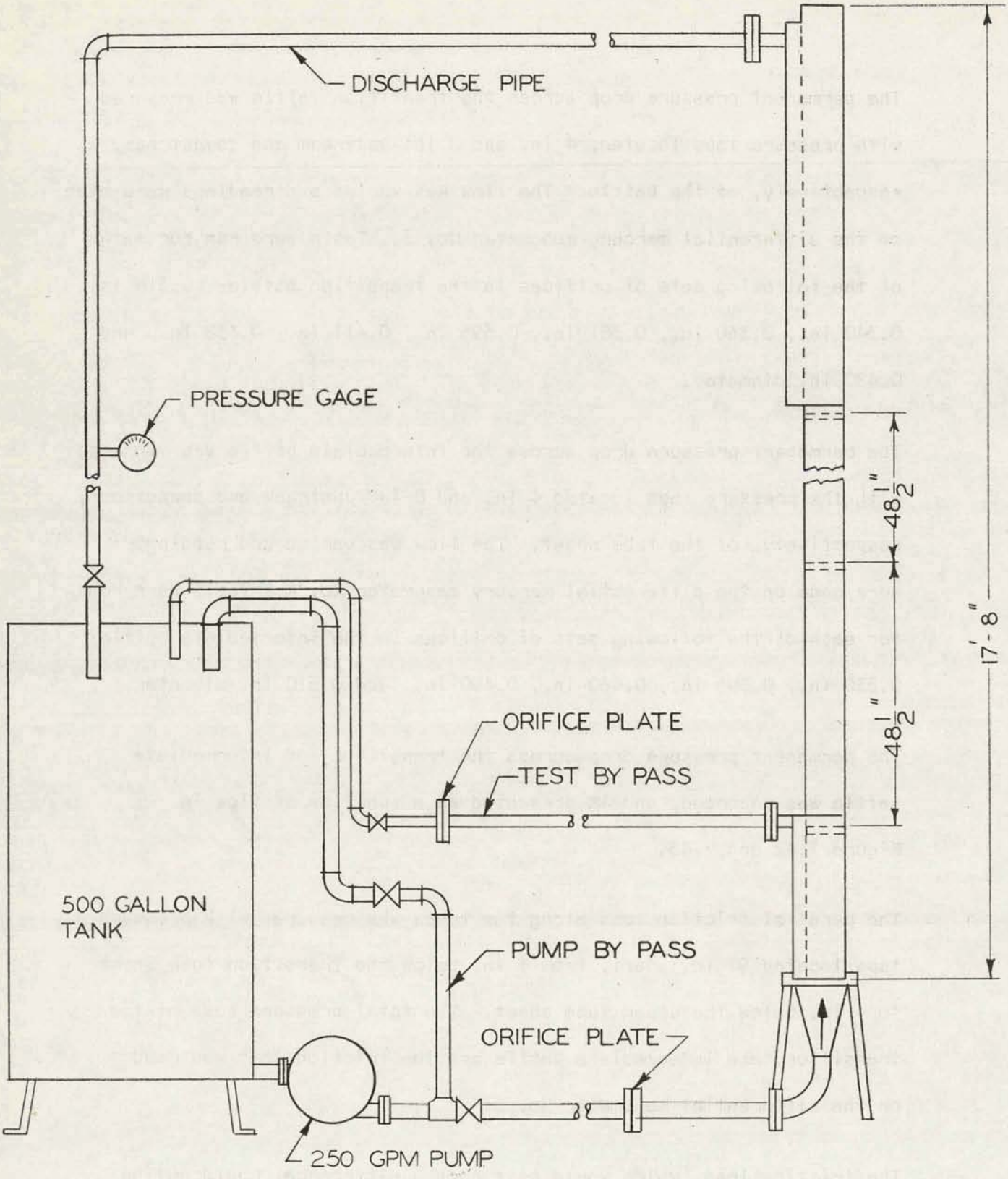

Figure 7.41 - Superheater Orifice Flow Schematic Diagram (43-024-425)

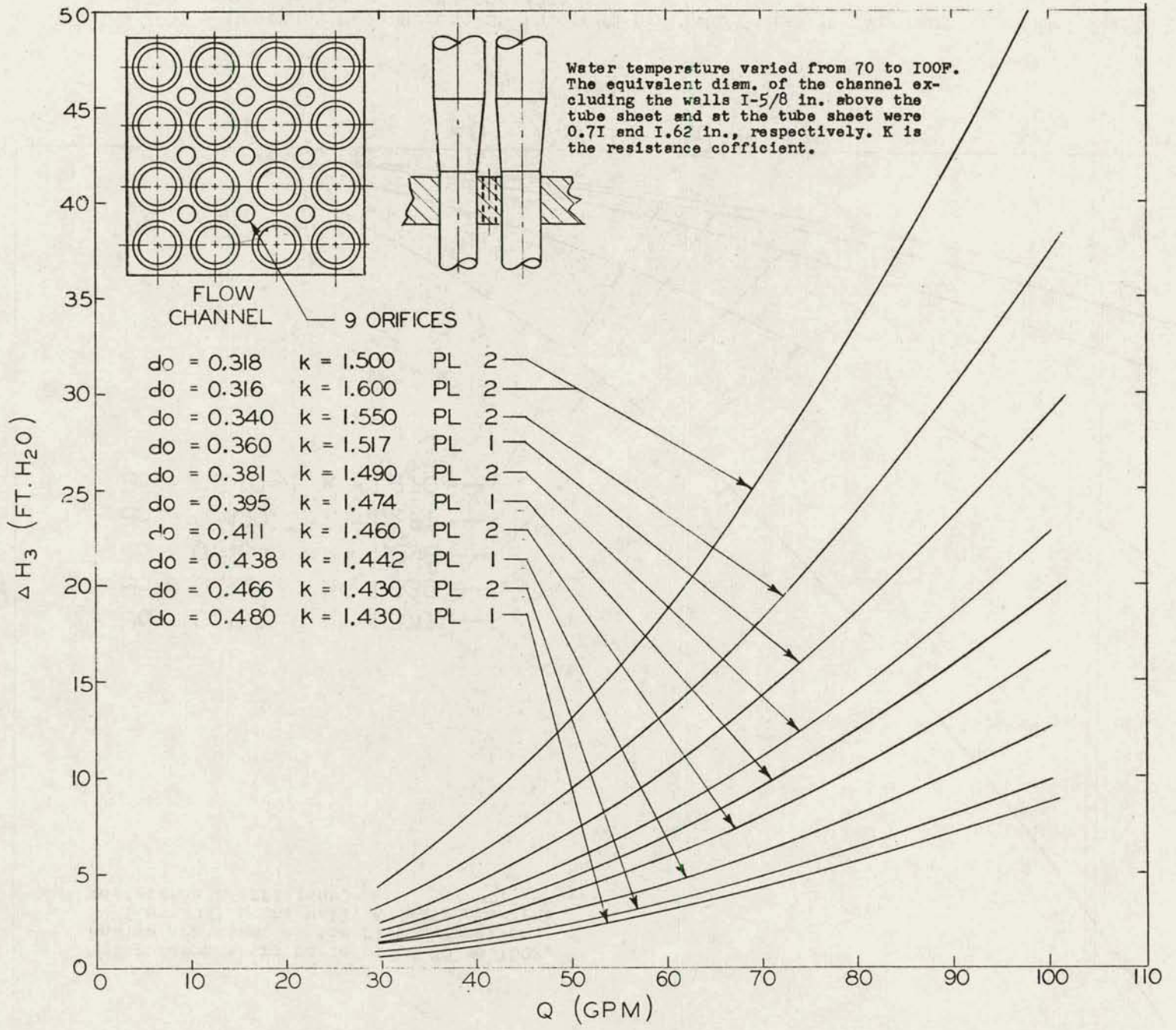

Figure 7.42 - Pressure Drop Across Transition Tube Sheet with Various Sized Orifice Diameter, d_o (43-024-429)

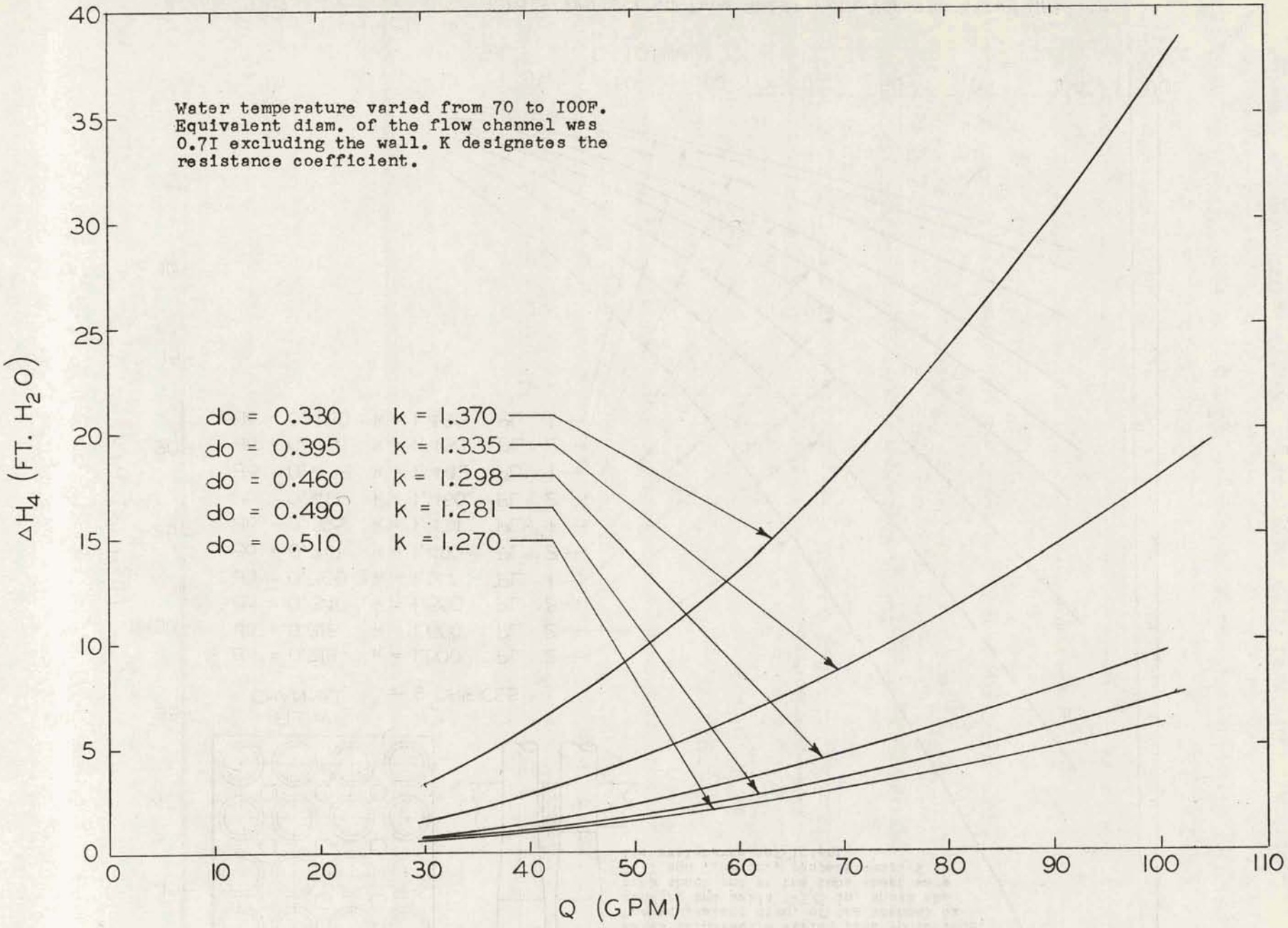

Figure 7.43 - Pressure Drop Across an Intermediate Tube Sheet for Various Sized Orifice Diameters, d_o (43-024-428)

Calculations. At the transition tube sheet, where the tubes were 0.800 in. O.D., the flow channel area was 16.36 sq in. The equivalent diameter was calculated to be 1.625 in. The walls of the box enclosing the tube lattice were neglected.

At the intermediate tube sheet, where the tubes are 1.080 in. O.D., the flow channel area was 9.73 sq in. The equivalent diameter was calculated to be 0.715 in.

The permanent pressure drop is a function of the resistance coefficient, K, and is expressed as follows:

$$\Delta H = \frac{K V_o^2}{2 g} \qquad (7.28)$$

where: V_o = velocity of water through the orifice, fps.

The average values of the resistance coefficient were plotted as a function of beta ratio in Figure 7.44.

Discussion. Since a small chamber will greatly affect the coefficient of discharge, it is imperative that the upstream edge of the orifice be sharp. In the test, each orifice was reamed to the indicated dimensions with a tolerance of $\pm$ 0.005 in. The scattering observed for some orifices tested was probably due to leakage between the baffles and the containment box walls, since some difficulty was encountered in inserting the lattice in the box.

The resistance coefficient, K, for each orifice size, was assumed constant from minimum to maximum flow (20 to 100 gpm). In no case was the difference larger than 6.5 per cent between minimum and maximum flow. This uniformity was attributed to an increase of the by-pass flow around the tube sheet when the differential pressure across the tube sheet was increased.

7.9 Superheater Water Flow

The water from the recirculation pumps enters the lower portion of the vessel and proceeds upward in the plenum, where most of it enters the boiler core through the grid plate and the fuel elements, and part of it enters the superheater, then flows upward through the baffle orifice holes.

The water entering the superheater is separated from the water around the boiler core fuel boxes over the whole length of the core by a peripheral shroud welded to the transition and intermediate tube sheets. Above the core region, the shroud is replaced by corner angles welded at the top and bottom to baffles. The superheater water flow outward through the longitudinal spaces between the corner angles and is mixed with the boiler core water steam.

The flow passing through the superheater is a function of the pressure drop through the boiler core fuel elements, the size of the orifice holes in the baffles, and the friction loss along the outer container tubes.

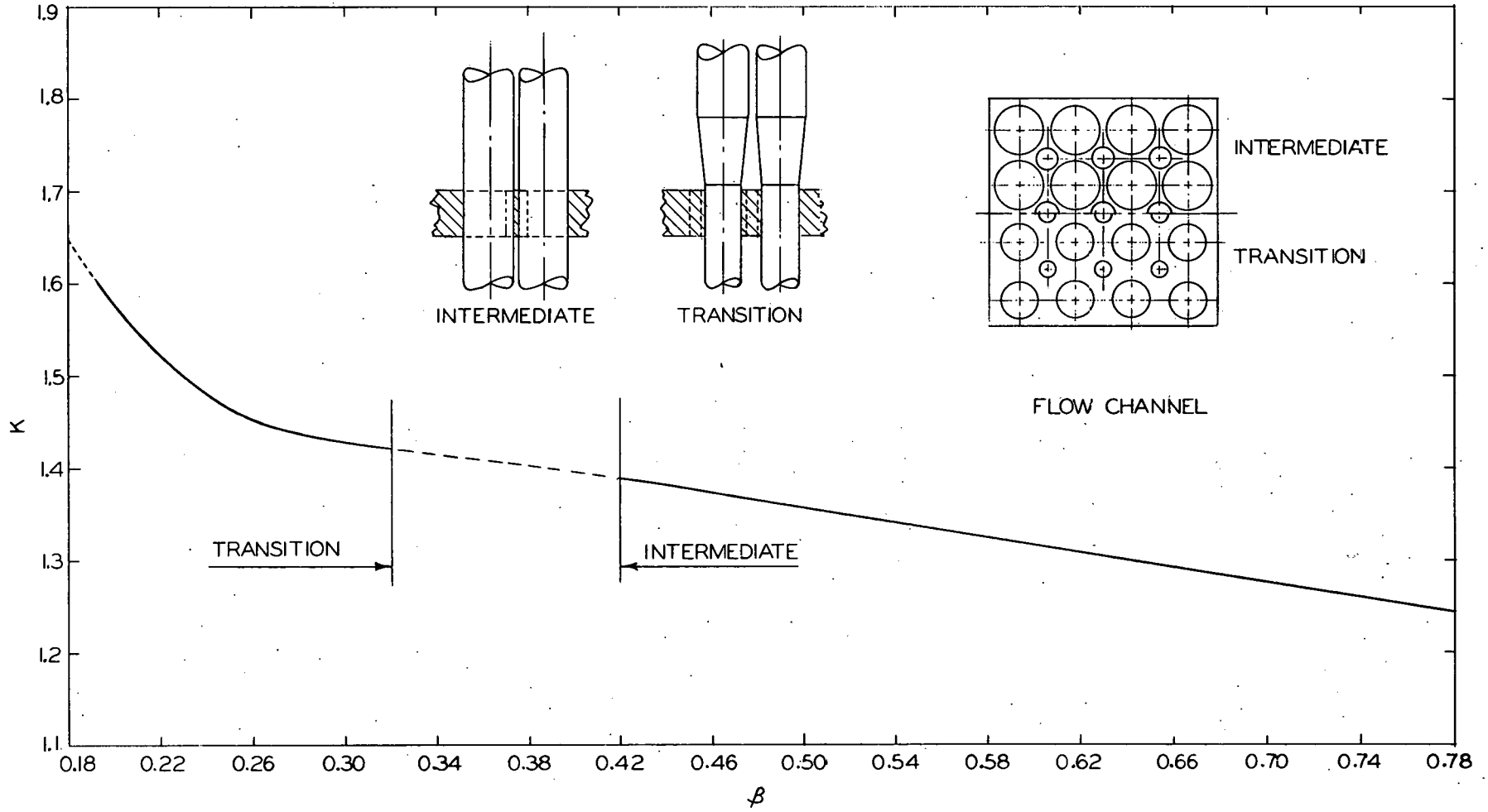

Figure 7.44 - Average Resistance Coefficient as a Function of B Ratio (The Ratio of the Orifice Diameter to the Equivalent Diameter) (43-024-427)

The minimum flow through the superheater corresponding to the minimum pressure drop through the boiler core fuel elements was the criterion for the superheater flow calculations. Based on heat transfer and nuclear physics requirements, the minimum flow and maximum void fraction permissible in the superheater was established.

The orifice sizes were determined from the orifice flow test, Sec. 7.8. The pressure drop throughout the superheater length was distributed as follows:

1.	transition baffle (bottom)	72%
2.	intermediate baffle (middle)	17%
3.	intermediate baffle (upper)	9.8%
4.	parallel friction loss	1.2%

The flow through the superheater will be 4.5 to 6.5 per cent of the total recirculation flow rate (65,000 gpm), based respectively on the minimum and maximum pressure drop through the boiler core fuel elements.

7.9.1 Superheater Flow Calculations

The distribution of the pressure drop throughout the superheater length was determined as follows.

Pressure drop in transition baffle - The permanent pressure drop is given as:

$$\Delta H = \frac{K V_o^2}{2 g} \qquad (7.28)$$

expressing the velocity, V_o, through the orifice in terms of the flow rate and total orifice yields.

$$\Delta P = \frac{0.113 \times 10^{-2}\ Q^2 K}{d_o^4\ n^2} \qquad (7.29)$$

Where:

Q = flow rate, GPM

d_o = orifice diameter, inches

n = number of orifices

K = factor dependent upon β, the ratio of orifice diameter to equivalent diameter.

The transition tube sheet has:

468 tubes - 0.800 in. O.D.

385 orifices - 0.375 in. diameter

From the orifice flow test, Section 7.8, it was found the β equals 0.224; thus K equals 1.51.

Thus, performing the required operations:

$$\Delta P_1 = 0.581 \times 10^{-6}\ Q^2 \qquad (7.30)$$

Pressure drop in intermediate baffle (middle)

468 tubes - 1.080 in. O.D.

385 orifices - 0.500 in. diameter

36 orifices - 0.406 in. diameter

From Sec. 7.8, average K equals 1.30; thus,

$$\Delta P = 0.1363 \times 10^{-6}\ Q^2 \qquad (7.31)$$

Pressure drop in intermediate baffle (upper)

468 tubes - 1.080 in. O.D.

385 orifices - 0.580 in. diameter

36 orifices - 0.406 in. diameter

From Sec. 7.8 average K = 1.25 thus,

$$\Delta P_3 = 0.786 \times 10^{-7} Q^2 \tag{7.32}$$

Friction Losses

Entrance, discharge and parallel losses have been estimated from the orifice flow test, Sec. 7.9:

$$\Delta P_f = 0.1 \times 10^{-7} Q^2 \tag{7.33}$$

Total pressure drop through superheater (See Figure 7.45).

$$\Sigma\Delta P = \Delta P_1 + \Delta P_2 + \Delta P_3 + \Delta P_f \tag{7.34}$$

$$\Sigma\Delta P = 0.806 \times 10^{-6} Q^2$$

Therefore:

ΔP_1 = 72.0% of $\Sigma\Delta P$

ΔP_2 = 17.0%

ΔP_3 = 9.76%

ΔP_f = 1.24%

7.10 Superheater Seal Test

The insulating gap between the outer and inner superheater container tubes is sealed at the top tube sheet. The outer container tube is fusion welded to the tube sheet. An insert maintains the seal between the inner and outer tubes at the top, and is fusion welded to the inner container tube. A seal between the outer tube and insert is accomplished by rolling (expanding) the inner tube and insert into the outer container tube. Tests were conducted to determine whether the rolled joint can be made pressure tight (489 F at 70 psi) and still be readily disassembled.

Sealing austenitic stainless steel tubes in a tube sheet of the same material is difficult since the elastic limit of the tubes is the same as that of the tube sheet. The tubes readily work harden from rolling, and tight joints are not easy to attain even when precise techniques are employed.

The test apparatus used in this experiment is shown in Figure 7.46. It consists of a cylinder of 6 in. diameter schedule 40 stainless steel welded at both ends to 6 in. 150 lb stainless steel flanges; 9 container tubes 1.080 in. O.D. x 0.020 in. thick wall plugged at one end with the sealing piece fusion welded to the tubes at the other end.

Test Procedure - The inner tube assemblies were inserted in the outer container tubes and expanded with a conventional condenser-tube roller.

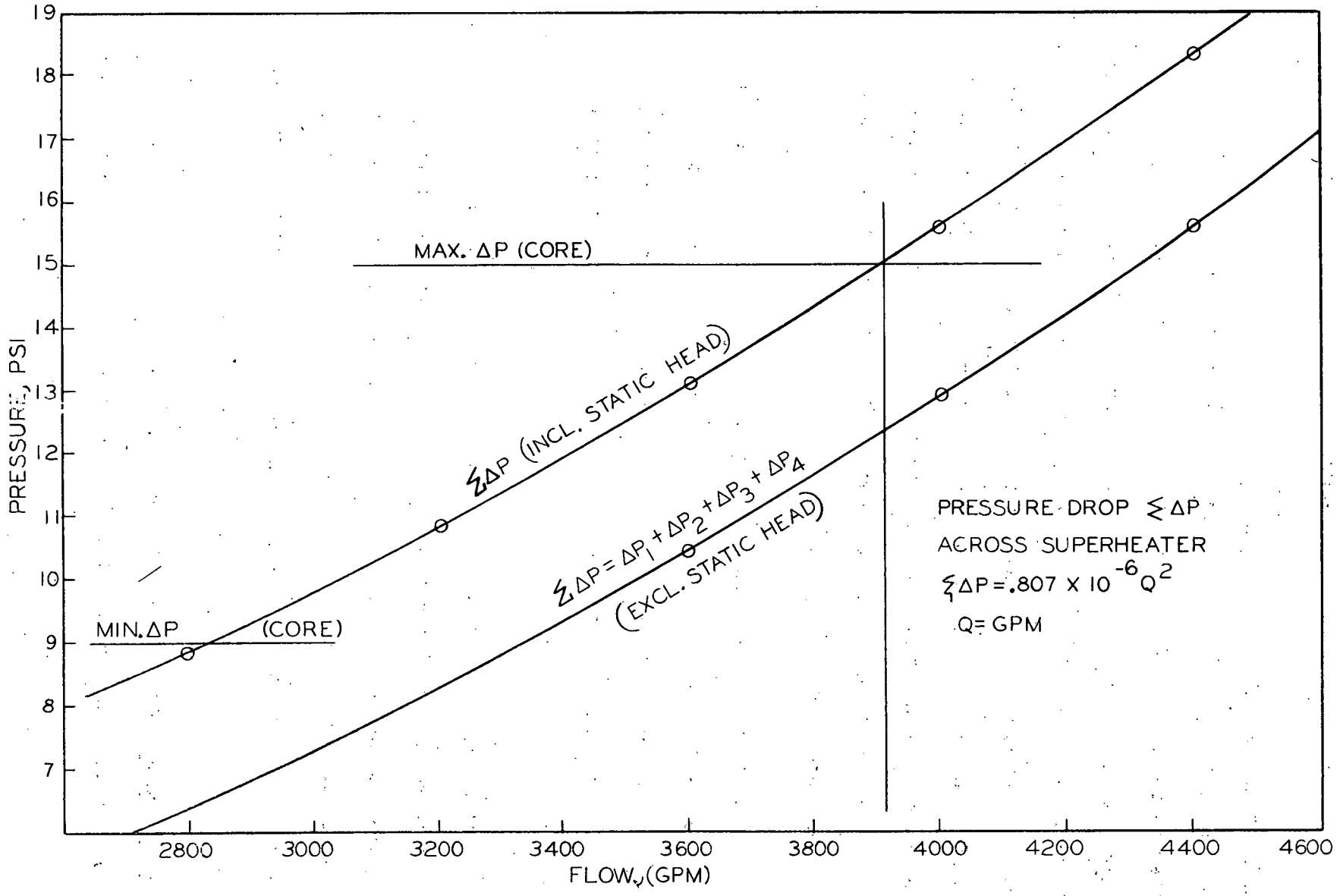

Figure 7.45 - Pressure Drop Across Superheater (43-025-181)

MK. NO. OR REF.	IT.	DESCRIPTION	MATERIAL	PART NUMBER DRAWING	PART NUMBER NO.	WT.
/	1	SUPERHEATER SEAL TEST ASSEMBLY		43-401-068	SOI	
1	2	HOUSING ASSEMBLY		43-381-679	SOI	
1	3	COVER		43-2IH-901	SOI	
5	4	TUBE ASSEMBLY		43-201-[illegible]	SOI	
9	5	CASING - [illegible]	[illegible]	THIS	SOI	
6	6	3/8-16 UNC-2A X 1 1/2 LG. HVY. S.E. HEX. BOLT	STEEL	2008346A1		
6	7	3/8-16 UNC-2B HVY. S.E. HEX. NUT	STEEL	2008333A1		
1	8	GASKET - 1/16 THK X 8 5/8 OD X 8 1/8 ID	URANIUM	THIS	SOI	

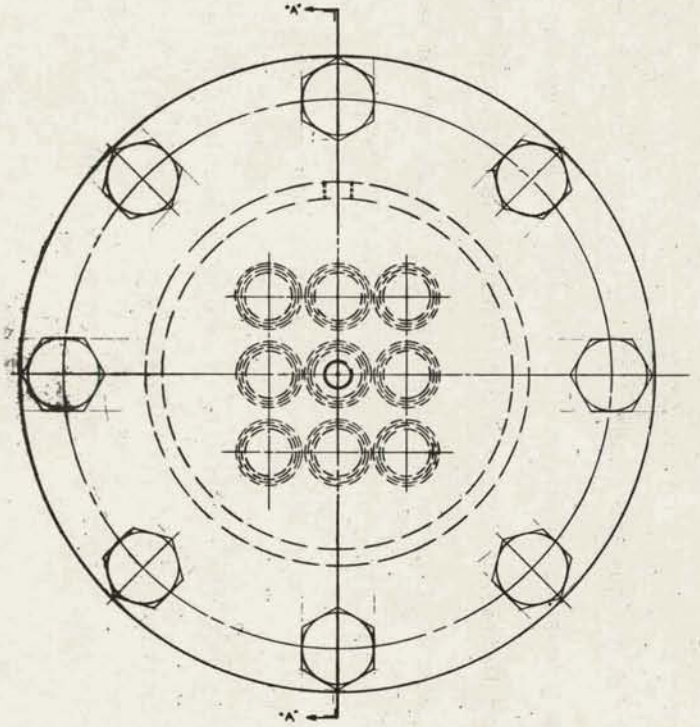

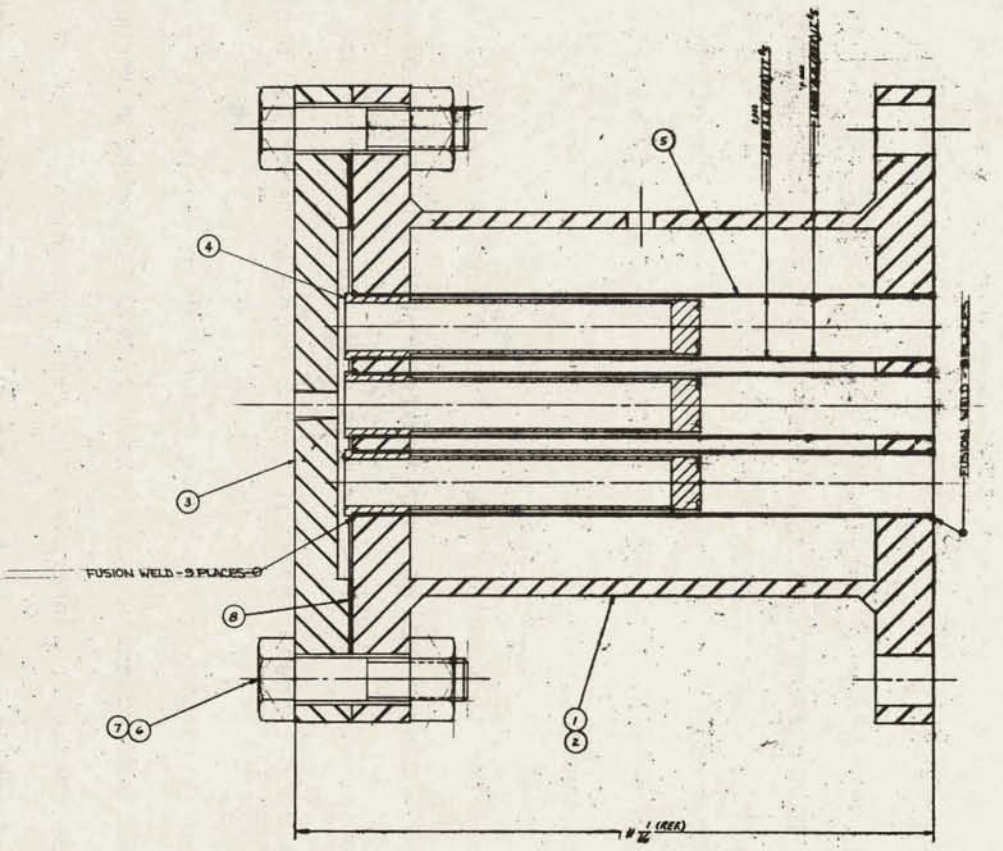

Figure 7.46 - Superheater Seal Test Assembly (43-401-068)

The torque applied on the tube roller was controlled to produce an optimum radial pressure on the sealing surface in order to insure a pressure-tight seal that could easily be disassembled.

Air pressure at 90 psi was applied on one side of the seal; the seals were tested by immersing the test apparatus in water and checking for bubbles.

In order to simulate thermal cycles encountered in reactor startup and shutdown operations, the test apparatus was heated to 500 F and cooled at room temperature several times. After each thermal cycle, leakage through the seals was checked as described above.

The integrity of the seals under hot conditions was also investigated. The test apparatus was heated to 500 F. Leakage through the seals was checked by immersing the test apparatus in oil at the same temperature and applying air pressure at 90 psi on one side of each seal.

Results - A torque of about 150 in-lb on a conventional tube roller produced pressure-tight seals. Adequate sealing was retained under simulated Pathfinder operating conditions. The optimum torque required for a given configuration depends on the amount of expansion required, the modulus of elasticity, and the moment of inertia of the sealing piece and the inner tube, and the tube roller condition and construction.

Nine seals had the following average dimensions after testing:

Outer tube	-	1.044 in. I D
Insert	-	1.041 in. O D - 0.928 in. I D
Inner tube	-	0.926 in. O D - 0.886 in. I D

The average expansion of the sealing piece outside (O D) diameter was 0.006 in. All seals were readily disassembled using a conventional condenser tube puller.

7.11 Superheater Tube Weld Test

Various joint designs were proposed for welding type 304 superheater container tubes to the type 304 SS upper tube sheet in the Pathfinder reactor. The weld that joins these two components must be leak-proof. The Allis-Chalmers Research Laboratories conducted an investigation to determine the most satisfactory of the proposed designs.

Materials and Welding Procedure - The tube material was type 304 Stainless Steel, 1 in. diameter and 0.020 in. wall thickness. The tube sheet material was type 304 Stainless Steel, 3/4 in. thick. Weld preparations in the tube sheet are shown in Figure 7.47. The tubes were inserted into the tube sheet (the fit-up is shown in Fig. 7.46) and were fused to the tube sheet with a Heliarc torch. The surface appearance of the six designs after welding is shown in Figure 7.48. Argon was used for the shielding gas. No filler metal was used except for the second pass of design 4, in which case a 1/16 in. diameter type 308 filler rod was used. A welding current of 30 amperes was used for design 1 and 40 amperes was used for the remaining designs. Design 1 and 6 had the best weldability characteristics in the weld tests.

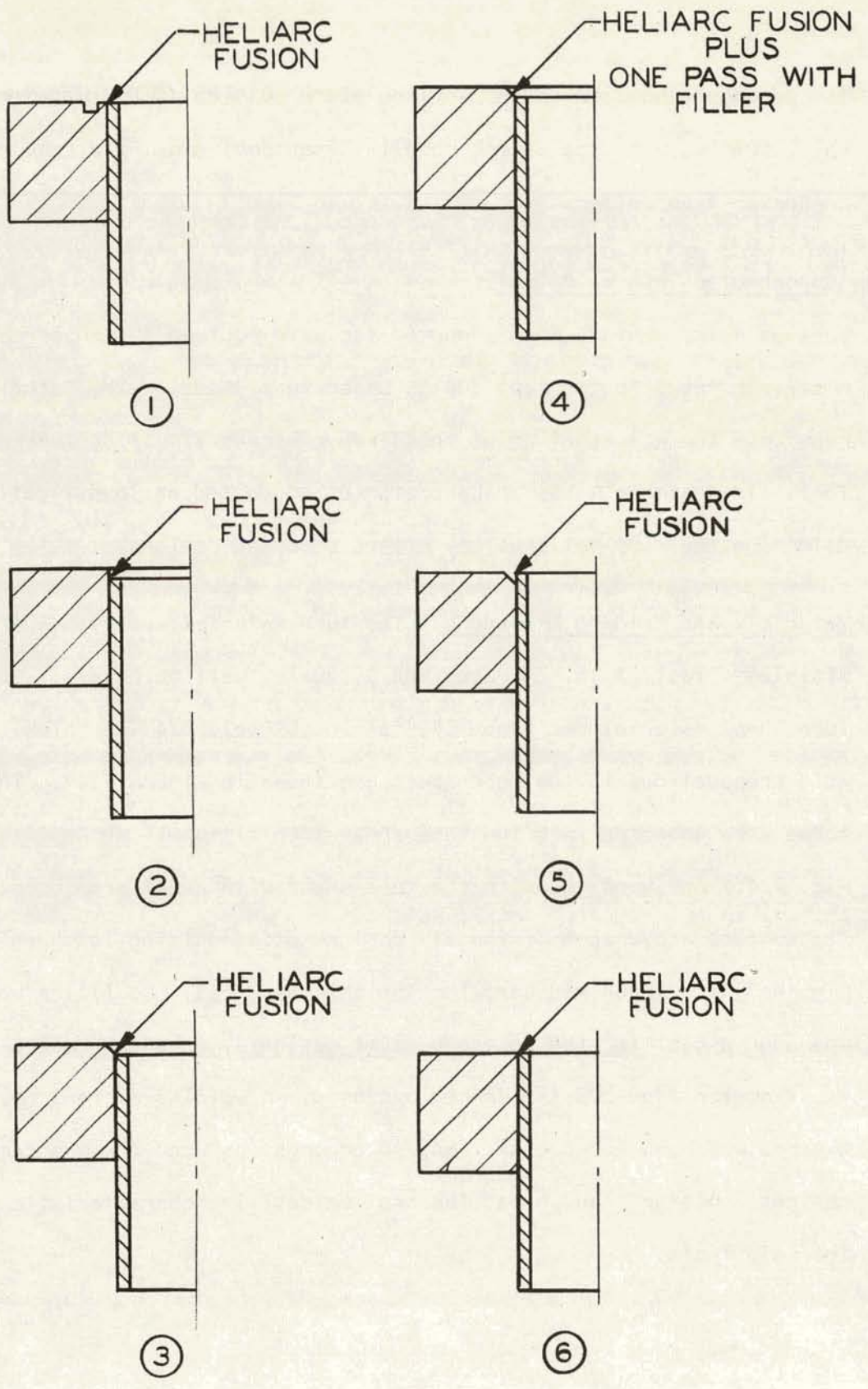

Figure 7.47 - Sketches of Various Tube to Tube Sheet Joint Designs (51-433)

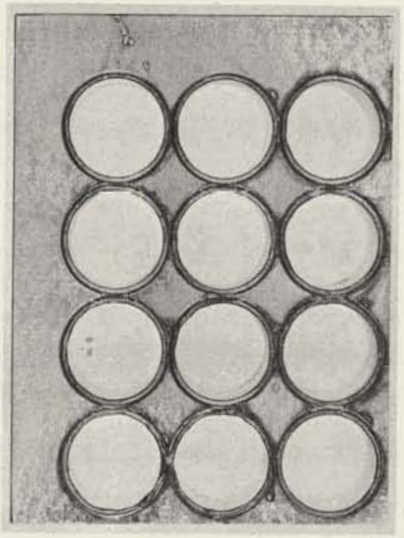

1

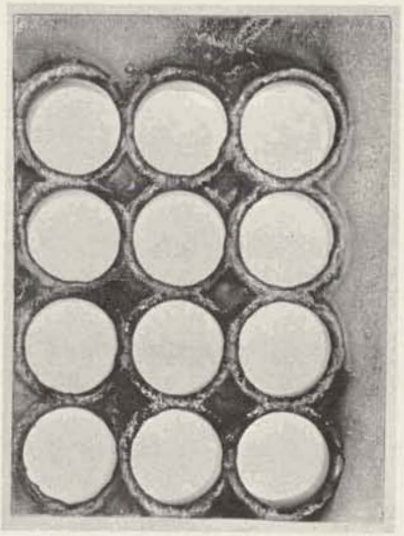

4

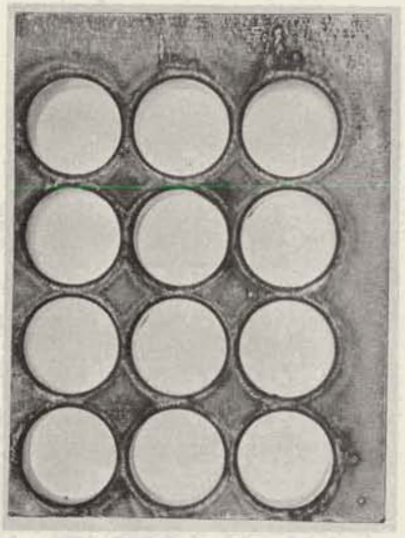

2

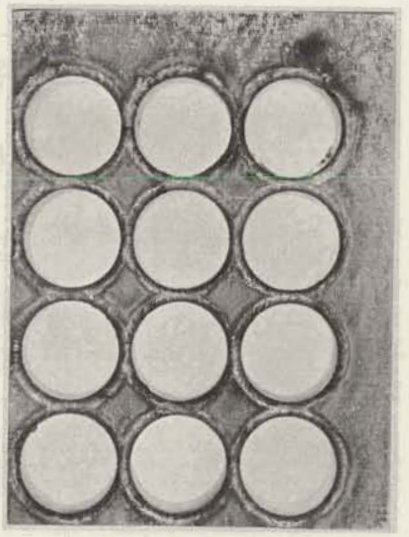

5

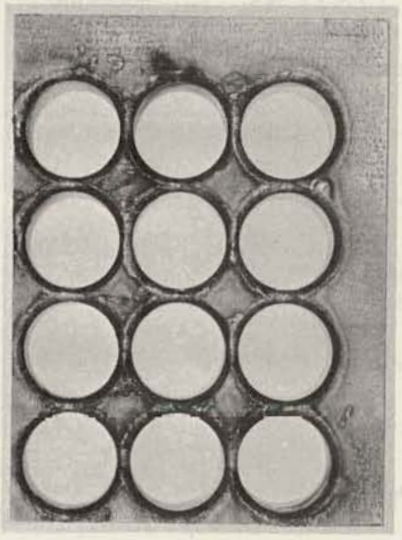

3

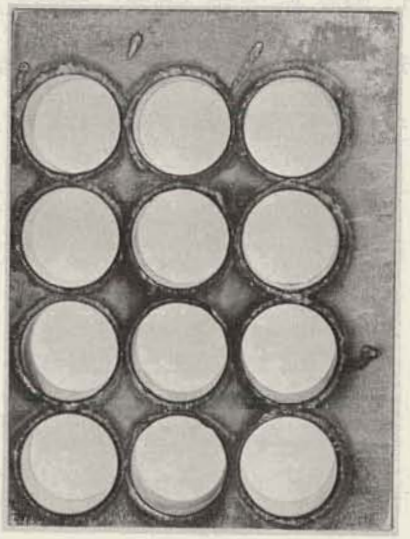

6

Figure 7.48 - Surface Appearance of Joint Designs After Welding (2486-A)

Physical Tests - Two methods were used to measure the distortion of the tube sheet caused by the heat of welding and the shrinkage of the weld (Figure 7.50). As shown in Figure 7.50 Section a, a straight edge was positioned so that the sagitta of the arc could be measured as shown. In Figure 7.50 section b, a straight edge was positioned as a cantilever, so that the deflection could be measured. Feeler gages were used for the measurements given in Table 7.2. The least distortion occurred when joint designs 1 and 6 were used.

TABLE 7.2

DISTORTION MEASUREMENTS

Weld Joint Design No. (See Fig. 7.47)	Distortion	
	Sagitta - "A" in.	Deflection - "B" in.
1	0.014	0.042
2	0.033	0.098
3	0.035	0.090
4	0.053	0.158
5	0.032	0.098
6	0.016	0.058

An attempt was made to determine the breaking strength of the weld. Using the set-up shown in Figure 7.51, a load was applied to the mandrel to force the tube out of the tube sheet since due to the short tube length, the tubes could not be gripped to pull them out of the sheet. The welds did not fail, even though all the tubes collapsed.

Metallographic Examination - Sections were cut from each of the welded joints and were mounted for metallographic examination. All fused areas had a microstructure of austenite plus pools of ferrite (about

10 per cent), as may be seen in Figure 7.49. The samples were then macro-etched and low power photomicrographs were taken of each joint design (Figure 7.52).

In design 1, the depth of fusion appeared to be inadequate. The control of penetration could be assured by using a tube-to-tube sheet welding gun. In design 4, an excessive overhand may be seen, which is undesirable. The additional filler added in making weld design 4 was not required.

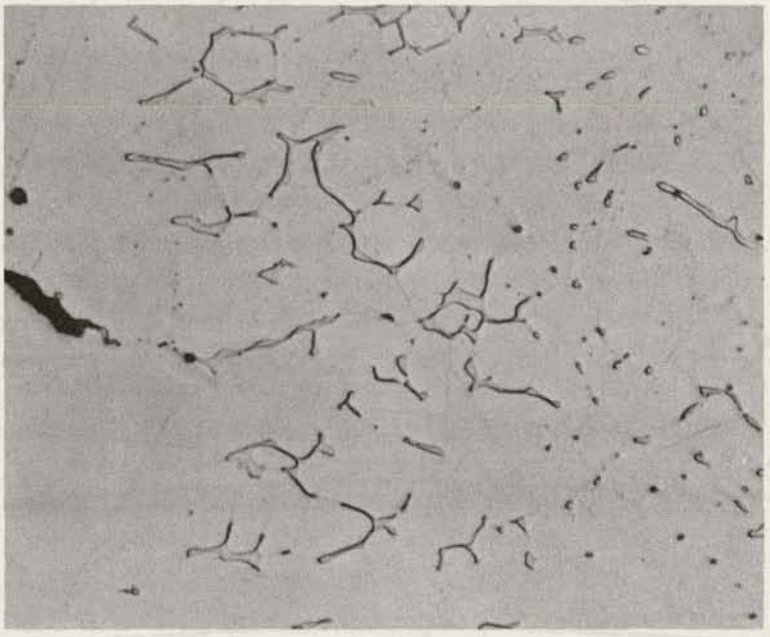

Figure 7.49 - Austenite-plus-ferrite structure which was typical of all fused joints between the tube and tube sheet. Magnification: 1000X Etchant: Oxalic acid, electrolytic. (Photo 2846-4-B)

Summary and Conclusions: Of the six joint designs proposed for Heliarc welding of Type 304 Stainless Steel tubes to a tube sheet, design 1 and

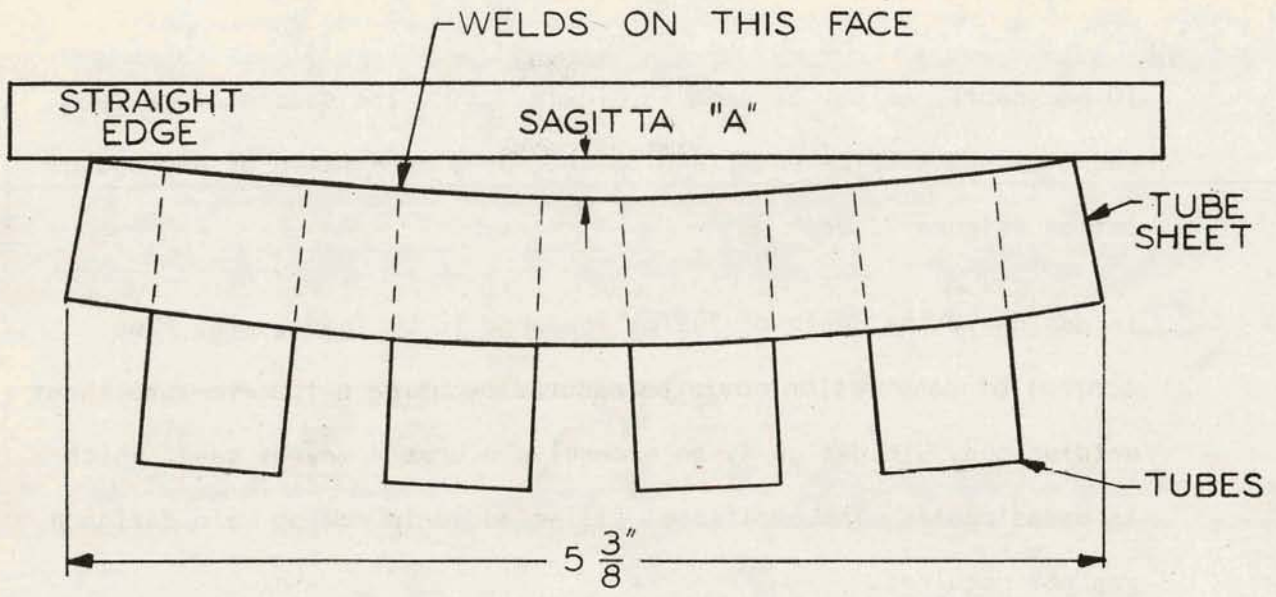

(a)

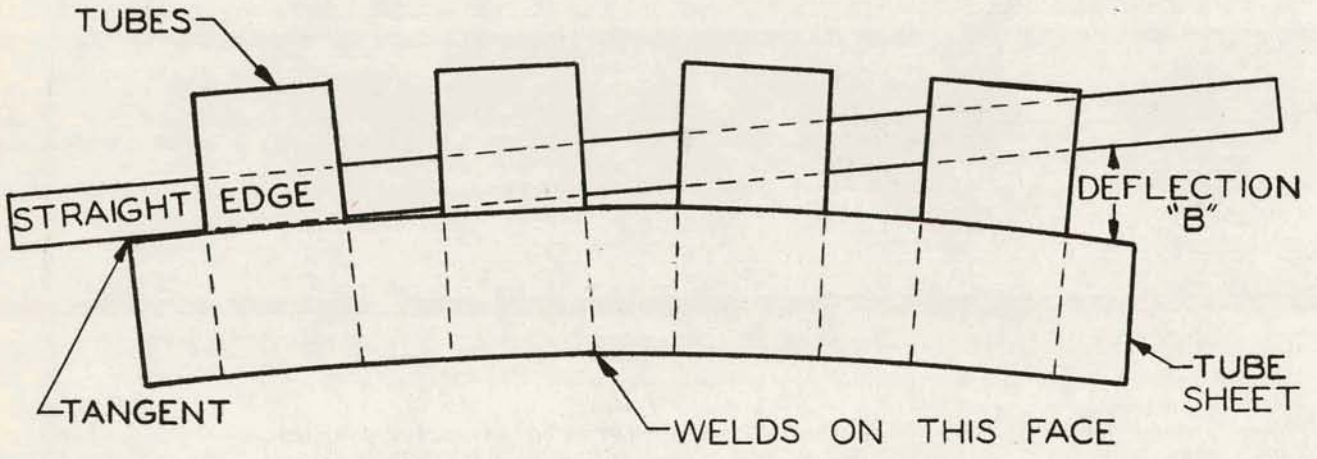

(b)

Figure 7.50 - Two Methods of Measuring Distortion of Tube Sheet (51-434)

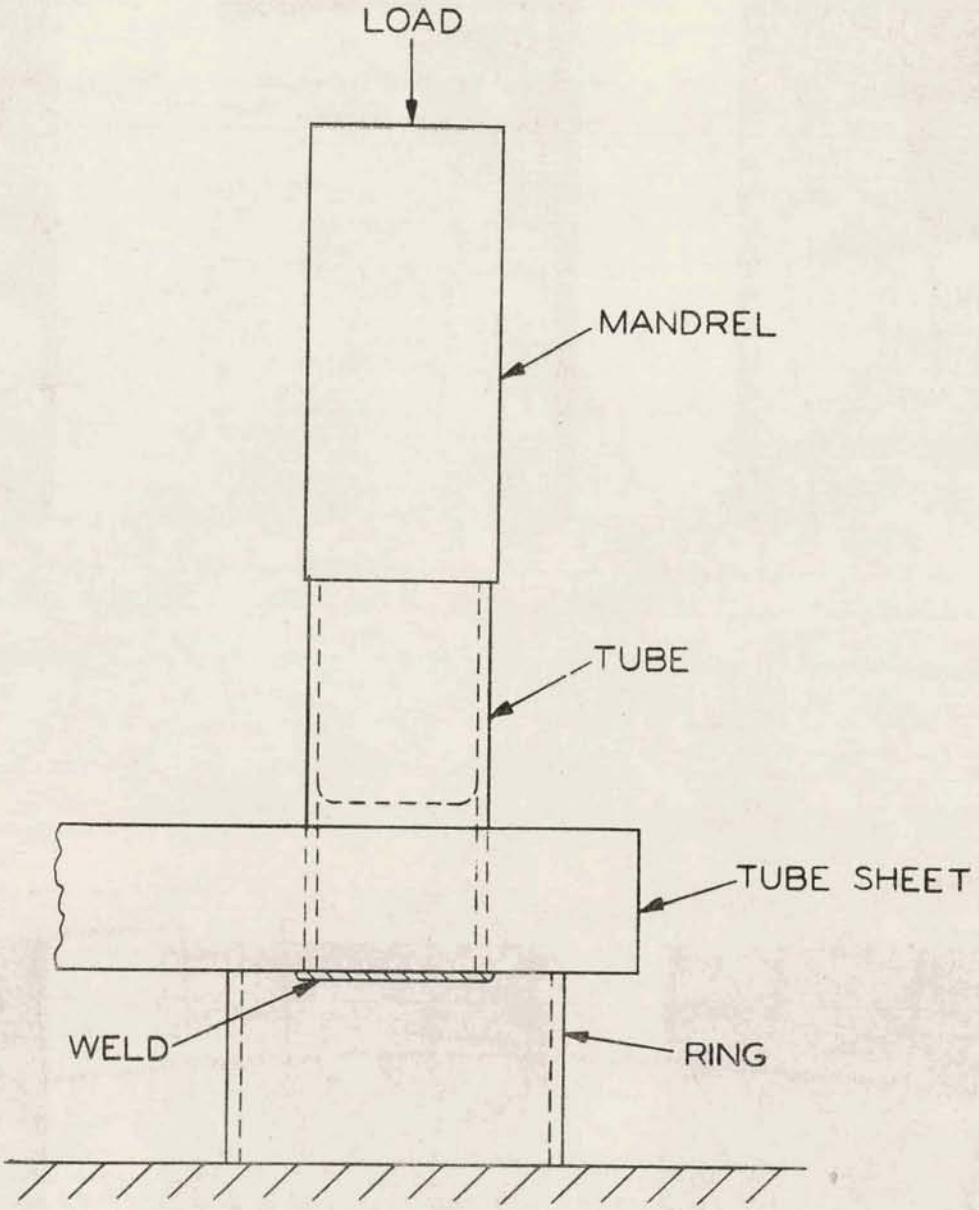

Figure 7.51 - Method Used to Determine Strength of Weld (51-435)

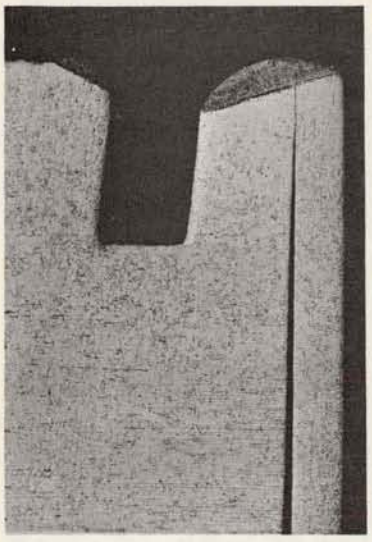

1

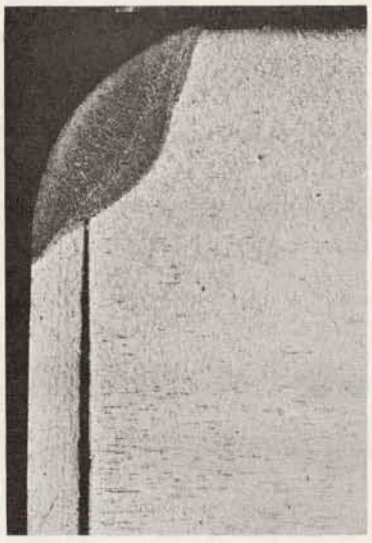

2

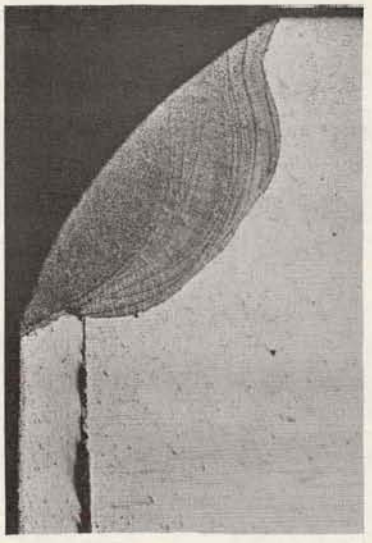

3

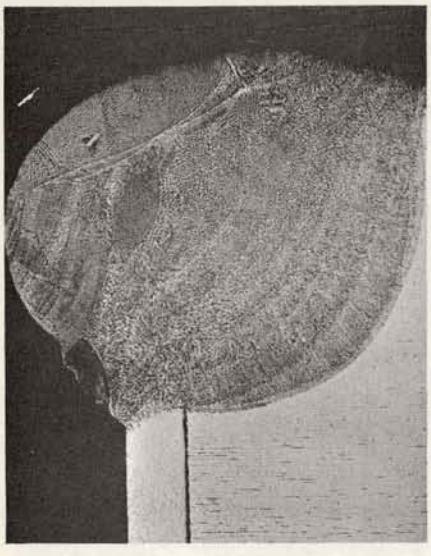

4

5

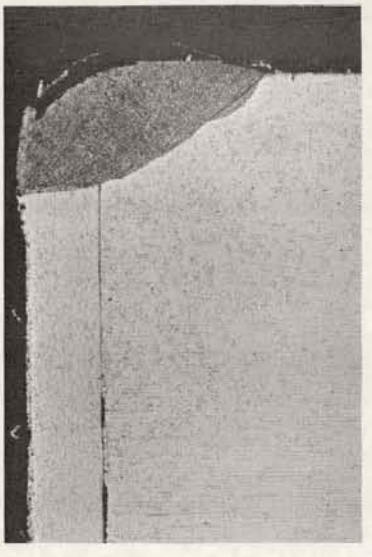

6

Figure 7.52 - Sections Through Tube to Sheet Welds----12.5 X Etchant: 10% Oxalic Acid (2846-C)

6 (Figure 7.47) were preferred because of ease in welding and low distortion. Tests to determine the strength of the welds indicate the necessary strength can be developed. The fused areas had a microstructure of austenite plus about 10 per cent ferrite, which is desirable to preclude hot cracking. Some welds had a shallow fusion, which could be corrected by using a semi-automatic welding gun.

Corrosion Loop Test (See Figures 7.53 through 7-63)

A dynamic loop test was performed on the following construction materials:

1. 316 - 316 SS and 304 - 316 simulated tube sheet-tube joints
2. expanded and annealed 316 SS
3. Inconel U bends and collapsed 316 SS tubes.

The test logged a total of 2304 hours under the following conditions:

Temp. - 500 F

Pressure - 1200 psi

Flow rate - low - limited by 1/4" tube

Chloride - averaged less than 0.1 ppm

pH - neutral

Oxygen level was approximately 8 ppm at the start of the test. No effort was made to control oxygen. It may be assumed that the corrosion process removed the oxygen rapidly, so that the average oxygen concentration was of the order of 10 ppb.

The specimens were removed after 1148 and 1734 hours and inspected visually. Each time all the specimens were returned to the loop for future exposure.

Test Results and Observations - At the conclusion of the test, visual and metallographic inspection of the specimens was made. The surface of all specimens was covered with a uniform dark grey corrosion product film. The film was slightly lighter in color on the thin sheet Inconel U bends than on those prepared for the heavy sheet. No explanation for this difference was apparent.

Microscopic examination showed no local attack either on U bends or in the tube - tube sheet crevice. No evidence of stress corrosion cracking was observed on the expanded or collapsed tubes. General surface attack had occurred on all specimens to a slight degree giving rise to an oxide film barely visible at the highest available magnification. (625X).

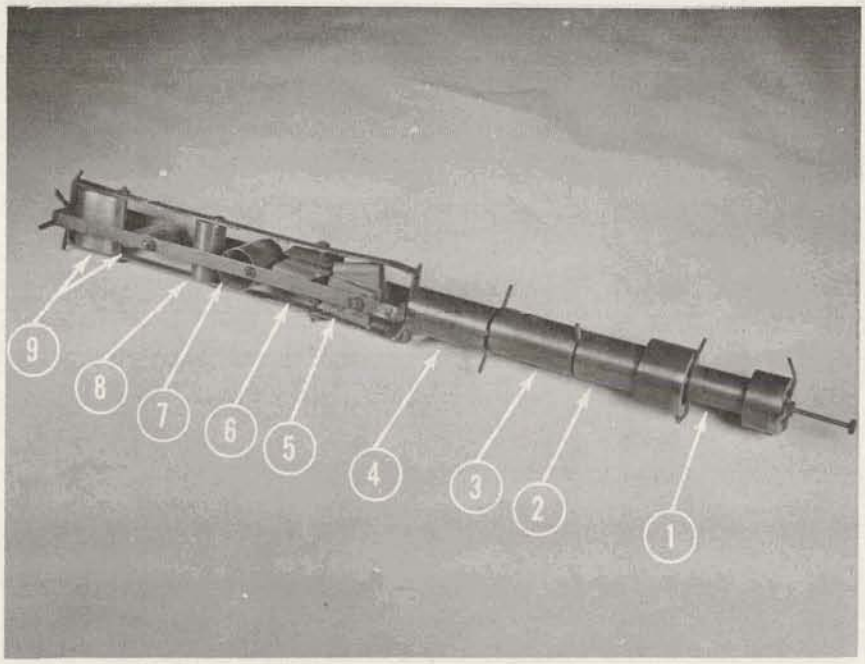

Figure 7.53 - Overall View of Test Holder ---- 0.20 X (1126-0-1)

LEGEND:

1. Assembly representing the lower collar (grid plate) and tubes. The tube is fusion welded to the simulated collar; radial clearance between the tube and collar of test approximately 0.0017". Tube and collar of stainless steel 316 fully annealed.

2. Assembly representing the upper collar and tubes. The tube, stainless steel 316, is fussion welded to the simulated collar stainless steel 304. At the weld region only, the tube was expanded in the collar prior to welding.

3. Typical outer container tube, stainless steel 316, expanded approximately 0.010".

4. Typical outer container tube, stainless steel 316, fully annealed

5. Inconel sheet 0.020" U bend

6. Inconel sheet 0.020" U bend

7. Typical outer container tube, stainless steel 316, fully annealed.

8. Typical outer container tube swedged end stainless steel 316, fully annealed.

9. Typical outer container flattened stainless steel 316.

NOTE:

Test holder shown at conclusion of 2304 hours in 500F and 1200psi water.

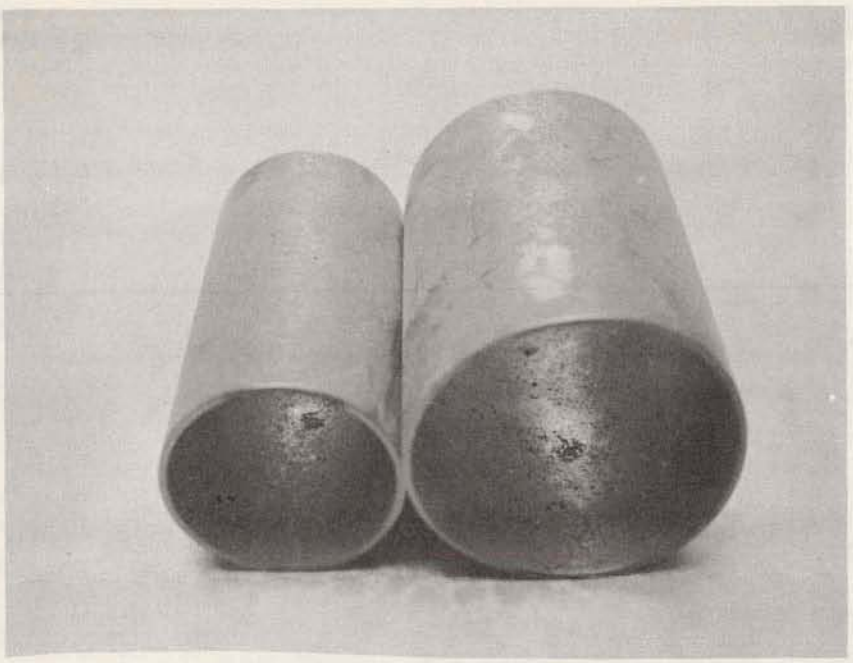

Figure 7.54 - View of Loose Crud Collected on Surfaces, (normal to flow in 2304 hrs. at 500 F and 1200 psi in loop test) (shape distortion is caused by angle of camera)....15X (112C-o-2)

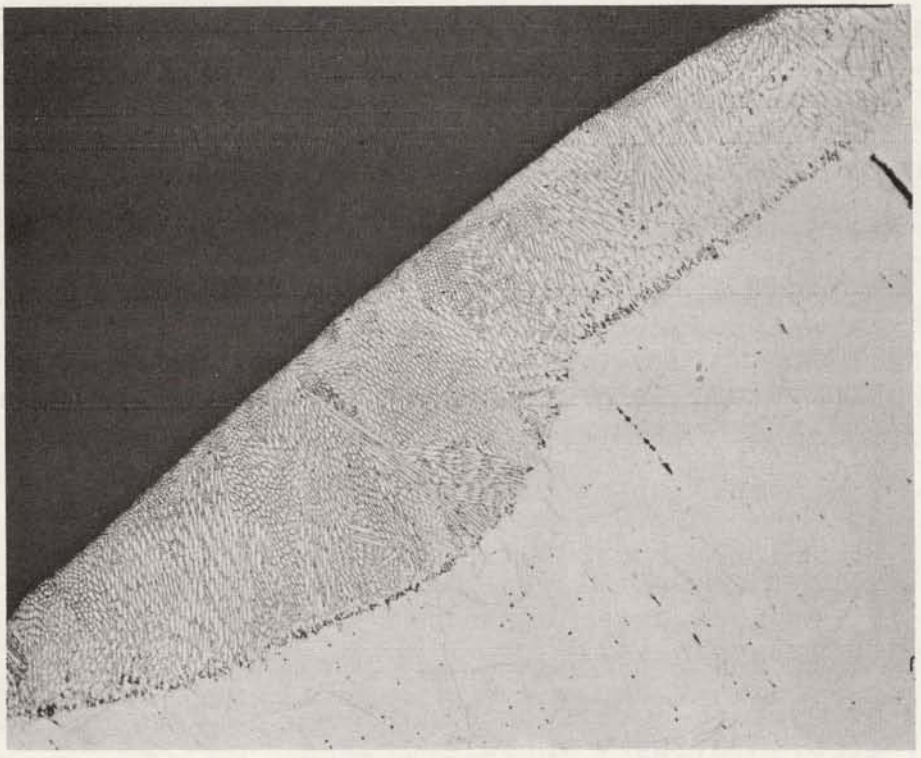

Figure 7.55 - View Showing Lack of Weld Penetration in Proper Area (test was run for 2304 hrs. at 500 F and 1200 psi in. water) .... 75 X (112C-1-1)

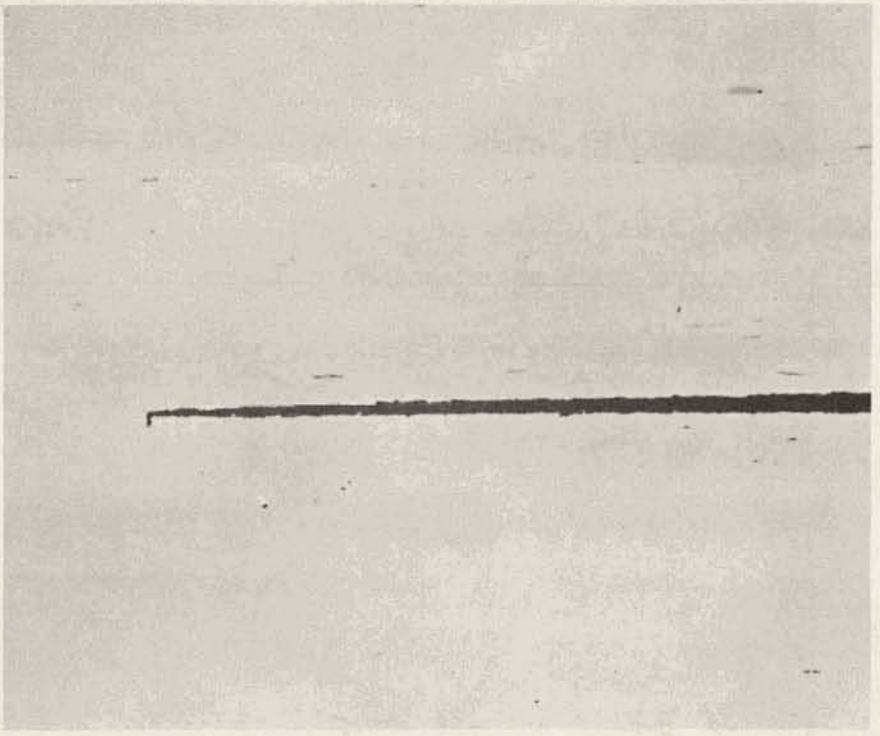

Figure 7.56 - View Showing Oxide at End of Weld Penetration (test was run for 2304 hrs. at 500 F and 1200 psi in water) .... 250 X (112C-2-1)

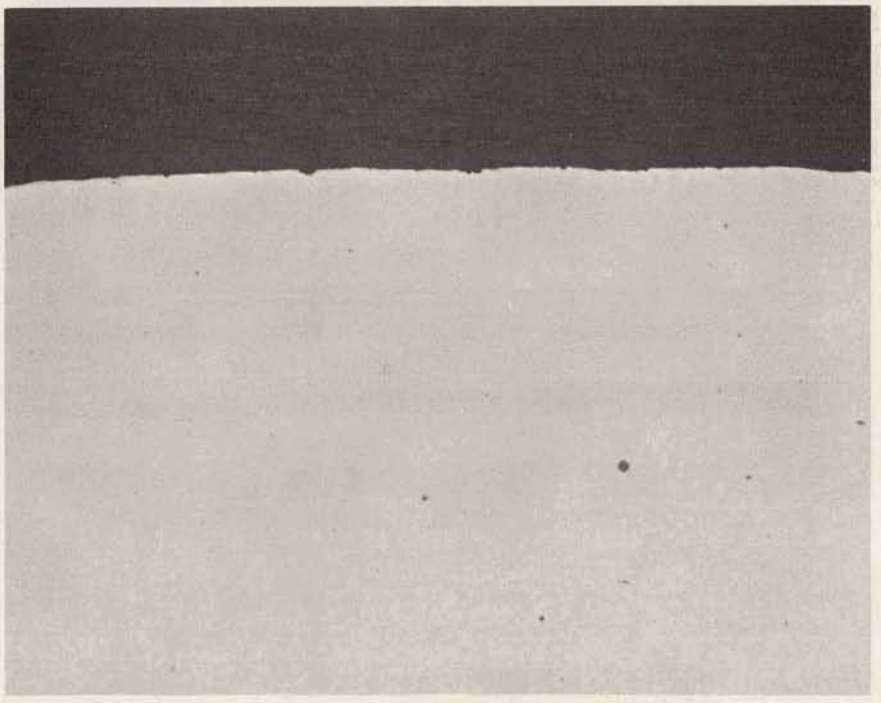

Figure 7.57 - View Showing Bent Surface of 316SS 25/32 in. Dia. Tube (after 2304 hrs. at 500 F and 1200 psi in test loop)....250X (112C-5-2)

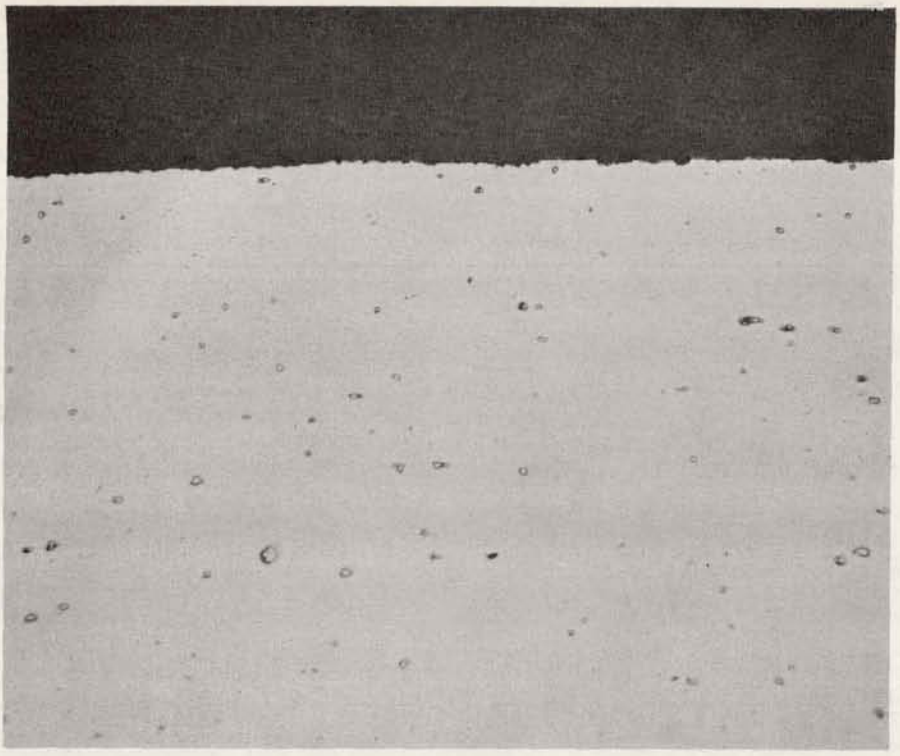

Figure 7.58 - View Showing Bent Surface of Inconel Sheet (after 2304 hrs. at 500 F and 1200 psi in test loop)----250X (1120-5-3)

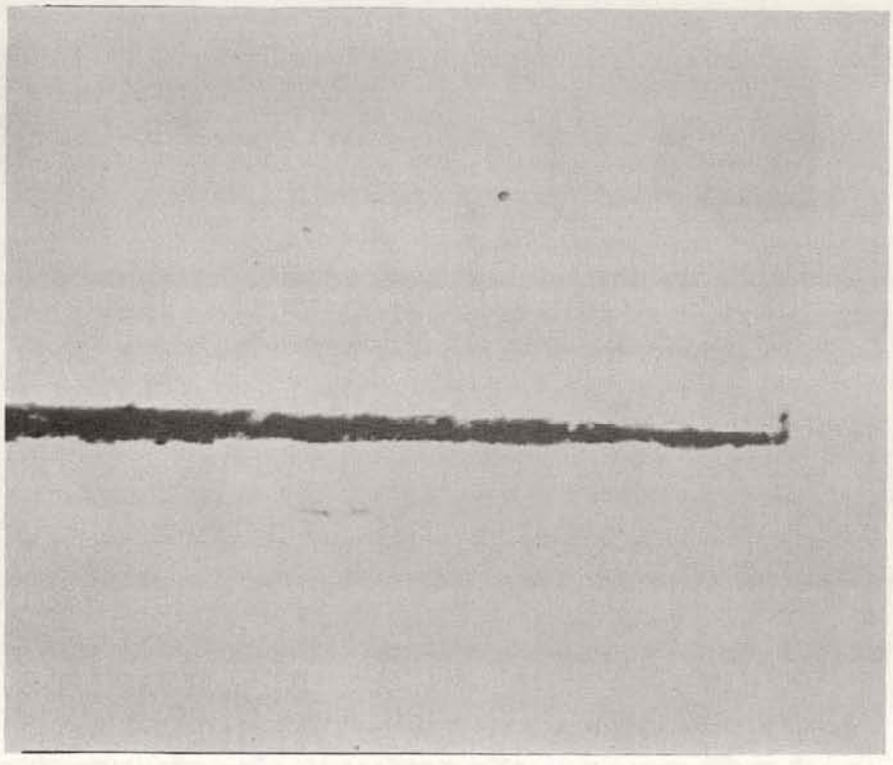

Figure 7.59 - View Showing Oxide at End of Weld Penetration, (test was run for 2304 hrs. at 500 F and 1200 psi in water) ----250X (1120-2-1)

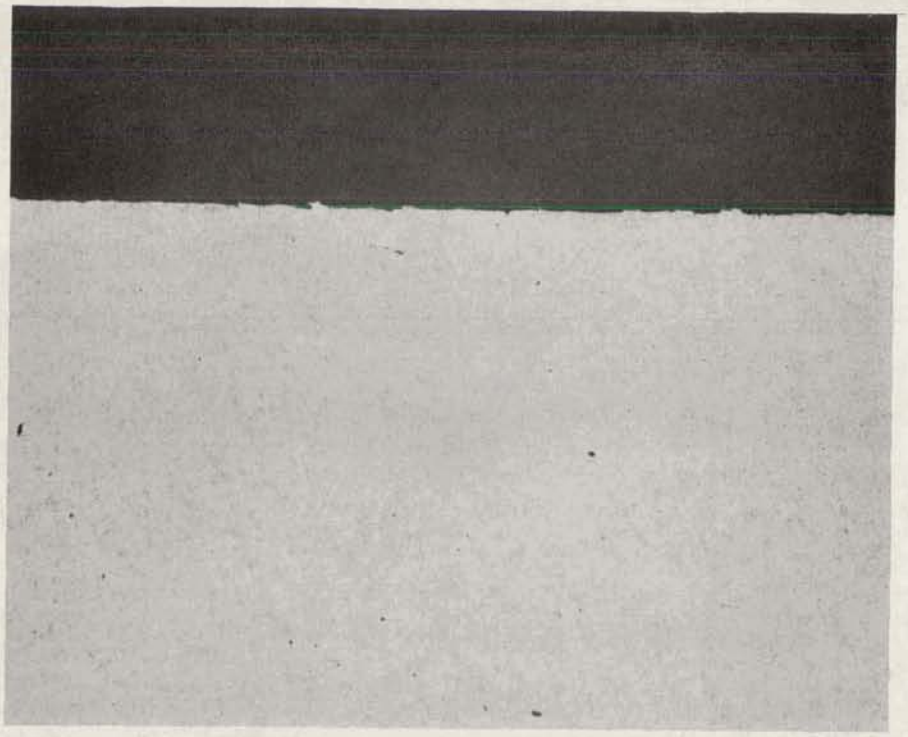

Figure 7.60 - View Showing Outside Surface of 316SS Fully Annealed (after 2304 hrs. at 500 F 1200 psi in test loop) ---- 250X (112C-4-1)

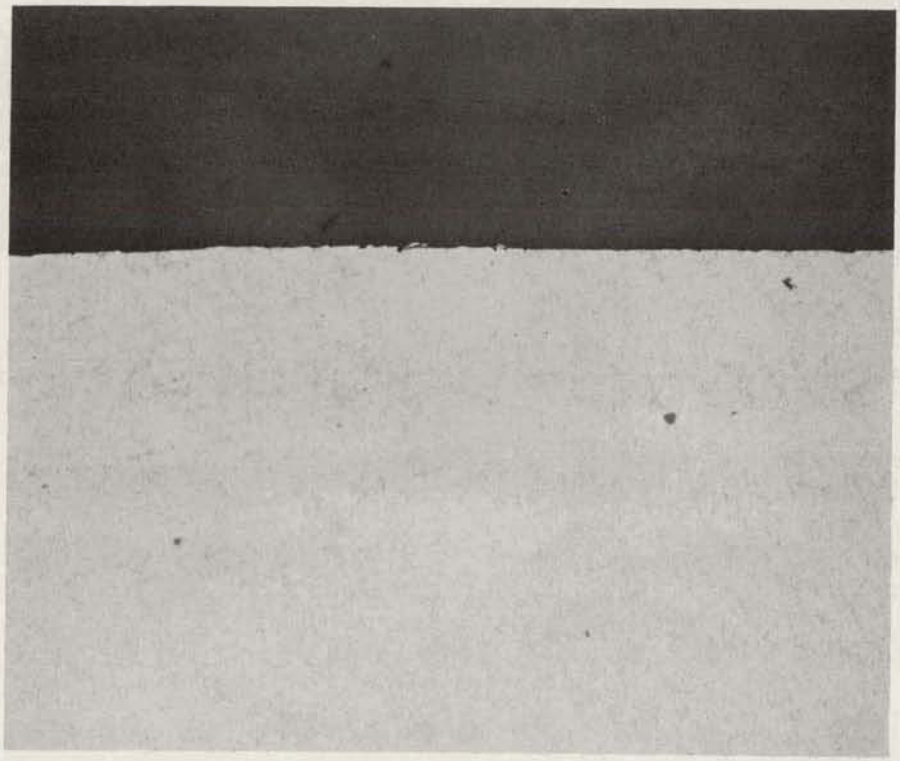

Figure 7.61 - View Showing Bent Surface of 316 SS 11/16 in. Dia. Tube (after 2304 hrs. at 500 F and 12 PSI in test loop) ---- 250X (112C-5-1)

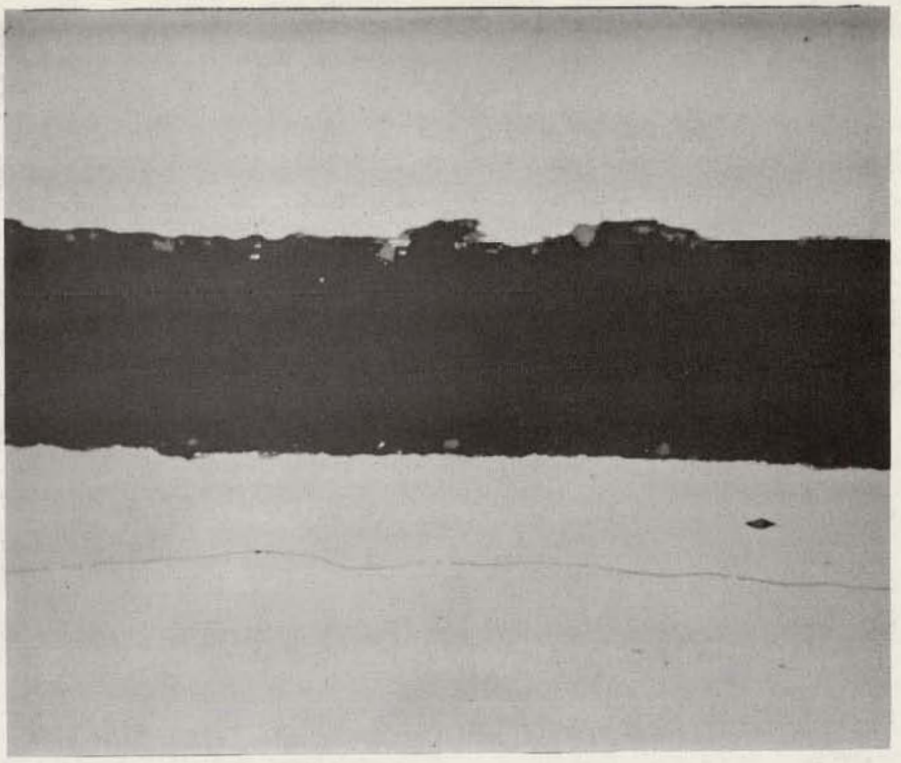

Figure 7.62 - View Showing Layer of Oxide Between Tube and Collar, (after 2304 hrs. at 500 F and 1200 psi in test loop) ---- 625X (112C-2-2)

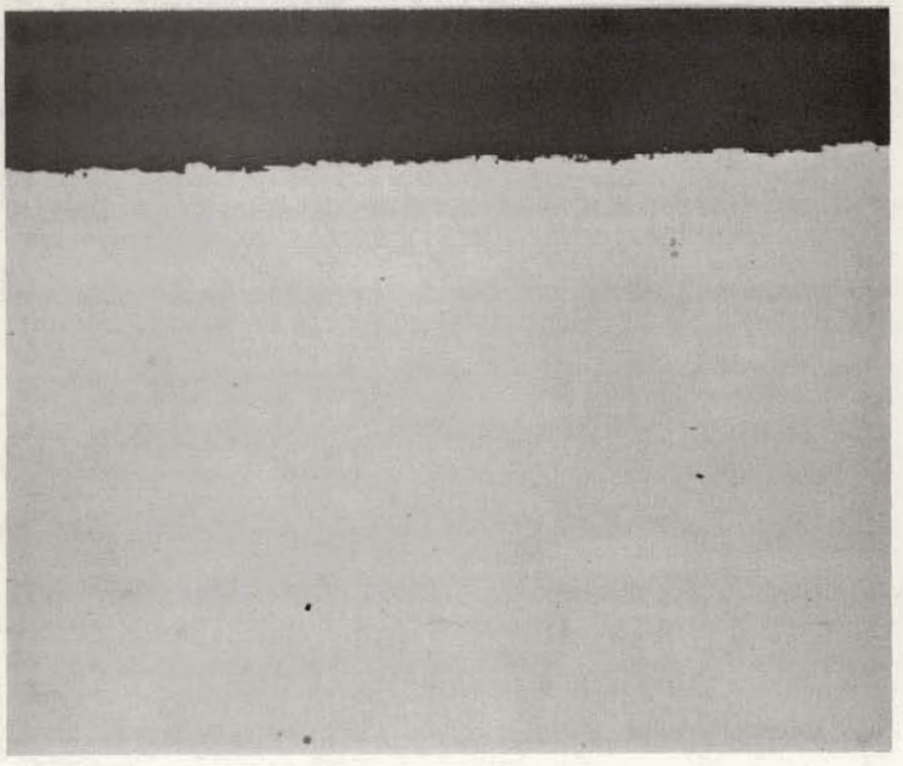

Figure 7.63 - View Showing Outside Surface of 316SS Expanded Tube, (after 2304 hrs. at 500 F and 1200 psi in water) --- 250X (112C-3-1)

BIBLIOGRAPHY

1. Eng, G. H., "Deflection and Stress Analysis of the Yankee Core Support Structure", YAEC-77, 1958.
2. Roark, R. J., "Formulas for Stress and Strain", McGraw-Hill Book Co., 3rd Edition, New York, 1954.
3. Glasstone, S., "Principles of Nuclear Reactor Engineering", Van Nostrand Co., Princeton, N.J., 1957.
4. Timoshenko, S. and MacCullough, G. H., "Elements of Strength of Materials", Van Nostrand Co., New York, 1945.
5. Wilson, J. F. and Grenda, R. J. "Removal of Entrained Moisture from Steam Using Natural Separation and Mechanical Dryers," ACNP-6105, 1961.
6. Sturm, R. G., "A Study of the Collapsing Pressure of Thin-Walled Cylinder", University of Illinois.
7. Soehrens, J. E., "The Design of Floating Heads for Heat Exchangers", ASME Paper No. 57-A-247, Dec. 1957.
8. Timoshenko, S., "Theory of Plates and Shells", 1st Edition, McGraw-Hill Book Co., New York, 1940.
9. "Tentative Structural Design Basis for Reactor Pressure Vessels and Directly Associated Components", U. S. Department of Commerce, Office of Technical Services.